Liquid-borne Nanoparticle Characterization and its Application to Nanometer-rated Liquid Filter Evaluation

A DISSERTATION
SUBMITTED TO THE FACULTY OF THE GRADUATE SCHOOL
OF THE UNIVERSITY OF MINNESOTA
BY

Tsz Yan Ling

IN PARTIAL FULFILLMENT OF THE REQUIREMENTS
FOR THE DEGREE OF
DOCTOR OF PHILOSOPHY

Dr. David Y.H. Pui

August 2013

Acknowledgements

I would like to express my sincere gratitude to my advisor, Prof. David Y. H. Pui for this guidance, stimulating ideas and continuous support throughout my study. I would also like to thank my committee members: Profs. Ephraim Sparrow, Thomas Kuehn and Timothy Wiedmann for providing valuable suggestions and comments on my dissertation research.

Thanks to all my colleagues in the Particle Technology Laboratory and Mechanical Engineering Department for their advice and help. I would like to thank Prof. Jing Wang, Dr. Seong-Chan Kim and Dr. Chaolong Qi for assisting me in the initial stage of my research work. Other former and current postdocs and students, including: Kyoungtae Kim, Jake Swanson ,Shawn Chen, Lin Li, Shigeru Kimoto, Qisheng Ou, Weon-Gyu Shin, Nick Stanley, Chang Hyuk Kim, Zhili Zuo, Kai Xiao, Leo Cao, Gustaf Lindquist and Drew Thompson, deserve thanks for helpful support and discussions.

Thank you to the contributors within the Center for Filtration Research including: 3M Corporation, Boeing Commercial Airplanes, Cummins Filtration Inc., Donaldson Company, Inc., Entegris, Inc., Ford Research and Innovation Center, Hollingsworth &Vose Company, MANN + HUMMEL GMBH, MSP Corporation, Samsung Electronics Co., Ltd, Shigematsu Works Co., Ltd, TSI Inc., and W. L. Gore & Associates, Inc., and the affiliate member National Institute for Occupational Safety and Health (NIOSH) for the technical and financial support. I also would like to specially thank Dr. Axel Zarrth from TSI Inc. for his help with using the nanoparticle nebilizer for my experiments. I also gratefully acknowledge the Department of Mechanical Engineering Fellowship, Abplanlp Sanders Research Fellowship and Doctoral Dissertation Fellowship from the Graduate School for the financial support of my studies.

Finally, I think my family and friends for their support and encouragements.

Abstract

Nanoparticles are often found in liquid-borne dispersed phases, in addition to the airborne and surface-borne phases. Characterization techniques for nanoparticles are needed for the environmental, health and safety studies of nanomaterials. On the other hand, membrane filtration has been demonstrated to be effective for the removal of liquid-borne nanoparticles. Such technique has found many applications, including: 1) contamination control in liquids used in industries which require high level of cleanliness, 2) control of the release of engineered nanoparticles for environmental health and safety and 3) drinking water purification and disinfection. For evaluating filtration performance of nanometer-rated filters, reliable techniques for counting and sizing liquid-borne nanoparticles are desirable. The objectives of this thesis are to 1) explore methods for characterizing liquid-borne nanoparticles and 2) apply these methods to study nanoparticle filtration problems.

In Chapter 2, calibration results of the Nanoparticle Tracking Analysis (NTA) technique in our lab are reported. The concentration measurements agree well with that estimated by suspension mass concentration within the range of 10^8-10^{10} particles/ml. To ensure the concentration measurements are made within the linear valid range, a single sample should be diluted and the NTA concentration measurements for the original and diluted samples should agree. Applying the NTA technique, the size distribution and concentration of nanoparticles in the water used in Abrasive Waterjet Machining (AWM) and Electrical Discharge Machining (EDM) processes were measured. The particles generally have a most probable size of 100-200 nm. The filtration systems of the AWM and EDM processes were found to remove of 70 and 90 % the nanoparticles present, respectively. However, the particle concentration of the filtered water from the AWM was still four times higher than that found in regular tap water. These nanoparticles are mostly agglomerated, according to the microscopy analysis. Since AWM and EDM are widely used, the handling and disposal of used filters collected with nanoparticles, release

of nanoparticles to the sewer and potential use of higher performance filters for these processes will deserve further considerations.

The development of an aerosolization technique to measure liquid-borne nanoparticles down to 30 nm and its application to filter evaluation is discussed in Chapter 3. This technique involves dispersing nanoparticle suspensions into airborne form with an atomizer or electrospray aerosol generator, and measuring the size and concentration by a differential mobility analyzer coupled to a condensation particle counter. With the electrospray aerosol generator, residue particles can be controlled to be less than 10 nm, allowing particles as small as 30 nm to be clearly distinguished from the size distribution measurements. Calibrations with 30, 50, 125 and 200 nm polystyrene latex particles showed that liquid-borne and airborne particle concentrations are proportionally related. This provides an effective way to quantify liquid-borne particles as small as 30 nm, which cannot be analyzed by state-of-the-art liquid particle counters. Comparing to NTA, the aerosolization technique gives more accurate representation for polydisperse size distribution.

The aim of Chapter 4 is to study the filtration process of a model membrane filter, the nuclepore filter. Initial filtration efficiency experimentally measured using the aerosolization and NTA techniques are comparable with each other. The capillary tube model modified from that developed for aerosol filtration was found to be useful to represent the experimental results, when a sticking coefficient of 0.15 is incorporated. This suggests that for the polystyrene latex (PSL) particles-nuclepore filter-water system, only 15% of the particle collisions with the filter results in successful attachment. The small sticking coefficient found can be explained by the unfavorable surface interactions between the particles and the filter medium.

The sieving mechanism, in which particles are removed when they are larger than the filter pore size, is primarily used to describe the filtration process. The capture of particles smaller than the pore size, by adsorption via diffusion and interception, becomes

effective when the combined electrostatic and van der Waals interactions between particle and filter surface are favorable. In Chapter 5, retention efficiency of a 50 nm-rated Polytetrafluoroethylene (PTFE) filter against nanoparticles of different materials (gold, PSL and silica), sizes (80, 50 and 30 nm), concentrations (2×10^9 to 4×10^{11} particles/ml) and size distributions (monodisperse and polydisperse) was measured. The decreasing trend of retention efficiency as a function of particle loading can be readily explained by the sieving mechanism. Among different particle materials, silica shows much lower retention efficiency compared to PSL and gold particles of the same size. This observation can be explained with the DLVO theory, which suggests that higher ionic strength of PSL and gold suspensions causes a decrease in the magnitude of energy barrier and favors their adsorption to the filter surface. In addition, this study observed higher retention efficiency for mixed particles compared to monodisperse ones and there is less than 10% of re-entrainment of particles collected by adsorption.

In Chapter 6, numerical simulations for change in membrane filter's retention efficiency in the presence of a particle previously captured within the filter are reported. Because of the complex porous structure of the membrane, the filter model is simplified into two cases: 1) capillary tube model and 2) single fiber model. Simulations for the capillary tube model show that a particle captured near the pore opening can increase the collection efficiency of 30 nm particles due to impaction and interception by about two times, depending on the relative size of the particles to the pore. From the single fiber model, a particle attached on the fiber can increase the combined impaction-interception single fiber efficiency by 10 times, depending on the location of the particle attached. The capillary tube simulation results can be incorporated into pore blockage model which considers filters as multiple layers of parallel pores. The single fiber simulations can explain the higher collection efficiency due to a previously captured particle. However, the single fiber theory alone cannot account for the observed decreasing trend with particle loading.

Table of Contents

List of Tables

List of Figures

Chapter 1 Introduction

1.1 Background

Liquid-borne nanoparticles

Nanoparticles are defined as particles with one or several dimensions of 1 to 100 nm by the American Society for Testing and Materials and the International Standard Organization [ASTM, 2006; ISO, 2008]. Nanoparticles exist in airborne, liquid-borne and surface-borne dispersed phases. In the liquid-borne phase, nanoparticles occur the nature, for example, rock and soil runoff as well as living or dead organisms [Gregory, 2006]. In addition, they can be generated by human activities. An important contribution is engineered nanoparticles, which are synthesized for use of their unique properties at the nano-dimensions. Engineered nanoparticles are usually stored in a liquid dispersion. Nanoparticles coated on various surfaces to enhance performance of nano-products may be released to the environment via wastewater streams upon washing or disposal. For the environmental, health and safety studies of nanomaterials in support of sustainable nanotechnology, it is therefore necessary to develop characterization techniques for liquid-borne nanoparticles to gain better understanding of their life cycle [Ling et al., 2013].

Another important application of the liquid-borne nanoparticle characterization is filter evaluation. Filtration is a major technique for the abatment of nanoparticle contamination in water and other liquids. For example, it is used to remove nanoparticles from wastewater before discharge as well as process water and other chemicals that are used in industries having high cleanliness requirement. An ideal filter should have high retention efficiency under wide range of working conditions and low pressure drop. Therefore, for the filter manufacturers and filter users, reliable nanoparticle characterization techniques are needed for evaluating nanometer-rated liquid filters. In the following sections, background information on the characterization techniques and properties of liquid-borne nanoparticles related to their filtration as well as membrane filtration will be discussed.

Liquid-borne nanoparticle characterization

Each characterization method for nanoparticles has its own advantages, disadvantages, applicable size and concentration ranges. Particles are best characterized at their original phase, with minimum handling or perturbation. For example, liquid-borne nanoparticles will form aggregates when dried or pH changes. However, transferring the particles from one phase to another, sometimes, allows additional information of the particles to be obtained. Decision on the use of a specific method will depend on the properties of the particles of interest. It should also be noted that different methods use different principles to measure the equivalent particle size distribution. Different particle size representations may have different significances. For example, the hydrodynamic size, which relates the drag experienced by the particles, will determine the diffusion behavior. On the other hand, the geometric size may be more relevant for particle filtration by interception mechanism [Wang et al., 2011]. The rest of this section will review common techniques for characterizing the size distribution and concentration of liquid-bone nanoparticles, which are important for filter evaluation.

Microscopy

Electron microscopy is applicable for resolving particles with nano-scale. Examples of electron microscopy include: Scanning Electron Microscopy (SEM), Transmission Electron Microscopy (TEM) and Atomic Force Microscopy (AFM). In addition to the area-equivalent size of the particles, a major advantage of microscopic observation is that particle morphology can be apparent. Additionally, electron microscopy methods allow the determination of the elemental composition of the particles if Energy Dispersive Spectroscopy (EDS) is included. The primary disadvantage of microscopy analysis is that the sample preparation procedures require drying and transferring the particles to a surface, which may cause particle aggregation [Hassellöv et al., 2008]. Secondly, microscopy analysis usually has a limited sample size. Sample preparation is elaborate and it is time consuming to obtain and analyze sufficient images in order to have statistically significant analysis [Mavrocordatos et al., 2007].

Coulter counting

Particles in an electrolyte solution passing through an orifice cause a momentary change in electrical resistance and hence a voltage pulse between two electrodes with current maintained constant. Most particles can be assumed to have infinite resistance, compared to the electrolyte solution and so the voltage pulse produced can reflect the particle volume. Particles can be counted as a series of pulses. An unique feature is that this method is independent of the shape and composition of the particles, because the measurement is only dependent on the volume of electrolyte displaced by the particles. Disadvantage of this technique is that the liquid phase has to be electrical conductive. The measurement is limited to the size of the orifice available [Gregory et al., 2006]. A carbon nanotube-based coulter has recently been commercialized for measurement of particles down to 50 nm [Henriquez et al., 2004; Ito et al., 2004].

Optical counting

Particles are made to pass through a laser beam where their scattered light is detected. Particles are counted and sized based on their light scattering properties. Because light scattering depends on the refractive index of particles, for particles of unknown composition, the results are reported as monodisperse polystyrene latex particles equivalent [Gregory et al., 2006]. Coincidence counting, in which two or more particles are considered as a bigger particle, has to be avoided [Weersing, 1969]. The lower detection limit is about 50 nm.

Dynamic light scattering

The basis of dynamic light scattering is that light scattered from a moving particle will have a slightly different frequency from the incident light. In a suspension, random Brownian motion of the particles causes scattered light to vary its frequency randomly. Interference between scattered light from different particles causes fluctuations in the

light intensity. The detection limit can go down to a few nanometer. However, it only gives particle size information but not concentration. In addition, the signal inversion for polydisperse particles is mathematically difficult [Gregory, 2006].

Centrifuge sedimentation

It uses centrifugation spinning to enhance particle sedimentation rate, which is size-dependent. Centrifuge sedimentation is combined with light transmission measurements to determine particle size distribution. An important advantage of the centrifuge technique is that it covers a wide particle size range from 10 nm to 50 μm. The limitation is that particles which have similar density as the solvent will have a low settling rate, leading to a higher detection size limit [McFadyen et al., 1993; Bondoc and Fitzpatrick, 1998 ;Gregory 2006].

Particle tracking

The particle trajectories due to diffusive Brownian motion can be followed using video microscopy. Particle size distribution is determined by correlating the particles' root mean square displacement to the Stoke-Einstein equation. Particle concentration is estimated based on the number of particles visualized in the video microscopy. The primary advantage is that the particles are visualized and data analysis is simpler than dynamic light scattering method [Filipe et al., 2010]. However, it has a small concentration dynamic range. More discussions on this method is given in Chapter 2.

Aerosolization

An atomizer or nebulizer is used to disperse liquid-borne nanoparticles into the airborne form. After subsequent evaporation of solvent in the droplets, the particle size and concentration can be determined by aerosol instruments, namely the Scanning Mobility Particle Sizer (SMPS). The advantage of this method is that it can achieve very high

sizing resolution with the aerosol instruments. However, it requires a low solute concentration in the solvent to overcome the residue particle interference. The aerosolization process may alter the actual particle size distribution. More discussions on this method is given in Chapter 3.

Finally, Table 1-1 summarizes the measurement specifications of the characterization methods discussed [Gregory, 2006; Hassellöv et al., 2006].

Table 1-1. Specifications of methods for liquid-borne nanoparticles characterization.

	Concentration limit (particles/ml)	**Equivalent size**	**Single particle or population method**	**Particle size range (nm)**
Microscopy	NA	Area	Single	1 to >1000
Coulter counting	$<10^6$	Volume	Single	50 to >1000
Optical counting	$<10^6$	PSL light scattering	Single	50 to >1000
Dynamic light scattering	10^5-10^9	Hydrodynamic	Population	3 to >1000
Centrifuge sedimentation	Detector dependant	Stoke	Population	10 to >1000
Particle tracking	10^7-10^9	Hydrodynamic	Single	30 to 1000
Aerosolization	$>10^9$	Electrical mobility	Single	10 to 1000

Particle interactions in liquids

The study of filtration of nanoparticles in liquds, with water being the focus in this work, has many common aspects as in aerosol study. The theories for particle mechanics, e.g., drag, diffusion, sedimentation, which govern particle motion and deposition onto a filter, are generally in common. In addition to particle mechanics, we need to consider the surface interactions between particles and filter surface. Surface interactions mainly include the van-der Waals forces and the double layer force. In this section, the basic concepts on liquid-borne nanoparticle surface interactions, which are related to filtration studies, are reviewed.

Surface charges and their representation

A particle or a surface in contact with an aqueous solution is likely to acquire surface charges. When a surface has constituent ion groups that have a greater tendency to ionize in presence of water, a residual charge on the surface is remained. Surfaces having acidic or basic groups will cause protons (H^+) to be released or acquired from the solution, depending on the solution pH. For example, metal oxides (e.g.: alumina Al_2O_3, iron oxide Fe_2O_3, titanium oxide TiO_2) can undergo ionization to gives Metal-O^- or Metal-OH_2^+, depending on the pH of the aqueous solution. The surface is positively charged at low pH and negatively charged at high pH. On the other hand, isomorphous substitution of ions with different charges or adsorption of ions also causes a surface to acquire charges [Gregory, 2006].

A charged surface in contact with a solution will attract oppositely charged ions (counterions), causing a uneven distribution of ions near the surface. The counterions are subject to two opposing tendencies: 1) electrostatic attraction to the charged surface and 2) the random motion due to thermal speed. Considering a negatively charged particle as an example (Figure 1-1), attraction from the negative particle causes positive ions to form a firmly attached layer around the surface of the particle. This layer is known as the Stern layer. Additional positive ions are still attracted by the negative particle, but the extent of charge unbalance decreases with the distance from the particle surface. The equilibrium between attraction by surface charge and random diffusion leads to the formation of diffuse layer of counter ions, until it reaches the potential in the bulk solution. The Stern layer and diffuse layer are collectively referred as electrical double layer [Lee, 1992]. A more detailed description on the double layer theory, which takes into account the finite size of ions, can be found in [Stern, 1924].

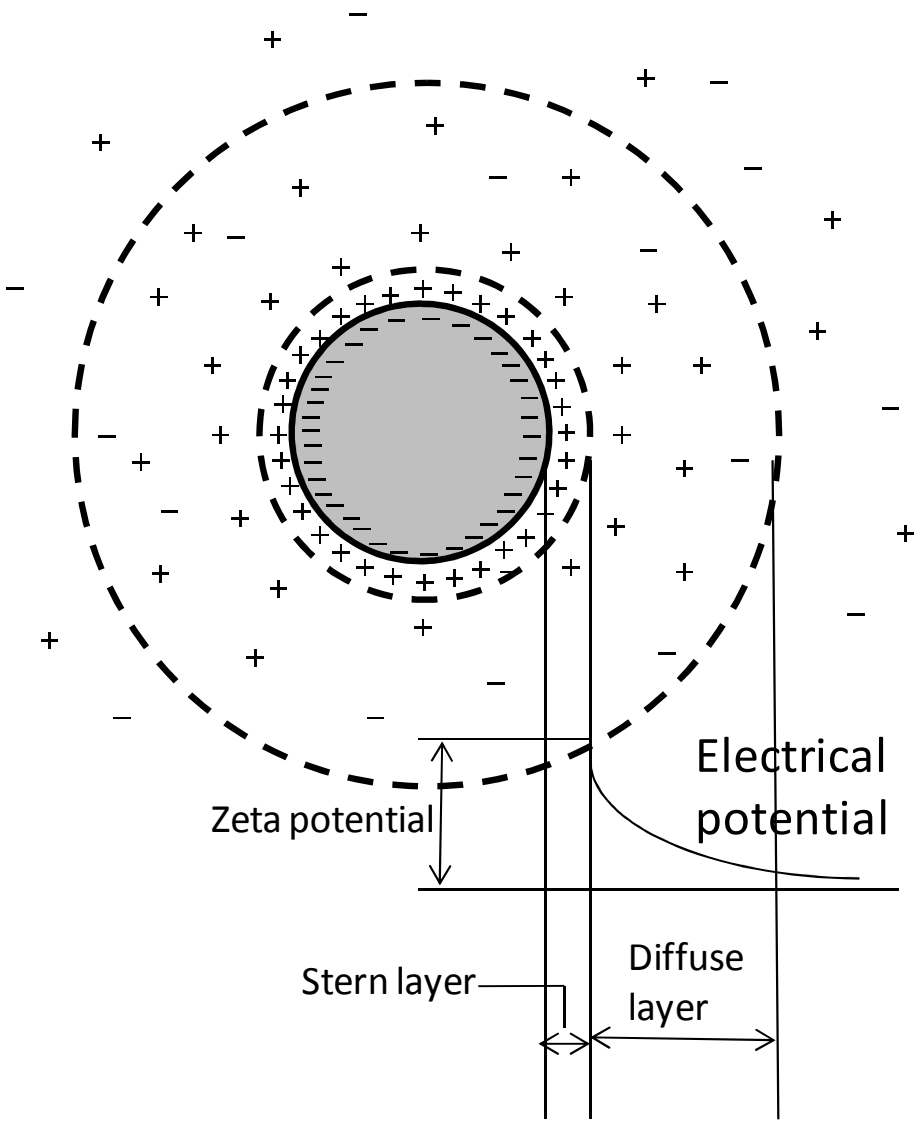

Figure 1-1. Electrical double layer and zeta potential of a charged particle [Lee, 1992].

The thickness of the electrical double layer affects the extent for the electrical force to be effective. The governing parameter is κ, and its value is given as follow:

$$\kappa = \left(\frac{\rho_\infty e^2}{\varepsilon \varepsilon_0 kT} \right)^{1/2} \qquad \text{Equation1-1}$$

where:

ε = Dielectric constant of the material

ε_0 = Dielectric permittivity of free vacuum space

k = Boltzmann constant

T = Absolute temperature

e = Electronic charge (1.602×10^{-19} C)

ρ_∞ = Bulk electrolyte concentration

From the Stern layer to the solution, the electrical potential varies in an approximately exponential manner. 1/κ is known as the Debye length, which gives the distance at which surface potential drops to 1/*e* of its original value. It represents thickness of the double layer. The Debye-length decreases with higher electrolyte ion concentration.

Surface interactions

Interactions between particles and/or surfaces are usually within a few nanometers, relatively short-range compared to other length scales of interest to particle filtration study. Therefore, they only become significant when particles are in close proximity with each other and/or filter surface. In general, they do not have much influence on the particle mechanics. The surface interactions are commonly represented as potential energy (*W*) or forces (*F*). These two quantities can be connected by considering the energy involved in bringing the particles from an infinite distance, where the interaction

is negligible, to a given separation D. Mathematically, this can be represented as [Gregory, 2006]:

$$W = \int_{D}^{\infty} F(x)dx \qquad \text{Equation1-2}$$

The two most important interactions are van der Waals (usually attractive) and electrical double layer (repulsive or attractive) interactions. They are described by the DLVO theory, named after Deryagin, Landau, Verwey and Overbeek who developed the quantitative theory of colloid stability [Verwey and overbeek, 1948; Derjaguin, 1954]. Other interactions include: hydration effects (repulsive), hydrophobic (attractive) and steric interaction (usually repulsive).

The van der Waals interactions arise from the attractions between atoms and molecules due to dipoles, induced dipoles or fluctuating dipoles. For sphere-flat plate geometry, the van der Waals energy of attraction per unit area is given as:

$$W_{vdw} = -\frac{AR}{6D} \qquad \text{Equation 1-3}$$

where:

A = Hamaker constant

R = Particle radius

D = Separation distance between particle and flat surface

The van der Waals interactions vary inversely with separation distance [Israelachvili, 2011].

The electrical double layer interaction arises from the surface charges. The actual surface potential of a particle is very difficult to measure experimentally. However, the zeta

potential, as indicated in Figure 1-1, is convenient to measure by electrophoresis, i.e., movement of charged particles in an electric field. The Zetasizer by Malvern is a common commercial instrument that can measure particles' zeta potential. It is assumed that the interactions can be estimated by the zeta potential. For sphere-flat plate geometry, the electrical double layer interaction is given as:

$$W_{edl} = RZ\exp(-\kappa D)$$

$$Z = 64\pi\varepsilon\varepsilon_0\left(\frac{kT}{e}\right)^2 \tanh\left(\frac{e\psi_1}{4kT}\right)\tanh\left(\frac{e\psi_2}{4kT}\right) \qquad \text{Equation1-4}$$

$$\kappa = \left(\frac{\rho_\infty e^2}{\varepsilon\varepsilon_0 kT}\right)^{1/2}$$

where:

ε	=	Dielectric constant of the material
ε_0	=	Dielectric permittivity of free vacuum space
k	=	Boltzmann constant
T	=	Absolute temperature
e	=	Electronic charge (1.602×10^{-19} C)
ψ_1, ψ_2	=	Surface potential of materials 1 (particle) and 2 (filter), respectively
ρ_∞	=	Bulk electrolyte concentration
D	=	Separation distance

It can be seen that the interaction depends on the zeta potentials of the two surfaces and the product of the separation distance and κ (in an exponential relation). With high electrolyte concentration, κ is high. The interaction decays rapidly with distance and is of short range [Israelachvili, 2011].

By considering the Equations 1-3 and 1-4 together, the combined surface interactions can be determined. Typical plots on overall interaction energy as a function of separation

distance for different ionic strength values are shown in Figure 1-2. The potential energy barrier needs to be overcome before the particle and surface experience an attractive force. The energy barrier is usually a lot higher than the average thermal energy, given as $\frac{3}{2}kT$. Therefore, additional momentum from the particles is needed to surmount the barrier for particle attachment onto a filter surface [Gregory, 2006].

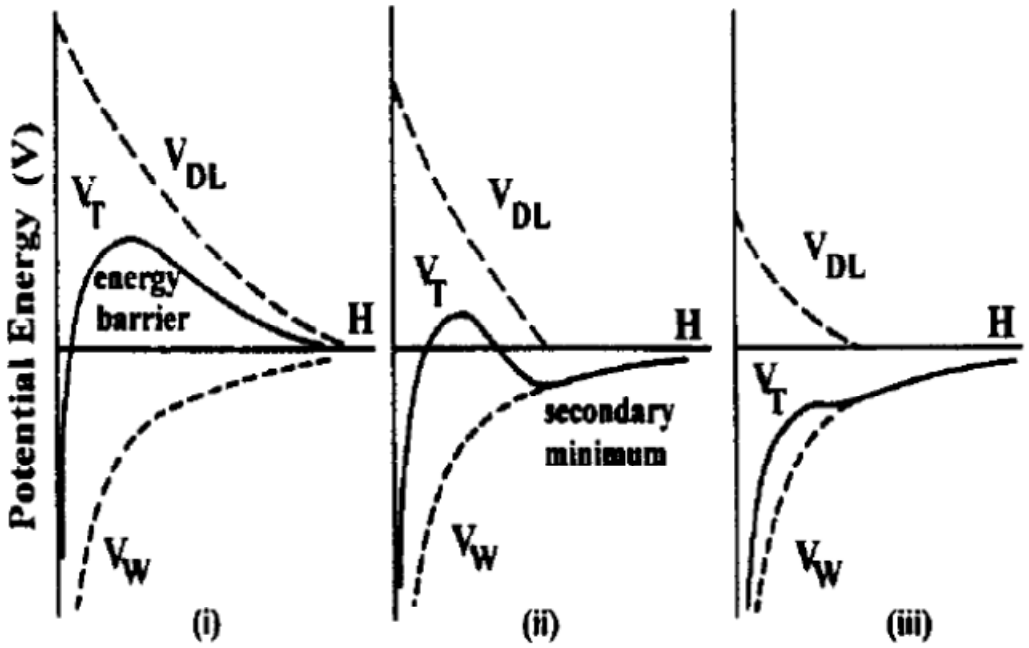

Figure 1-2. DLVO potential energy of interaction between two surfaces having the same sign of charge. (i) low ionic strength; (ii) intermediate ionic strength; (iii) high ionic strength [Oliveira, 1997].

Liquid filtration

Liquid-bone particle filtration can be broadly classified into: 1) membrane filtration and 2) granular deep bed filtration. Membranes are thin layer of porous material usually made of polymer or ceramic. Membrane filtration has the advantages of process simplicity, modular construction and low space requirement. In addition, with the development in new membrane materials, filtration performance can be continuously improved [Tien and

Ramarao, 2007]. Membrane filtration is widely used in the control of semiconductor contamination and nanoparticle removal from water. It has been reported that particle counts in ultra pure water have a direct relation to the yield loss in semiconductor manufacturing industry [Wali et al., 2009]. 20 nm rated Polytetrafluoroethylene (PTFE) membrane filters are used to remove particles from wafer cleaning chemicals [Nose et al., 2007]. Membrane filtration has been studied for the separation of different engineered and biological nano-materials from water [Han et al., 2008; Jassby et al., 2010; Lander et al., 2012; Wu et al., 2013]. Based on the effective pore size of the membrane and hence the size of the impurities removed, membrane processes can be generally characterized as follows: 1) microfiltration, 2) ultrafiltration, 3) nanofiltration and 4) reverse osmosis. Table 1-2 summarizes the features of these processes [Gregory 2006; Geise, 2010; Pendergast and Hiek 2011]. It should be noted that the values are not absolute and different references may have different ranges. Filtration of nanoparticles covers size range from microfiltration to nanofiltration.

Table 1-2. Typical characteristics of membrane processes

Process	Operating pressure (bar)	Molecular weight cut-off	Size cut off (nm)	Example particles
Microfiltration	<4	>500k	50-10000	Fungi, bacteria, oil emulsion
Ultrafiltration	2-10	1k – 1000k	15-300	Colloid solids, virus, protein
Nanofiltration	5-40	100-20k	1-50	Antibiotics
Reverse osmosis	15-150	<200	<1	Inorganic ions

Membrane filtration can be operated in two different modes: 1) dead-end and 2) cross-flow, in which fluid flows perpendicularly and parallel to the filter surface, respectively. In this thesis, dead-end filtration is considered. Membrane filtration study concerns about the particle retention efficiency, pressure drop and fouling. Pressure drop affects the energy consumption during filtration operation. Fouling is the process in which contaminants from the feed deposit on the membrane surface and cause a decrease in flux

rate. The focus of this thesis is on particle filtration efficiency. More detailed review on related filtration processes is given in Chapters 4-6.

1.2 Research objectives

The objectives of this thesis are to 1) explore methods for characterizing liquid-borne nanoparticles and 2) apply these methods to study nanoparticle filtration problems. It is expected that connecting the nanoparticle measurements in different phases (air, liquid and surface) will enhance the characterization capability. An obvious example is microscopy analysis for particle morphology and elemental composition by depositing liquid-borne nanoparticles onto surfaces. Taking advantage of the well-developed airborne particle analyzers, this thesis will explore using aerosol methods to characterize the size and concentration of liquid-borne nanoparticles. In addition, this thesis also evaluates a liquid-borne nanoparticle analyzer: the Nanoparticle Tracking Analysis by NanoSight LM10 (NanoSight Ltd., United Kingdom), which is newly available to the market. The applicability of these methods for nanometer-rated liquid filter evaluation will be discussed.

Membrane filters are used for removing different nanoparticles from water/liquids for different applications. However, as discussed in this chapter, the performance of membrane filters will depend on the properties of the particles. In addition, filter performance may vary with particle loading due to prolong use. This thesis will study retention efficiency of different types of membrane filters against nanoparticles of different materials. Both the initial and transient performance will be study. The results will be compared to filtration models. Computational fluid dynamics (CFD) tools will also be applied to understand the phenomena. The goal is to enhance our understanding on membrane filtration against liquid-borne nanoparticles.

1.3 Thesis organization

This thesis is organized in the following manner. A brief review on the topic of this thesis is given in this chapter. For the rest of the thesis content, each chapter contains a separate paper already published or under preparation. Chapter 2 discusses the use of the Nanoparticle Tracking Analysis (NTA) technique for liquid-borne nanoparticle characterization. Its application is demonstrated by charactering waste water from machining processes. Chapter 3 discusses the use of aerosol instruments for counting and sizing liquid-borne nanoparticles. The applicability of this technique for filtration study is also discussed. In Chapter 4, the two techniques discussed in the previous chapters are applied to study initial filtration efficiency of standard nuclepore filter. Chapter 5 reports the experimental studies on the effects of particle loading, size distribution and materials on the filtration performance of Polytetrafluoroethylene (PTFE) membrane filter. In Chapter 6, CFD simulations are used to understand the observations from the experiments. Chapter 7 gives conclusions of this work.

Chapter 2

Applying the Nanoparticle Tracking Analysis technique for nanoparticle characterization and filtration

2.1 Introduction

Because of the rapid development of nanotechnology, the use of engineered nanoparticles in many consumer products, including garments, sporting goods, cosmetics, paints etc., has been increasing [Nowack et al., 2007]. There have been concerns about the release of engineered nanoparticles through waste disposal, leading to their occurrence in the environment [Rezić, 2011; Gallego-Urrea et al., 2011; Zänker and Schierz, 2012]. Common materials of these engineered nanoparticles are different metals, namely: silver, zinc, titanium, gold, metal oxides, carbon nanotubes (CNTs) and fullerenes [Weinberg et al., 201; Zänker and Schierz, 2012]. In addition, nanoparticles can also be unintentionally produced. Examples include nanoparticles from combustion, electrical arc discharges in motors and mechanical wear of materials [Gallego-Urrea et al., 2010].

There are potential environmental and biological effects associating with the metal and metal oxide nanoparticles [Nel et al., 2006; Wiesner et al., 2006; Warheit et al., 2007; Boxall et al., 2007; Handy et al., 2008; Farré et al., 2009; Menard et al., 2011; Peralta-Videa et al., 2011]. In terms of environmental impact, because these nanoparticles are generally of low solubility and degradability, they are likely to accumulate in the system. It was reported that alumina nanoparticles can cause reduction in root elongation and germination [Yang and Watts, 2005]. Biologically, studies have shown that nanoparticles can be taken up by a wide variety of mammalian cells [Lynch et al., 2006; Rothen-Rutishauser et al., 2006]. Alumina nanoparticles are shown to cause oxidative stress and generate free radicals that could disrupt the endothelial cell membrane [Sharma and Sharma, 2007; Schrand et al., 2010]. Copper nanoparticles have also been demonstrated to have toxicological effects in different organs of mice [Chen et al., 2006]. Despite many studies, the impacts of metal and metal oxide nanoparticles are not well known, because

of the complex interactions between engineered and natural nanoparticles, nanoparticle surface functionalization that arises from environmental influences and the rapid development of the nanotechnology field [Zänker and Schierz, 2012].

The risk assessment of nanoparticles requires two pieces of information: 1) hazards or toxic effects of the nanoparticles and 2) exposure as indicated by the amount present in the environment (air, water, soil) [Mueller and Nowack, 2008]. Metal and metal oxide nanoparticles present in sewage may be removed at a waste water treatment plant by partitioning onto wastewater biomass and only to re-enter the environment via agricultural land application of wastewater treatment biosolids. Nanoparticles that are not removed will remain in the effluent stream and enter the surface water environments [Weinberg et al., 2011]. Therefore, for assessing the impact of nanoparticles on the environment or human beings during their entire life-cycle, it is important to characterize their physical and chemical identities as well as quantity released [Benn and Westerhoff, 2008; Gallego-Urrea et al., 2010].

Abrasive Waterjet Machining (AWM) and Electrical Discharge Machining (EDM) are machining processes widely used for cutting and material removal. AWM uses a jet, i.e., small section of water at high velocity and pressure, as a tool to cut the target material by means of erosion. Abrasive slurry is added to enhance the cutting power [Wang, 1999]. EDM makes use of the high temperature during electrode discharge between the work piece and electrode to remove the unwanted material from the work piece through melting and evaporation [Abbas et al., 2007]. During AWM and EDM operations, debris materials, in form of particles of different sizes, are formed and remain in the water used in the processes. In fact, AWM and EDM have been suggested as methods for synthesizing nanoparticles and microparticles [Lin, 2005; Cabanillas 2010; Cabanillas et al., 2010]. Because of the presence of particles in the water, filtration system is included in the AWM and EDM processes. We briefly describe the filtration systems from which we collected samples. The AWM system has both pre- and post- filter systems. The pre-filter system cleans the water before water is sent to the jet to protect the jet nozzle. The

post-filter system removes the abrasive and debris particles before the water is discharged into the sewer. The system consists of 1) a three-stage tank for settling the large abrasive particles and 2) filter cartridges installed with micrometer-rated filters. In the EDM system, water with adjusted conductivity is re-circulated within the system during operation. A micrometer-rated filter is installed to remove particles during re-circulation. Despite the filtration systems installed in the equipments, AWM and EDM processes can be a potential source of unintentionally produced nanoparticles.

Nanoparticle Tracking Analysis (NTA) technique was used for particle characterization in this study. NTA determines particle size distribution by measuring the diffusive Brownian motion of nanoparticles using video microscopy and correlating that to the particle size using the Stoke-Einstein relation. It also determines the particle concentration based on the number of particles visualized in the video microscopy. The instrument allows detection of liquid-borne particles in the size range (polystyrene latex equivalent) of approximately 50 to 1000 nm. The NTA has been used for measuring liquid-borne nanoparticles in different applications, namely: carbon nanotubes, engineered nanoparticles (e.g., fuel additives: ZnO_2, CeO_2, pigments in inks and paints: TiO_2, optical nanotechnology: Ag, Au), pharmaceuticals and nanocapsules for controlled drug delivery and virus particles [Trushkevych et al. 2008; Lundhal et al. 2008; Domingos et al. 2009; Nassar et al. 2009]. It was commented that the NTA gives accurate size measurement, but imprecision of the particle concentration given by this technique has been observed [Filipe et al., 2010]. A major reason for the imprecision is that the number of particles visualized in the videos, from which the NTA software estimates the actual particle concentration, is influenced by various video capture and analysis parameters. For example, a higher camera gain, longer exposure time or lower detection threshold value can cause the NTA software to “see” more particles from the video, even the same suspension sample is used . Therefore, the objectives of this work are to 1) determine the capability of NTA to measure nanopaticle concentration, 2) determine if nanoparticles are generated during AWM and EDM processes, 3) characterize the

nanoparticles found physically and chemically and 4) assess whether the current filtration system is adequate for preventing release of nanoparticles.

2.2 Experiments

NTA calibration

The concentration measurement by NTA (NanoSight LM10, NanoSight Ltd., United Kingdom) was first calibrated with 150 nm PSL particles (Duke Scientific Corp.) of different concentrations. Particles were diluted from the supplied package in deionized water to the concentration acceptable for NTA measurements, i.e., between 10^7 and 10^9 total particles/ml (NTA manual). The number concentration measured was compared to that estimated by the size, material density and mass concentration of the PSL particles. The experiments were performed with 5 different camera gains, which act to multiply the intensity reading from each pixel in the video images. It should be noted that NTA requires the user to adjust some parameters (e.g., brightness, gain, detection threshold) to facilitate particle identification and processing. The measurements of the particle size distribution and concentration have been found to be dependent to these parameters, particle materials as well as the particle polydispersity [Domingos et al., 2009; Gallego-Urrea et al., 2011; Ling et al., 2011]. To ensure consistency and improve the statistical significance of the measurements, we performed 10 repeated measurements (each for 60 min) for each concentration sample, with constant parameter settings.

AWM and EDM water characterization

All the water samples were collected from the Physics Shop in the University of Minnesota, Twins Cities. From the AWM machine, samples were collected before the water enters the settling tank and after it passes the filter cartridges. From the traveling wire EDM machine (Mitsubishi FX10) , water samples upstream and downstream of the filter in the re-circulating system were also collected when it was being operated to cut a piece of aluminum metal. All the samples were collected during normal operation of the

equipments. Nanoparticles present in the collected samples were characterized by the NTA technique and Scanning Electron Microscopy (SEM) analysis. The NTA technique was used to measure the size distribution and concentration of the nanoparticles. Since NTA measurements are conducted in the liquid phase, it is considered to cause minimum perturbation to the water samples. The water sample collected before the AWM settling tank contained abrasive particles in size of more than 10 μm. These particles are likely to interfere with the nanoparticle measurements due to the high intensity of the scattered light. Since the focus of this study is on nanoparticle characterization, the AWM samples were allow to settle for 30 minutes to exclude the coarse abrasive particles before subsequent analyses.

Scanning Electron Microscopy (SEM) and Electron Dispersive Spectroscopy (EDS) analyses were also performed to complement the NTA measurements. SEM and EDS measure the two-dimensional size/ shape and the elemental composition of the nanoparticles, respectively. The model used in this study is JOEL 6500. To prepare specimens for analysis, an appropriate volume of each AWM /EDM sample was passed through 50nm-rated nuclepore filters. The nanoparticles present in the samples were collected onto the surface of the nuclepore filters. A section of the filter, approximately 5mm by 5mm, was obtained for the SEM and EDS analyses.

2.3 Results and discussions

NTA calibration

Our group has experience in measuring size distribution of standard particles using NTA. It has been shown that NTA can accurately measure size distributions of standard-size reference nanoparticles [Filipe et al., 2010]. Therefore, the focus of calibration will be on concentration measurement. The response of the NTA towards different particle concentrations and different camera gain values is shown in Figure 2-1, which shows plots of the NTA measured concentration against the number concentration estimated by mass concentration. Several features are noted. Firstly, the lower limit of the measurable

particle concentration is about 10^8 particles/cm^3, which is determined based on whether a significant number of particles can be observed from the video. Secondly, a higher camera gain gives a higher estimated particle concentration, because more scattered light blobs from the particles can be visualized. It also suggests that the NTA software does not have corrections on particle concentration measurements for different measurement parameters used. When the software parameters were adjusted to maximize nanoparticle visualization (Gain = 680), the plot yielded a proportional correlation with slope close to unity (1.07). Using gold nanoparticles, Gallego-Urrea et al. [2010] also reported there is maximum discrepancy of a factor of 2.6 between the NTA measurements and the expected real concentration. The instrument is calibrated by the manufacturer using PSL particles with a nominal size of 100 nm. Visualization of the nanoparticles illuminated by the laser beam, from which particle concentration is determined by the software, will depend on the size and materials of the particles being measured. Therefore, the concentration measurement by NTA can be regarded as a quick estimate with accuracy with a factor of about 2.

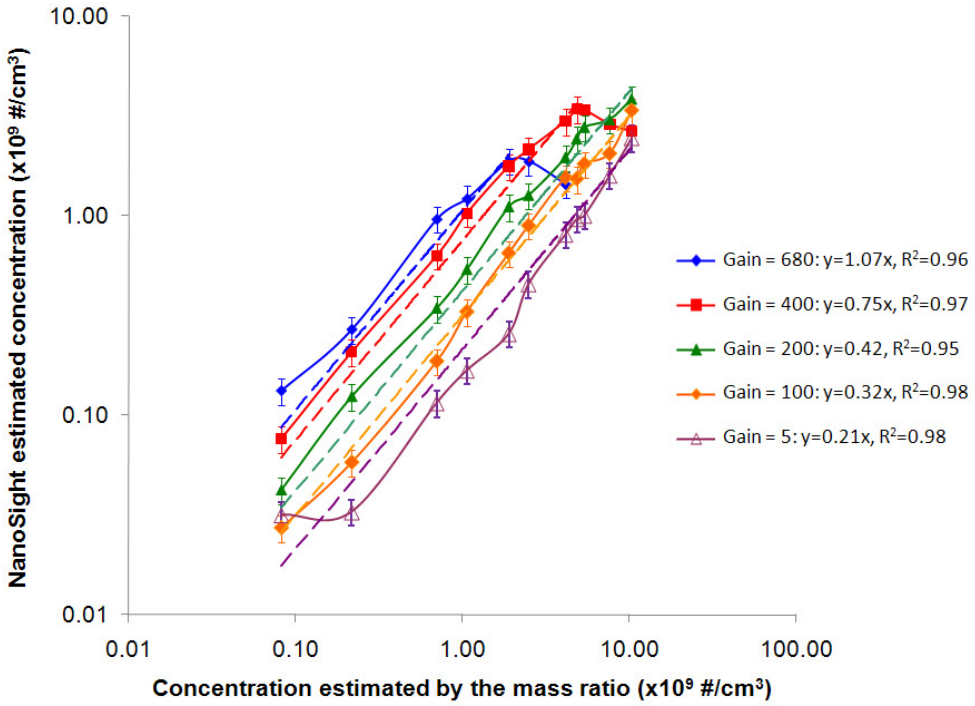

Figure 2-1. Calibration results of Nanoparticle Tracking Analysis technique. Legend shows the camera gain values used in the measurements and the equations of the linear fittings of the data points.

In general, the particle concentration estimated from the instrument varies linearly with the actual concentration. Therefore, by applying a specific correction factor, which is the slope of each linear fit, for each camera gain, the actual concentration (equivalent to PSL particles) can be obtained. It should be noted that the correction factors shown in Figure 2-1 are specific to 150 nm PSL particles in water and will be different for particles of different sizes and materials. At high concentration and high camera gain, the linearity is lost. The dynamic range depends on the camera gain chosen. Therefore, it is very important to ensure the particle concentration measurements are made within the linear concentration range. It is recommended that a single sample should be diluted with particle-free solvent with a known ratio and the NTA concentration measurements for the original and diluted samples should agree with the dilution factor. For the filtration experiments in which upstream and downstream particle concentration can differ by more

than 100 times, proper dilution of the particle samples will be needed before sending them for NTA measurement.

AWM and EDM sample analysis by NTA

Figure 2-2a and 2-2b show the size distributions of particles found from AWM and EDM samples, respectively. The data are represented with a bin width of 50 nm. Error bars represent the standard deviations among 10 repeated measurements. Each plot shows the size distributions of water before and after filtration treatment. In general, the water samples show a pronounced peak maxima at 100–200 nm. Particles larger than 200 nm usually dominate in mass concentration, instead of number concentration. It should be noted that the intensity of light scattered by a particle is proportional to the sixth power of the particle diameter. Therefore, the NTA measurement has reduced sensitivity for particles smaller than ~50 nm [Gallego-Urrea et al., 2010]. The decrease in concentration on the lower end of the size distribution can be either due to the actual size distribution or reduced measurement sensitivity. There is appreciable variability in the size distributions among repeated measurements. This could be due to the low particle concentration in the samples, relative to the recommended concentration range optimum to the measurements (10^8 particles/ml). The long video time and repeated measurements are expected to improve the statistics.

a)

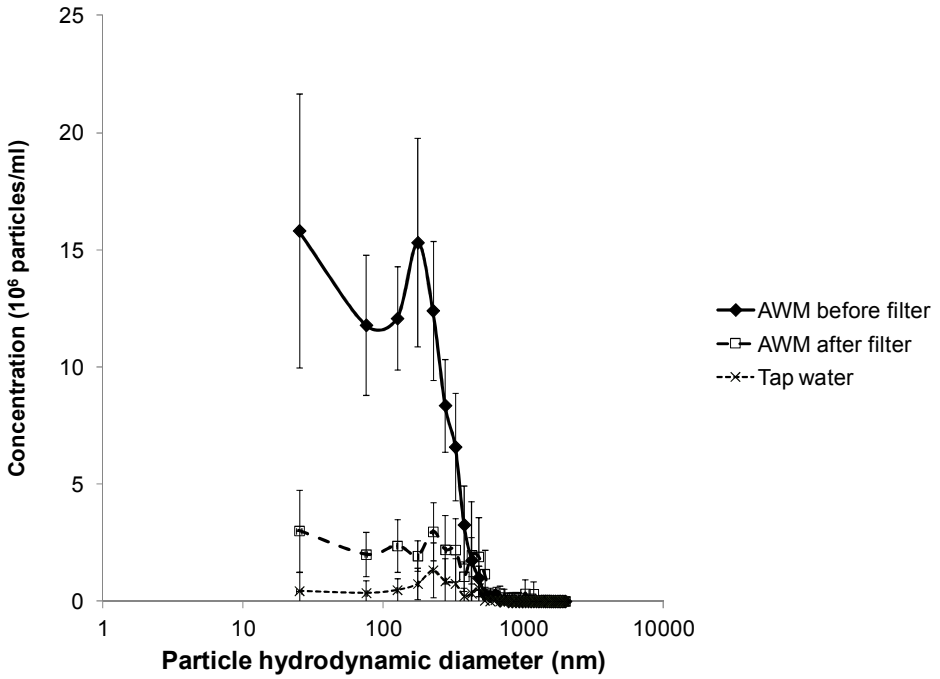

b)

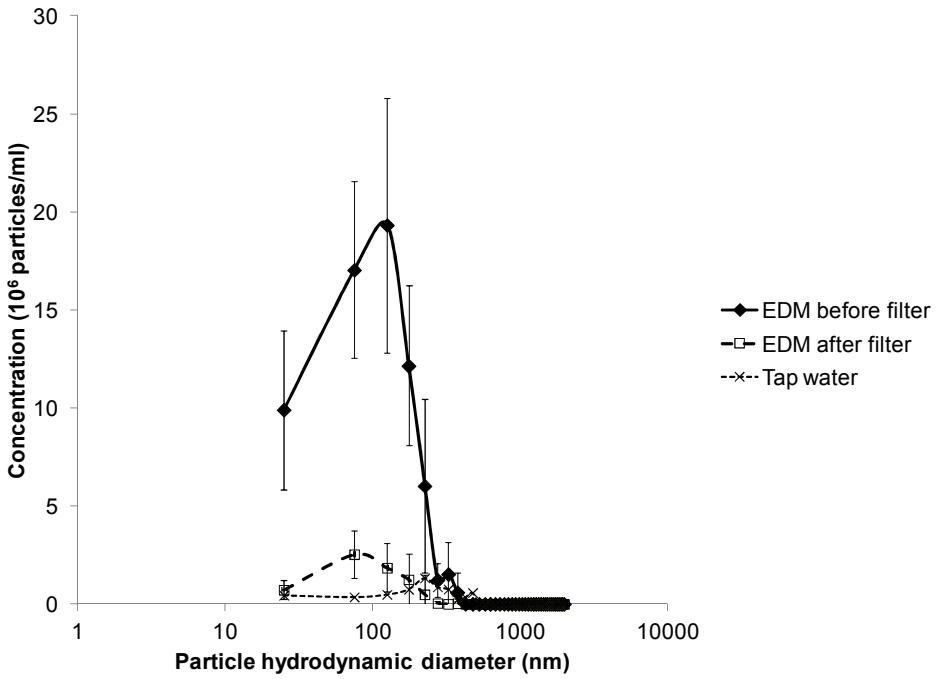

Figure 2-2. Size distributions of particles found from samples of a) AWM and b) EDM, measured by the NTA technique.

Also included on Figure 2-2, for comparison, is the size distribution of particles found in typical tap water, which was obtained from our lab. The total particle number concentration is 3×10^7 particles/ml. Kaegi et al. [2008] reported the concentration of nanoparticles found in drinking water to be of the order of 10^8 particles/ml based on Laser Induced Breakdown Detection (LIBD) measurement. This discrepancy is caused by the different cut-off size of the two methods. While the LIBD includes particles down to 10 nm, results from the NTA are restricted to particles > 50 nm. The size distribution of particles usually fall onto a straight line when represented as particle concentration against size on a log-log scale, i.e., an exponential relation [Kaegi et al., 2008]. The flattening of the lower end of the size distribution of particles found in tap water measured by NTA indicates the drop of counting efficiency of smaller particles. According to Figure 2-2, the filtration systems in AWM and EDM processes can significantly reduce the nanoparticles present in the water used. The overall filtration efficiency is estimated to be about 70% an 90%, for the AWM and EDM systems, respectively. However, in the sample collected from the downstream of the AWM filtration system, which is ready to be discharged to sewer, the total nanoparticle concentration (= 1.3×10^8 particles/ml) is still about four times higher than that found in tap water.

AWM and EDM sample analysis by SEM

SEM-EDS analyses on the nanoparticles collected on the nuclepore filters revealed their size, shape and elemental identity. Figure 2-3 shows the SEM images of the AWM samples. From Figure 2-3a, both micron-sized and nano-sized particles are generated and remained in the water during the operation of AWM process. Comparing the samples before and after the AWM filtration system, as shown on Figure 2-3a and 2-3b, respectively, it can be seen that particles with size larger than a micron are removed by the AWM filtration system, but an appreciable amount particles in an order of 100 nm remained. The nanoparticles generated from the AWM process are not spherical. Instead, they are irregularly shaped and agglomerated.

Figure 2-4 shows the representative zoomed-in SEM images and the corresponding EDS spectra of particles found from AWM samples. Micron-sized particles present in the water before entering the filtration system, which are likely from the abrasive particles, are multi-component. EDS spectra indicat the presence of silica, alumina, magnesium and iron (Figure 2-4a). Nanoparticles found in the water after the filtration system indicated the presence of similar composition, but each component is present singly. Silica and Alumina are likely to come from the mechanical wear of the abrasive particles. Iron particles are likely from the materials that have been cut with the AWM equipment. We believe the carbon and platinum peaks can be attributed to the surrounding materials from the nuclepore filter, carbon tape used for SEM sample preparation and coating material to make the samples conductive.

a)

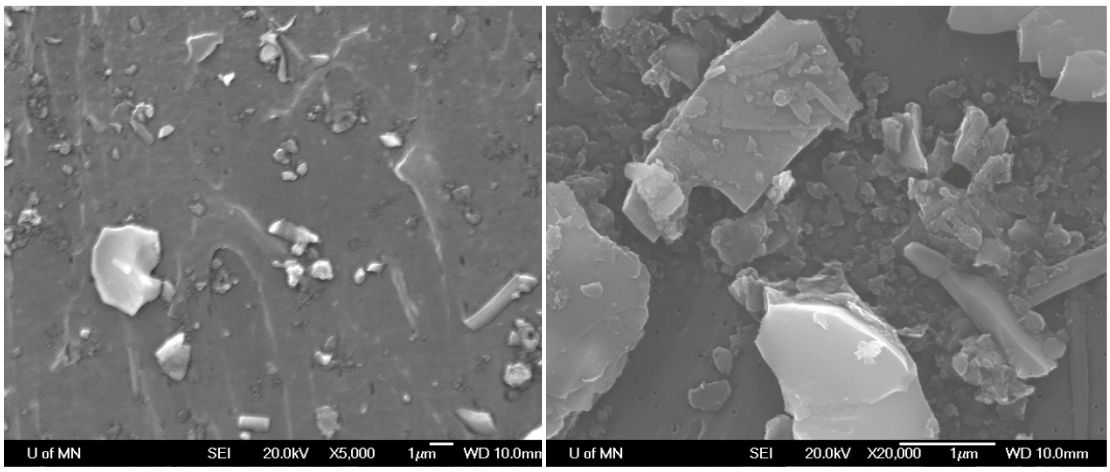

b)

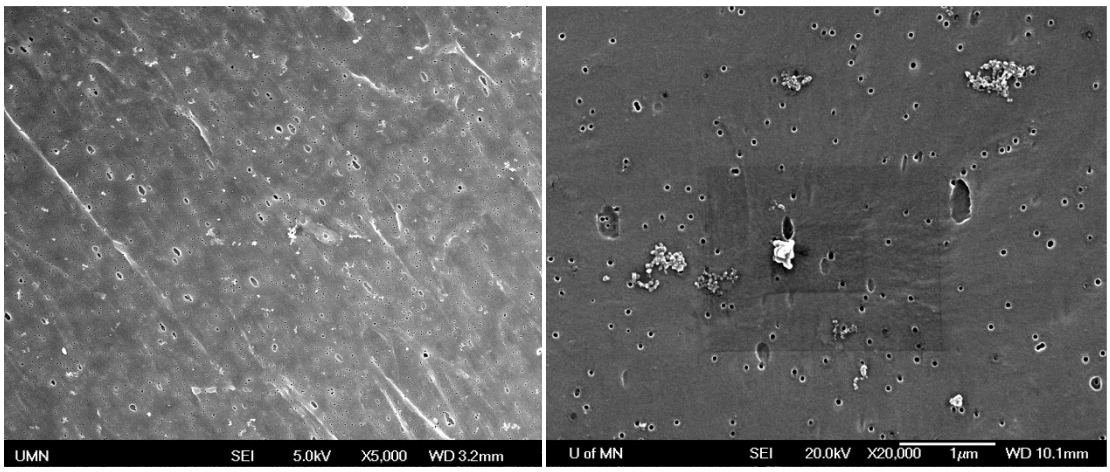

Figure 2-3. SEM images of particles found from AWM samples a) before and b) after filtration system. For both samples, same volume was passed through the Nuclepore filter, but the sample before filtration system was 10 times diluted with HPLC grade water.

a)

b)

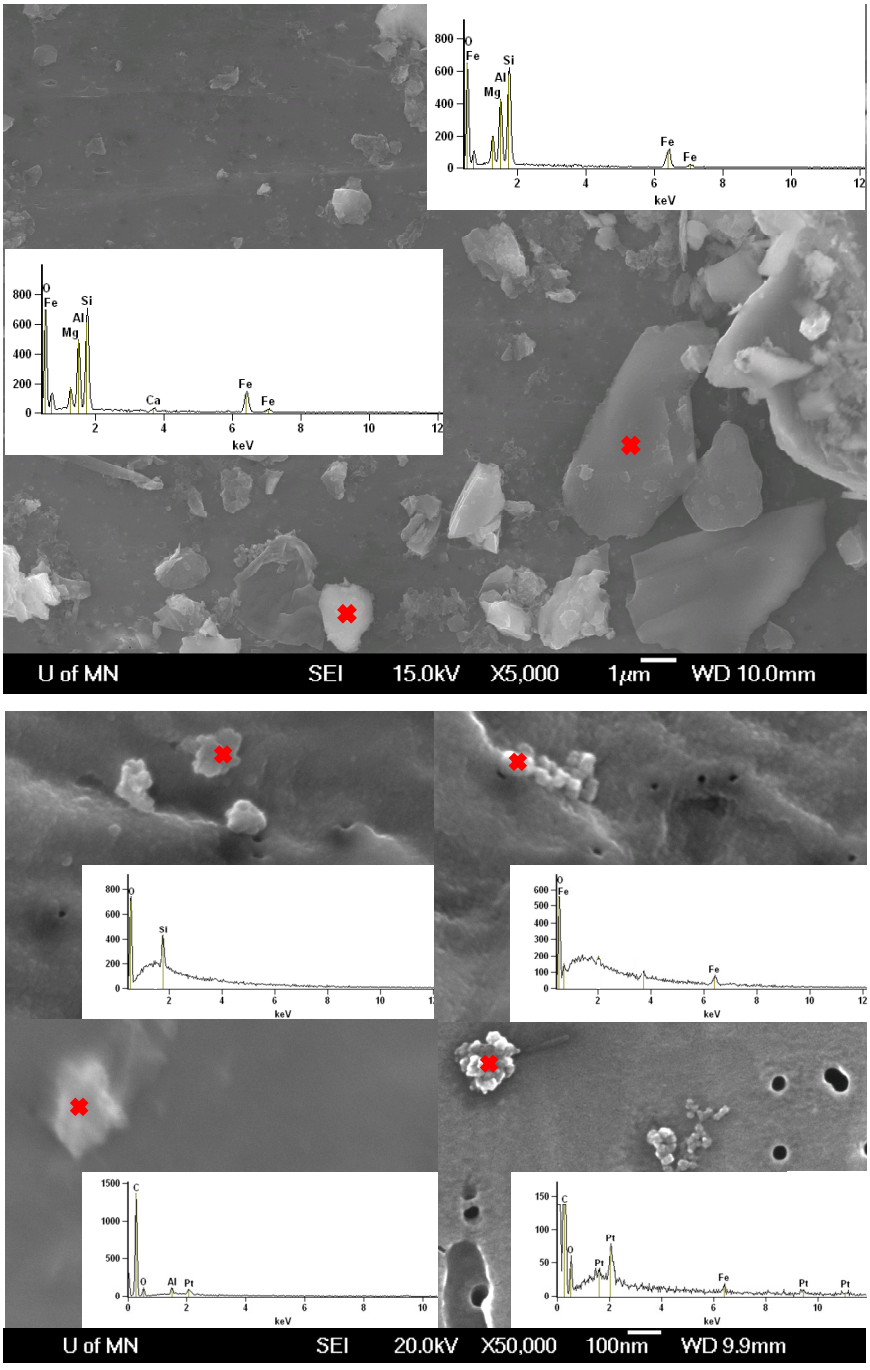

Figure 2-4. SEM images, with higher magnification, of particles found from AWM samples a) before and b) after filtration system. Insert: Representative EDS analysis of the particles marked with a cross.

SEM images of particles found from EDM are shown in Figure 2-5. Micron- and nano-sized particles are present in the water before the re-circulation filter (Figure 2-5a). Downstream of the filter, there are still some particles less than 0.5 micron observed (Figure 2-5b). Comparison of Figures 2-5a and 2-5b shows that the majority of particles are removed, in agreement with the NTA measurements. EDS analyses on selected particles indicated the presence of alumina particles (Figure 2-6). This is because the samples were collected when the EDM was operated to cut a piece of aluminum. In a TEM-EDS analysis of particles found in drinking water, it was found that particles of a few tens of nm in diameter consist of organic materials (high-molecular weight humic substances and polysaccharides) and particles larger than 1 μm are mainly mineral products (clay), iron oxides, silica and calcium carbonate [Kaegi et al., 2008]. Therefore, nano-sized iron, alumina and silica found in SEM-EDS analyses in this study are likely generated by the AWM and EDM processes.

a)

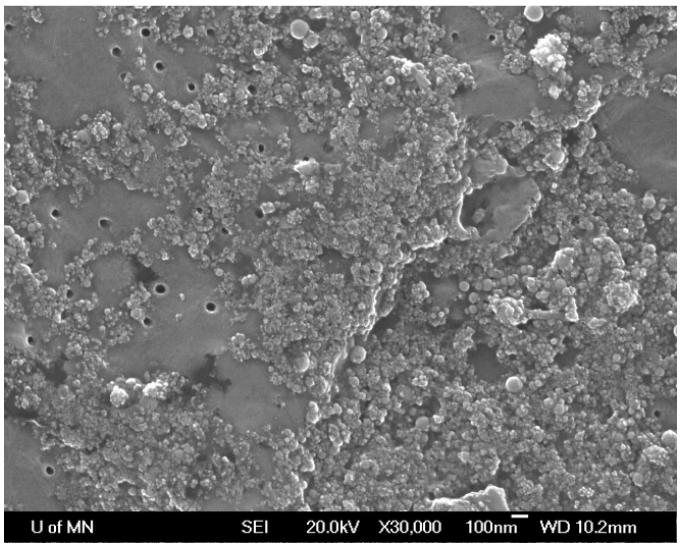

b)

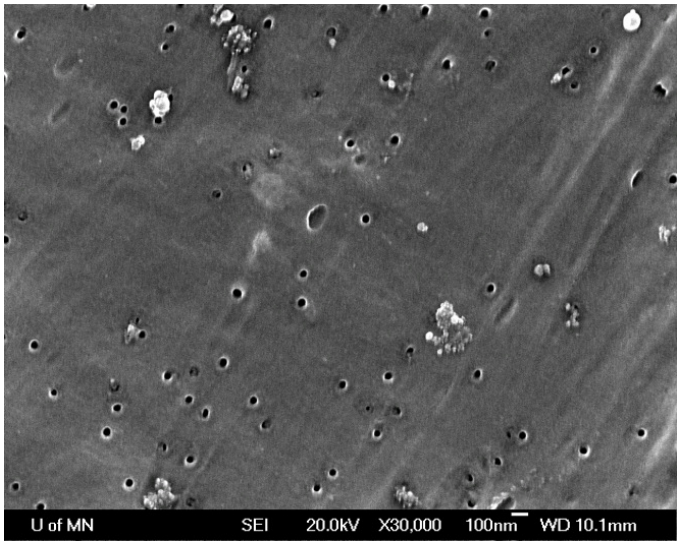

Figure 2-5. SEM images of particles found from EDM samples a) before and b) after filtration system. For both samples, same volume was passed through the Nuclepore filter.

a)

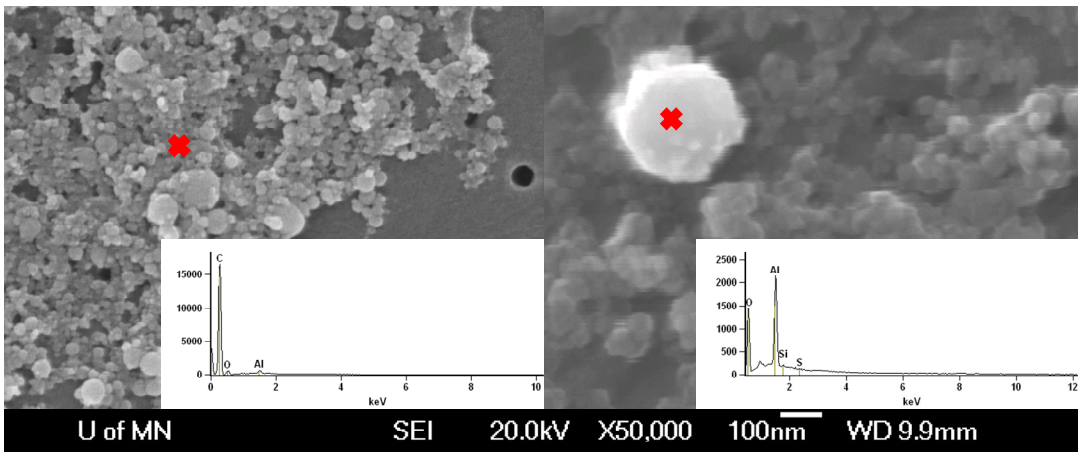

b)

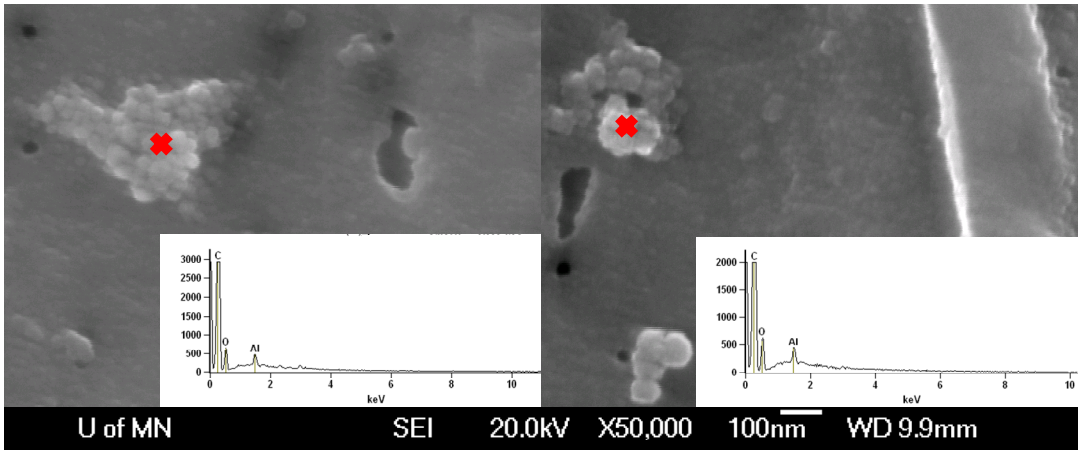

Figure 2-6. SEM images, with higher magnification, of particles found from EDM samples a) before and b) after filtration system. Insert: Representative EDS analysis of the particles marked with a cross.

Filtration of liquid-borne particles was found to begin with a sieving dominant regime followed by a transition regime and a cake filtration regime as particles accumulate inside the filter pores and on the filter surface. The filtration efficiency decreases rapidly and then more gradually during the sieving dominant regime and transition regime, respectively. With an appreciable amount of particle loading, the filtration efficiency increases with particle loading. The initial decrease in efficiency with loading is caused by some of the smaller pores in the filter becoming plugged by the particles, thus forcing

more fluid through the larger pores. As a cake is built up on the upstream face of filter surface, it provides additional filtration which partially compensates for the drop in filter efficiency caused by the plugging of the small pores. Eventually, the surface cake layer builds up to a level such that efficiency increases [Lee and Liu, 1994]. Therefore, filtration efficiency changes as particles load onto the filter. Filters in these systems are usually replaced when the pressure drop is higher than a certain value. We do not have the information of the extent of usage of the filtration systems used in the AWM and EDM equipments, but the filter pressure drop is below the value when the filter should be replaced. The filtration efficiency reported in this study can only give an estimate on the general performance of the filters against the particles generated during the AWM and EDM processes.

AWM and EDM have extensive applications in fabricating industry [Momber et al., 1998; Hashish and Hilleke, 1999]. In addition, research has been undergoing to improve the understanding and performance of these processes [Wang et al., 2003; Ho and Newman, 2003; Pandey and Singh, 2010] . It is expected that their usage will continue to increase and the nanoparticles generated should not be neglected. The used filter systems in AWM and EDM are loaded with high concentration of nanoparticles. It is worthwhile to have some considerations on the disposal of the filters. Firstly, extra cautions are needed when operators replace or handle the used filters to avoid human exposure to nanoparticles. In addition, if the filters are treated as conventional municipal waste, they will be sent to landfill or incineration. There is a lack of understanding about the behavior of nanoparticles during waste incineration. The corresponding fractions that stays in the slag and becomes airborne are not known [Mueller and Nowack, 2008]. AWM and EDM are applicable to many different materials, including ceramics [Gudimetla et al., 2002] and composite materials [Wang, 1999]. The effects of a mixture of nanoparticles with different materials is not well known.

Using a model analysis, Benn and Westerhoff [2008] predicted that typical wastewater treatment facilities are effective to remove silver nanoparticles which are three orders of

magnitude higher than the commonly observed concentration, such that the effluents would not exceed the USEPA water quality criteria for salt water and fresh water. Assuming similar removal efficiency for other types of nanoparticles, it is expected that the addition of unintentionally produced nanoparticles from AWM and EDM will not exceed the load that wastewater treatment plants are capable of handling. The fate of the nanoparticles collected in the wastewater treatment facilities will deserve further investigation. Life-cycle model can be used to quantify release of engineered nanoparticles released into the environment. The worldwide production volume of engineered nanoparticles is one of the required inputs to the model. It was predicted that CNT and nano-Ag pose little risk but nano-TiO_2 in water may pose a risk to aquatic life [Mueller and Nowack, 2008]. However, it is likely that unintentional nanoparticle generation and those emitted from production sites were not considered. Therefore, effort will be needed to find out the potential sources of unintentionally generated nanoparticles and study the properties of these nanoparticles and quantify their occurrence.

2.4 Summary

The NTA in our lab has been calibrated with monodisperse 150 nm PSL particles. With software parameters properly adjusted to maximize nanoparticle visualization, NTA concentration measurements agree well with the number concentration estimated by suspension mass concentration. A proportional correlation is yielded with slope close to unity. To ensure the particle concentration measurements are made within the linear concentration range, a single sample should be diluted and the NTA concentration measurements for the original and diluted samples should agree. When using NTA to analyze particle samples from filtration experiments, which may have significant concentration difference, proper dilution of the samples is needed. Using the NTA and microscopy techniques, we observed that nanoparticles, with peak size between 100 and 200 nm are present in water samples collected from AWM and EDM processes. The filtration systems in AWM and EDM processes can reduce the number of nanoparticles by about 70 and 90 %, respectively. SEM analysis suggested that these nanoparticles are

mostly non-spherical and agglomerated. Elemental analysis by EDS indicated that they come from the debris of the cut materials. Since AWM and EDM are widely used, the handling and disposal of used filters collected with nanoparticles, release of nanoparticles to the sewer systems and potential use of higher performance filters for these processes will need to be considered.

Chapter 3

Measurement of retention efficiency of filters against nanoparticles in liquids using an aerosolization technique

3.1 Introduction

Liquid filtration has been an effective technique to separate suspended particles from a liquid by passing it through a porous membrane or medium [Grant and Liu, 1991; Lee et al., 1993; Brown and Jenner 1995; Madaeni and Fane 1996]. Liquid filtration technique is widely used in chemical engineering, semiconductor, pharmaceutical, food and beverage industries [Oganesyan et al., 2001] It also plays a significant role in control and prevention of water related pollution, for example, mitigation of the risks of engineered nanoparticle release into aqueous/ aquatic environments. Increasing concerns of limited water resources have generated growing interests in wastewater treatment. A large body of literature has been devoted to liquid filtration in water and wastewater treatment [Ghayeni et al., 1999; Chang et al., 2002; Rosenberger et al., 2006].

Quality of the filter media is important for filtration performance. Liquid filters are often characterized by means of 1) the geometrical pore size obtained from electron microscopy, 2) the gas permeability, 3) the bubble point and liquid displacement [ISO 2942:2004; Zhao et al., 2000]. But these representations often do not correlate well with sieving characteristics of liquid filters, and may not agree accurately with the retention efficiency [Nakao, 1994; Waterhouse and Hall, 1995; Singh eta l998]. The bubble point test responds to a small fraction of pores that are much larger than those in the remaining fraction, and the sample preparation for electron microscopy may affect the interpretation of the pore size [Duke, 2003]. Therefore, the most direct way to evaluate the performance of a filter is to obtain its retention efficiency experimentally.

Challenge particles for filter testing include microorganisms and bacteria as well as other solid particles: silica, gold and polystyrene latex particles [Lee and Liu, 1994]. Removal

of bacteria and other microorganisms in wastewater treatment and sterilization water has been extensively investigated [Ghayeni et al., 1999; Elsaied et al., 2001; Wang et al., 2007; Wang et al., 2008]. Testing by organisms is mainly for characterizing sterilizing efficiency of a membrane [Waterhouse and Hall, 1995]. However, it is difficult to characterize the true physical process involved because the size of the organisms is not verifiable during the testing. It is also time consuming to carry out the test [Lee and Liu, 1994]. Among the solid particles, polystyrene latex, silica and gold particles are generally used.

Quantifying liquid-borne particle concentration can be done using laser-based liquid particle counters. Lee et al. [1989] studied the sizing accuracy of several commercial particle counters using spherical polymer particles and non-spherical polydisperse alumina particles. Retention efficiency of PSL particles and irregular shaped, real world particles by microporous membranes has also been measured using an automated filter test system coupled with a laser particle counter to measure the upstream and downstream particle concentrations [Lee et al., 1994b]. The particle size in the above mentioned studies was generally in the range of 0.1 to 1 μm. The laser particle counters offer marginal performance for particles less than 100 nm in PSL equivalent size, because small particles scatter only little light. Other limitations include the variation in counting efficiency in response to variation in refractive index contrast between particles and fluid, and interference from bubble formation [Knotter et al., 2007]. Liquid-borne particle detection and filtration evaluation can also be done using magnetically susceptible materials and a suitable sensor [Rajagopalan et al., 2008], fluorescent particles and a spectrophotometer [Duke, 2003]. These methods are limited to particles with specialized properties, despite their capability to distinguish particles as small as 0.01 μm.

The particle number concentration in liquids generally increases with decreasing particle size [Lee and Liu, 1994; Lee and Liu, 1994c]. Besides, the quantity of engineered nanomaterials is expected to grow significantly in the next eight to ten years [Roco, 2006]. With the large-scale development and use of nanotechnology, the amount of man-

made nanoparticles in environmental matrices (air, soil, water) will increase the likelihood of uptake by living systems [Biswas and Wu, 2005; Wiesner et al., 2006]. Liquid filtration plays a significant role in the prevention of nanoparticle release into the aqueous environments. There is a definite need for faster and more effective testing methods for nanoparticle retention efficiency.

Air-borne nanoparticle classification and detection has been well developed. With a Differential Mobility Analyzer (DMA) and Ultrafine Condensation Particle Counter (UCPC), air-borne particles in the size range of 3-700 nm can be classified and detected by varying the ratio of the aerosol flow and sheath flow of the DMA. Aerosolizing the liquid-borne particles by an atomizer for classification and detection is therefore a possible means to enhance the sensitivity of the liquid-borne particle characterization. Therefore, researchers have been exploring aerosol techniques for counting and sizing liquid-borne nanoparticles. The challenge for this method is to preserve the original size distribution as in the liquid-borne phase. It needs to produce single particles which are agglomeration-free and avoids the influence from the impurities (soluble or insoluble) present in the liquid phase. The nonvolatile surfactant, sometimes necessary to stabilize the nanoparticles in liquid-borne phase, is also considered as part of the impurities. After evaporation of the volatile solvent, the nonvolatile impurities can either form smaller residue particles, which interfere with the particles of interest on the size distribution plot, or coat onto the particles of interest, increasing the size and changing the chemical nature of them.

To overcome these problems, Lenggoro et al. [2002] applied electrospray operating in the cone-jet mode, instead of an atomizer, to disperse liquid-borne nanoparticles into air-borne phase. Since the electrospray is capable of generating finer droplets compared to conventional atomizers, one can ensure that only one particle is contained in a droplet, avoiding particle aggregation. The small droplets also minimize the effects of nonvolatile impurities after solvent evaporation. Lenggoro et al. [2007] further demonstrated that a tubular furnace can evaporate residue particles and coatings on the nanoparticles of

interest, leading to size measurement with better accuracy. Park et al. [2012] also suggested that the effect of impurities can be suppressed by reverse osmosis process under high pressure. The nanoparticle nebulizer developed by TSI Inc. can generate droplets smaller than conventional atomizers. The aerosolization method has been applied to monitoring water quality and primary marine aerosol formation in seawater [Park et al., 2011].

Taking the advantage of the sensitivity of airborne nanoparticle detection, we aim to 1) explore the possibility of determining the size distribution and the (relative) concentration of particles present in liquid suspensions by an aerosolization method, 2) apply the aerosol techniques to determine the retention efficiency of nuclepore filters (a model filter with well-defined pore size) as a function of particle size, and 3) compare the particle measurement performance to the Nanoparticle Tracking Analysis (NTA) technique.

3.2 Experiments

PSL particle suspension preparation

Particles used in this study include PSL particles with various sizes (Duke Scientific Corporation) and gold nanoparticles (Ted Pella Inc.). The original suspensions from the suppliers were diluted with deionized (DI) water, to the concentration needed. The DI water was assumed to be particle-free. Particle concentration is in the range of 10^7-10^9 particles/ml, determined by a liquid particle counter (CLS-1000, PMS). To ensure the suspensions were well dispersed and agglomerate-free, they were sonicated before being used to challenge the filters or aerosolizing.

PSL particle dispersion

Figure 3-1 shows the schematic diagram of the experimental set-up, consisting of the dispersion and measurement parts. Diluted PSL suspensions were dispersed by the

Constant Output Atomizer, COA (Model 3075, TSI Inc.) or an Electrospray Aerosol Generator, ES (Model 3480, TSI Inc.) depending on the size of the latex particles used. Residue particles contributed from the water impurities and surfactant used to stabilize the suspensions may interfere with the latex particles in their airborne size distributions. COA, which generates larger droplets, gave larger residue particles at ~30nm, while ES generates smaller droplets, and gave residue at ~10nm. The COA was operated in the recirculation mode, and the pressure was maintained at 20 psig (gage pressure). In operating the ES, the applied voltage, sheath air flowrate and pressure in the chamber were maintained at 2 kV, 2 lpm and 4 psig, respectively.

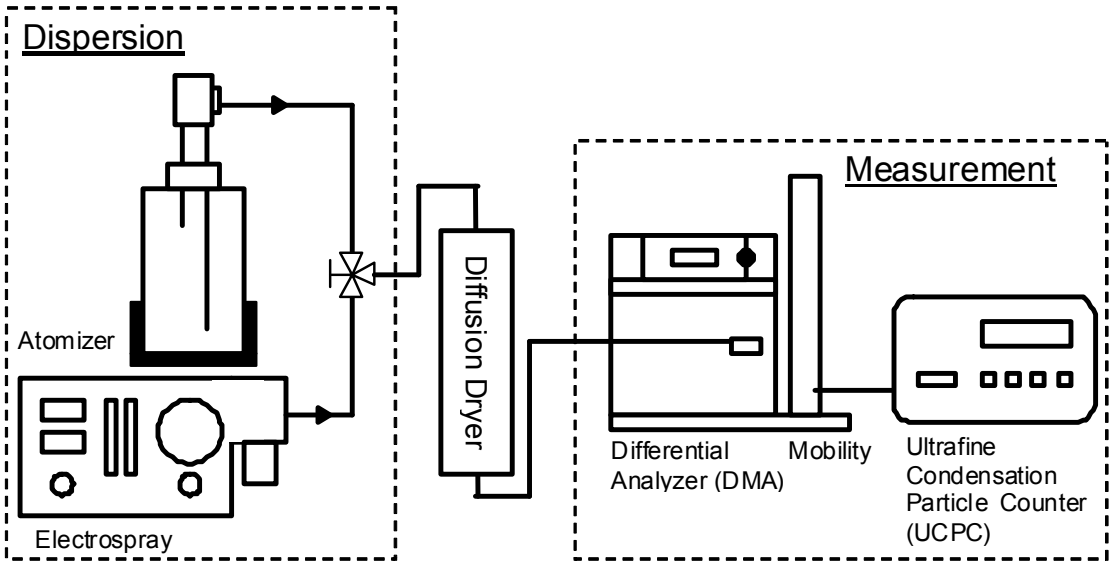

Figure 3-1. Experimental setup for dispersing liquid-borne PSL particles and counting airborne particles.

Airborne particle concentration measurement

Airborne particles were measured by the setup shown in Figure 3-1, consisting of a Differential Mobility Analyzer, DMA (Model 3081, TSI Inc.) or a Nano Differential Mobility Analyzer, Nano-DMA (Model 3085, TSI Inc.) and an Ultrafine Condensation Particle Counter, UCPC (Model 3025, TSI Inc.). Size distributions of the particles generated from the aerosol dispersion system were first measured, using the voltage-scanning mode, to ensure residue particles do not interfere with the PSL particles to be analyzed. The voltage applied to the DMA was then fixed to classify the latex particles of the desired size, and its airborne concentration was measured with the CPC. The CPC recorded the particle concentration every second, for one minute with the COA and five minutes with ES to ensure the aerosolization process was stable. Fluctuations of the concentrations measured were within 10% of the averaged values.

Liquid-borne and airborne concentration correlation

The objective is to explore the possibility of determining the size distribution and the (relative) concentration of particles present in suspensions by the aerosolization method. To infer the liquid-borne particle concentration from the airborne concentration after dispersion, the relationship between the two concentrations were found by calibration. PSL suspensions were diluted with DI water with known ratio, and the air-borne concentration as a function of dilution ratio was recorded accordingly. The range of concentration calibrated was kept relevant to the filter retention tests.

Retention of nuclepore filter determination

Experimental setup for filter evaluation is shown in Figure 3-2. A peristaltic pump drew the PSL suspensions to pass through a 47 mm filter holder, where the test filter was placed. Nuclepore polycarbonate track-etched membrane filters (Whatman) with pore sizes rated at 400 nm and 200 nm were tested. The peristaltic pump maintained a constant liquid flowrate at 50 cm^3/min through the filter. The pressure gauge upstream of the filter

holder was used to monitor the pressure build up during filtration testing. The liquids downstream were collected for about 3 min for enough volume for dispersion. Therefore, the time-averaged retention efficiency was measured.

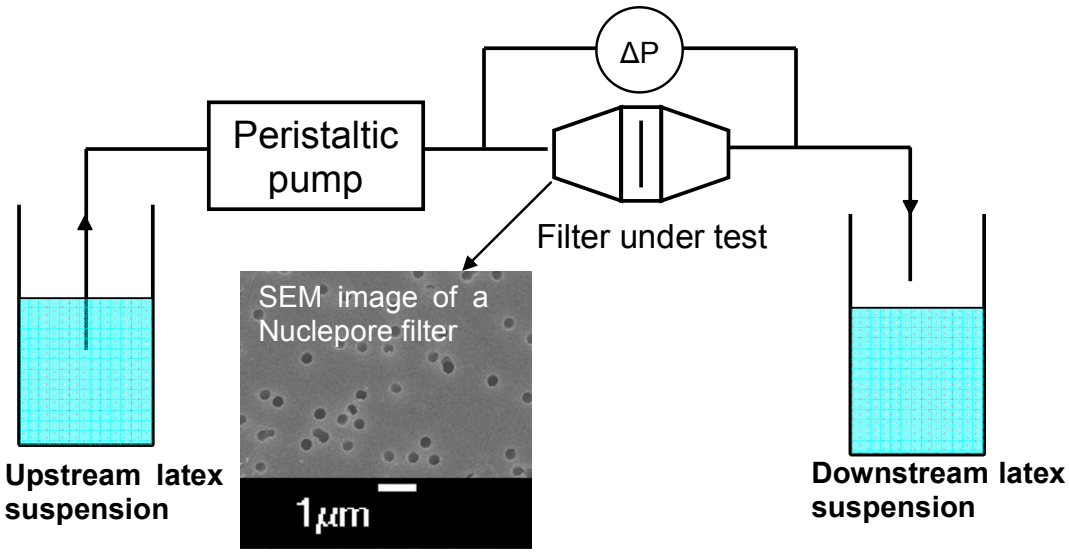

Figure 3-2. Experimental setup for filter evaluation. Insert is a SEM image of a typical Nuclepore filter showing the uniform pore size.

Comparison with the NTA technique

Particle dispersion was performed by a nanoparticle nebulizer (TSI Inc.), which is designed for dispersing droplets smaller than the conventional atomizers or nebulizers. It is suitable for the purpose of characterizing nanoparticles by the aerosolization method, in replacement of the electrospray aerosol generator. Since PSL particles below 50 nm have a relatively broad size distribution (standard deviation 3.2 nm for 150 nm PSL particles vs >7 nm for 30 nm PSL particles), gold nanoparticles, which have a narrower size distribution, were used to compare the resolution of both techniques: aerosolization and NTA. The suspensions include monodisperse 80, 50 and 30 nm gold particles and a mixture of them with equal number concentration. The concentration limit for the two

methods should be noted. SMPS gives results with good statistics with particle concentration > 10^9 particles/ml, while the NTA has a concentration window between 10^7 and 10^9 particles/ml. Therefore, proper dilution was needed.

3.3 Results and discussions

Particle generation with COA and ES

Figure 3-3 shows the typical size distributions obtained from a) the COA for 125 nm latex particles and b) the ES for 30 nm latex particles. Droplets produced which contain no latex particles dry to form residue particles consisting of the impurities and stabilizing surfactant in the liquid. These aerosols are undesirable since their concentration is considerably higher than the monodisperse PSL particles themselves. Under the operating conditions, residue particles generated by a COA spanned up to about 70nm. Residue particles overlapping with or being too close to PSL particles should be avoided. Therefore, the COA cannot be used for aerosolizing challenged particles smaller than 70 nm. From Figure 3-3b, residue particles from the ES can be controlled to be smaller than 10 nm, allowing latex particles < 70 nm to be uniquely identified. However, compared to the COA, particle generation by ES involves more controlling parameters, including the conductivity and flowrate of the suspensions, and the applied voltage to the capillary. The liquid flowrate is also orders of magnitude lower than that of the COA, causing the ES to have a greater chance to disperse particles unstably. Therefore, it is desirable to use the COA to ensure stability of the particle generation whenever suitable.

a)

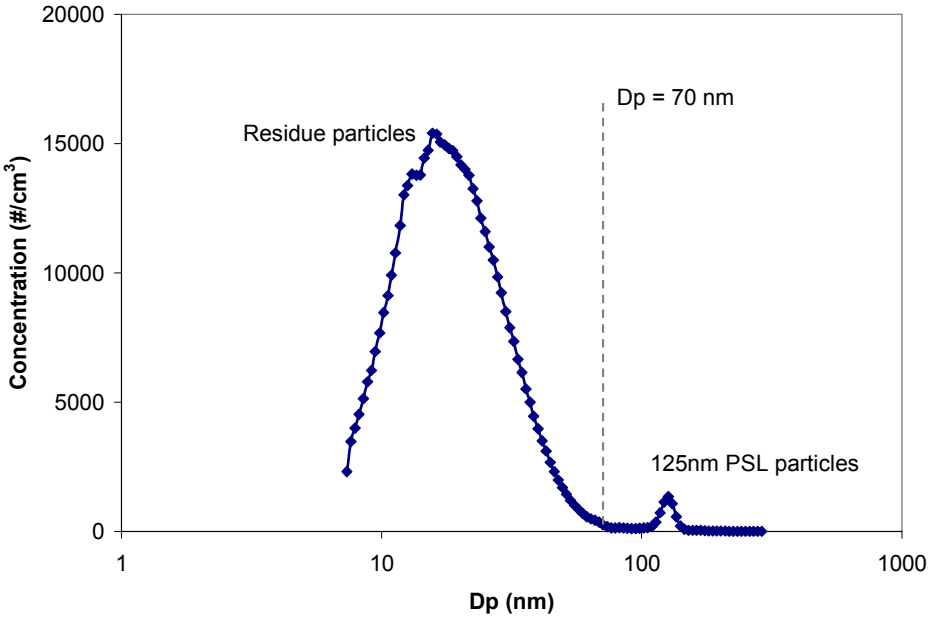

b)

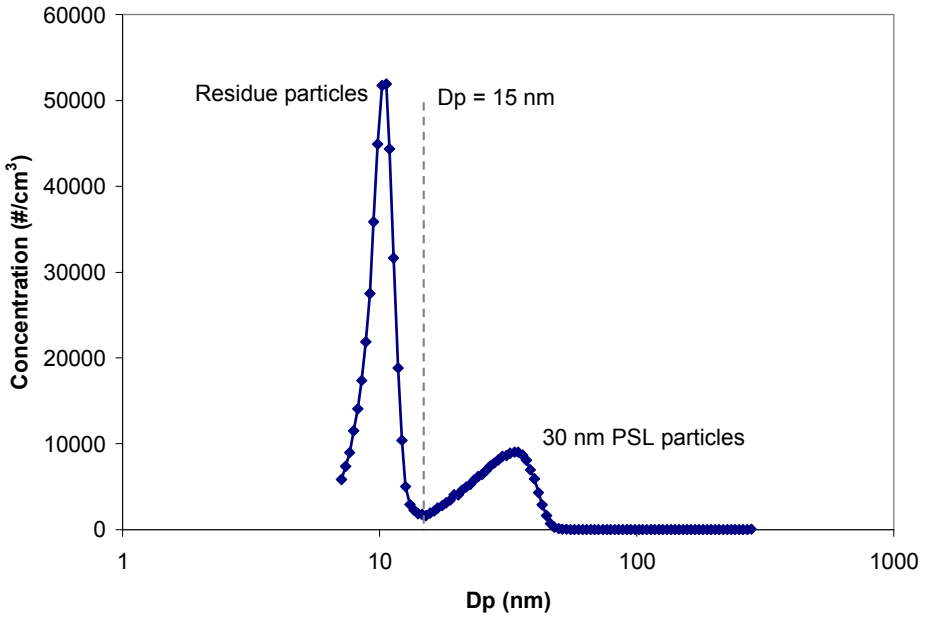

Figure 3-3. Typical size distributions obtained by (a) atomizing 125 nm PSL particles and (b) electrospraying 30 nm PSL particles.

Liquid-borne and airborne concentration correlation

Figure 3-4 shows the calibration results, demonstrating the linear relation of liquid-borne and air-borne particle concentrations. Linear fittings with the intercept forced to be zero were shown. The sum of error square (R^2), which indicates how well the data were fitted, are > 0.98 for all cases. The experimental data have also been fitted without forcing zero intercept. While the linear regression with a non-zero intercept fits the data points better, representation of the data points by a linear line intercepting at zero does not differ too much (R^2 < 1% difference). To simplify the calculation, in our experiments, a proportional relation between the airborne and liquid-borne concentration was assumed, i.e.,

Liquid-borne particle concentration = Constant x Air-borne particle count

Similar results have been obtained by Hogan et al. [2006] which showed that the total number concentration of electrosprayed virus particles is directly proportional to the virus titer in the electrospray suspension. Therefore, the retention efficiency can be represented as:

$$Efficiency = 1 - \frac{Downstream\ liquid-borne\ particle\ concentration}{Upstream\ liquid-borne\ particle\ concentration} \qquad \text{Equation 3-1}$$
$$1 - \frac{Downstream\ airborne\ particle\ counts}{Upstream\ airborne\ particle\ counts}$$

a)

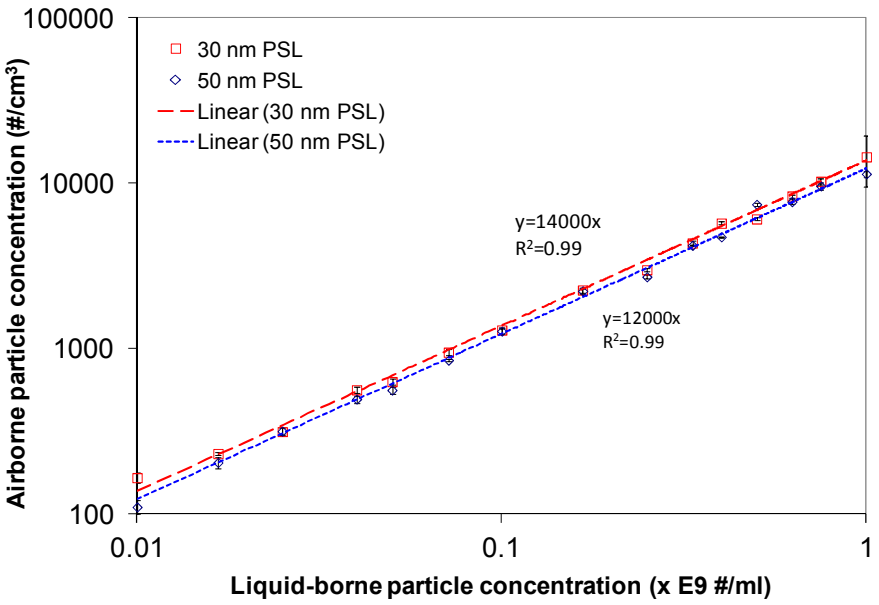

b)

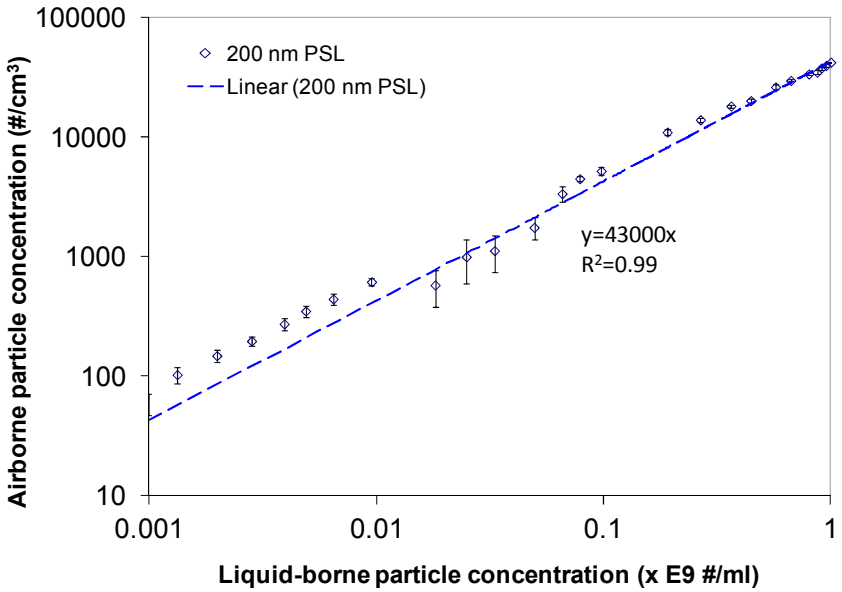

Figure 3-4. Relation of liquid-borne PSL particle concentration and airborne concentration after dispersion by (a) ES and (b) COA. Error bars represent the standard deviation over the measurements. Concentration ratio = 1 represents dilution of 1 drop of latex particle suspension (about 0.01-0.1 g) into 100 ml DI water.

Evaporation is one of the concerns of using an atomizer for quantitative analysis. It increases the concentration of the particles in the suspensions and affects the airborne particle concentration when dispersed. Another important precaution in using the atomizer is to maintain the temperature of the suspensions, on which the viscosity is dependent. Evaporation may occur on the droplets which then hit the impaction wall of the atomizer and return to the reservoir. Temperature and viscosity of the recirculated suspensions may change, affecting the atomization process and subsequently the number of airborne particles. A separate experiment was performed to confirm the stability of the particle output from the COA. The COA was run to generate PSL particles from a suspension for 20 minutes, and no monotonic change in airborne particle concentration was observed. In our experiments, the atomization of each sample took less than 15 minutes, and evaporation and temperature variation was believed to be insignificant. It should be noted that the atomizer can be configured such that droplets formed are not re-circulated to the reservoir to avoid the evaporation and temperature variation problems.

Another precaution of this method is to ensure that only individual particle will be aerosolized and no droplets contain more than one particle, which will become undesirable doublets upon evaporation. The maximum number concentration, *MNC*, of monodisperse particles in a liquid suspension to be atomized and the corresponding singlet ratio, *R*, is related as shown in Equation 3-2. *R* is defined as the ratio of droplets with but one monodisperse particle to all droplets that contain one or more monodisperse particle Raabe [1968].

$$MNC = \frac{6(1-R)e^{-4.5(\ln \sigma_g)^2}}{\pi (VMD)^3 \left[1 - 0.5e^{(\ln \sigma_g)^2}\right]} \qquad \text{Equation 3-2}$$

where:

VMD = atomizer droplet Volume Median Diameter (cm)

MNC = number of monodisperse particles of the suspension (particle/ml)

σ = geometric standard deviation of the droplet distribution from the atomizer

This determines the maximum particle concentration in the suspensions that can be used. The COA used in this study produced particles with VMD and σ equal to 1.03 μm and 1.5 (Manual, TSI Inc.). R is greater than 0.99 when particle concentration in the order of 10^7 particle/ml was used. On the other hand, droplets formed from ES are much smaller, about 150 nm in diameter (Manual, TSI Inc.), significantly reducing the formation of doublets.

The third precaution of this technique is to ensure low impurity concentration of the solvent, water in this work. Impurity of the solvent will impact the results of this technique in two ways: 1) Residue particles, which are non-volatile impurity formed from evaporation of the original droplets containing no PSL particles, affect the identification of the PSL particle peaks from the size distributions. 2) The non-volatile impurities form a layer on the PSL particles, which hinders determination of the correct particle size. In our current experiments, the non-volatile residue particles have peaks at 30nm and 10nm for COA and ES, corresponding to impurity levels of 0.0007 and 0.002 g/cm^3, respectively (assuming unity density for non-volatile impurity). Another precaution is to ensure complete evaporation of the solvent before the dispersed particles are being sized by the DMA. A diffusion dryer should be included between the dispersion and measurement units (Figure 3-1).

Retention of nuclepore filter determination

400nm and 200nm rated nuclepore polycarbonate filters were challenged with PSL particles of sizes ranging from 50 to 500 nm. Nuclepore filters are often considered as a convenient model of capillary porous body consisting of a bulk of uniform-sized, cylindrical-shaped pores and with simple surface configuration [Oganesyan et al., 2001]. PSL particle concentrations upstream and downstream of the filters were obtained with the aerosolization methods, and retention efficiency were computed using Equation 1. Retention efficiency as a function of particle size was plotted in Figure 3-5. For filter samples of the same pore size, experiments were repeated twice with latex particles of the

same size. The computed efficiencies from two independent experiments were generally comparable. Variation may be due to the inhomogeneity and variation of quality between each filter as well as handling procedures of the filtration experiments.

Particle capture in liquid filtration is usually described as sieving, depth filtration (adsorption) and cake filtration [Grant et al., 1988]. Sieving mechanism is solely determined by the ratio of the filter pore size to the particle size (diameter for spheres). Intuitively, particles are captured by sieving if they are larger than the pore openings of the filter. From Figure 3-5, particles larger than and equal to 200nm were mostly captured by the 200nm rated nuclepore filter, and almost all 500nm particles were captured by the 400nm rated filter. Dashed lines were included to guide the readers' eyes for reading the plot. The retention efficiency results in this work can be attributed mainly to the sieving mechanism. The non-zero efficiency for particles smaller than the rated pore sizes indicates that retention of particles by adsorption of diffused particles was also at play. It has been shown that the sieving mechanism dominates in the filtration of PSL particles with nuclepore filters. Experiments were carried out by Oganesyan et al. [2001] where the pore sizes were deliberately selected to be wider than the sizes of latex particles and no retention was detected.

The number concentration of the 100 nm PSL suspension used for challenging the filter was estimated, by a liquid particle counter, to be 10^7 -10^9 particle/cm^3. With the use of 150 cm^3 suspension, there were not enough particles to form a cake on a 47 mm filter. Under these operating conditions, pressure build-up was less than 15 psi, a value common to other tests with particles of other sizes, and filters of other pore sizes. Therefore, the cake filtration mechanism was not likely involved. To confirm that both dispersing techniques are complementary to each other, upstream and downstream samples from the challenge test of the 200nm rated Nuclepore filter with 100nm latex particles were dispersed by both the COA and ES for analysis. While the absolute air-borne particle concentrations given by the COA and ES were different, the two dispersion

techniques showed comparable retention efficiencies (10-12% and 14% with COA and ES, respectively).

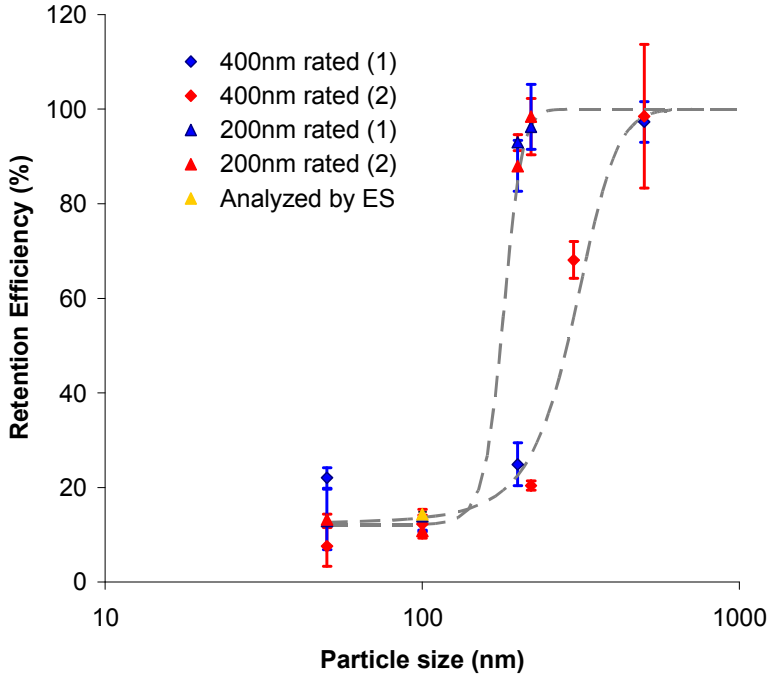

Figure 3-5. Retention efficiency of 200 nm and 400 nm rated Nuclepore filters. Each data point represents the average of two experiments. Curve fitting for the data with logistic functions yields: $y = 12 + 88 \times \frac{1}{1 + \exp[-0.08 \times (x - 180)]}$ and $y = 12 + 88 \times \frac{1}{1 + \exp[-0.02 \times (x - 300)]}$ for the 200nm and 400nm rated Nuclepore filters, respectively.

Comparison with the NTA technique

Figure 3-6a shows the size distribution of 30 nm gold particles measured with nanoparticle nebulizer-SMPS and NTA. On the SMPS size distribution, the first and second peaks correspond to the residue and gold particles, respectively. Residue particles have significantly higher concentration compared to the gold particles. However, since the residue particles are small (mode diameter at 10 nm), they do not interfere with the gold particles on the size distribution. In many cases, they can be removed by using a diffusion screen or by electrostatic classification using a Differential Mobility Analyzer (DMA).This also indicates the nanoparticle nebulizer can produce droplets smaller than the COA. Figure 3-6b shows the size distributions of mixed 80, 50 and 30 nm gold particles with equal number concentration. On the SMPS plot, while the residue particles are present in high concentration, they are kept in small size, not interfering with the particles of interest. The peaks at 30, 50, 80 nm can be distinctly resolved. The NTA plot shows a biased measurement towards the larger particles. From the comparison on the two measurements, it is obvious that aerosol technique gives more accurate representation for nanoparticles with polydisperse distribution. Therefore, when testing filter with polydisperse particles, the aerosol technique is preferred for particle analysis. However, one drawback is that it usually requires higher particle concentration to give results with good statistics.

a)

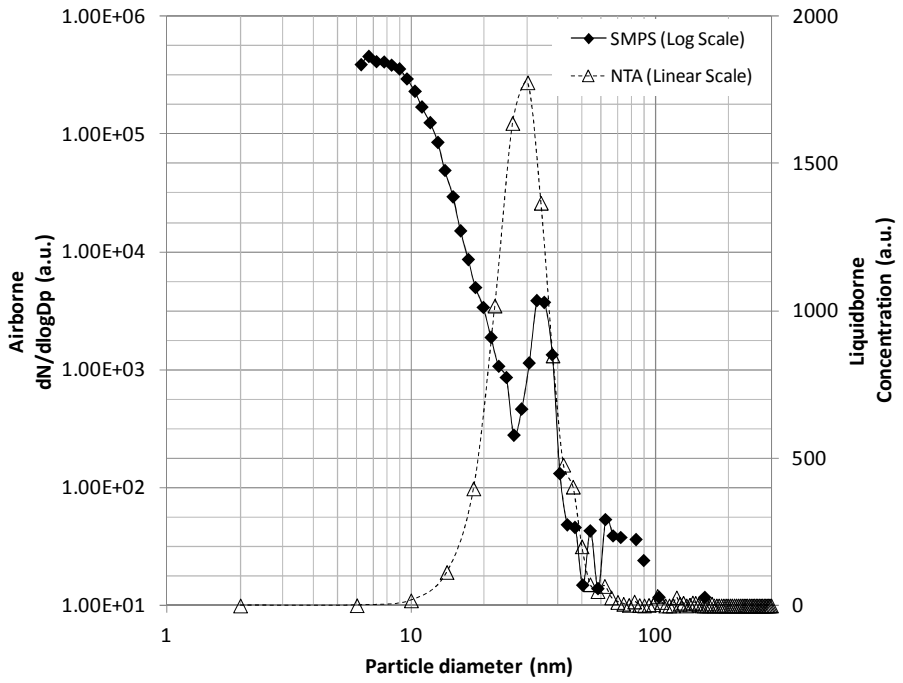

b)

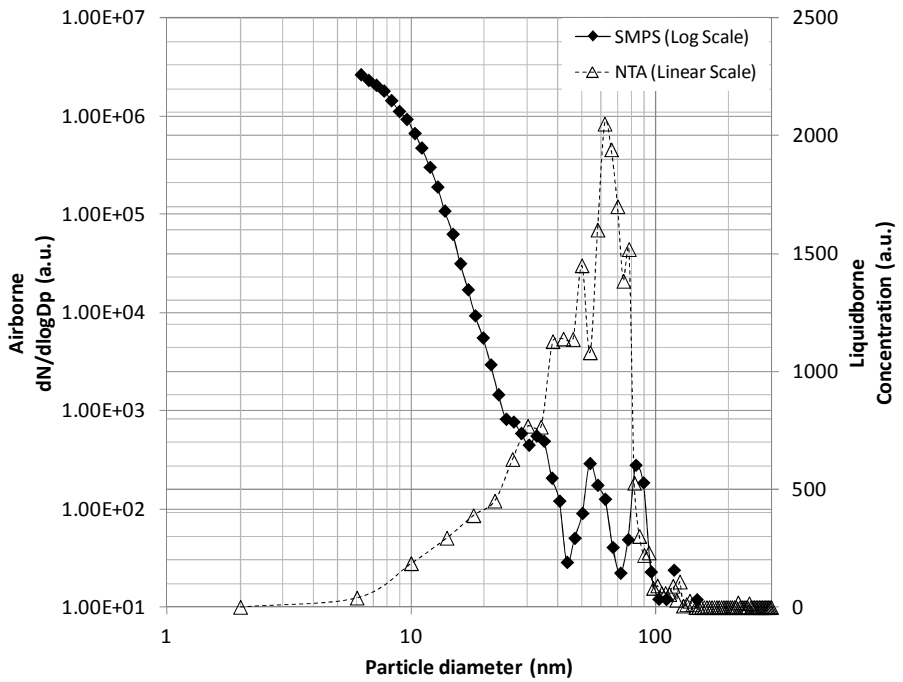

Figure 3-6. Size distributions of gold particles measured with SMPS and NTA : a) 30 nm, b) mixed 80, 50 and 30 nm gold particles with equal number concentration. The SMPS measurement is represented with resolution of 32 channels/decade. NTA measurement is represented with resolution of 4nm/channel.

3.4 Summary

In this study, we demonstrated the use of airborne dispersion technique for quantitative determination of liquid-borne nanoparticles. With the use of ES or nanoparticle nebulizer, nanoparticles as small as 30 nm can be dispersed and clearly identified by the airborne measurements. This allows an easy way to quantify liquid-borne particles as small as 30 nm, which cannot be analyzed by state-of-the-art liquid particle counters. Proportional relationship between the airborne and liquid-borne particle concentrations over two decades has been shown. No sign of deviating from the proportional relationship has been observed with further higher particle concentration in the water. The upper concentration limit will be imposed by the formation of appreciable doublets upon atomization which is governed by Equation (2). On the other hand, the lower concentration limit will be imposed by the measurement fluctuations. An important application for this technique is to evaluate filter retention efficiency by counting the particle concentrations upstream and downstream of the filters being tested. Standard nuclepore filters were tested to demonstrate the feasibility of the proposed technique. Retention efficiency of nuclepore filters as a function of particle size has been obtained, and the results are consistent with the nominal pore sizes and sieving mechanism. Comparing the technique to NTA, the aerosol technique gives more accurate representation for nanoparticles with polydisperse distribution.

Chapter 4

Measurement of filtration efficiency of nuclepore filters challenged with polystyrene latex nanoparticles: experiments and modeling

4.1 Introduction

Clean water is always of great demand. Drinking water, which is free of pathogens (bacteria and viruses), is critical for ensuring human health. Halogen disinfection is one of the major approaches to control microbial pathogens [Madaeni 1999]. However, they generate harmful byproducts and give rise to resistant pathogens. Filtration can be one of the chlorine-free alternatives for drinking water treatment [Savage and Diallo, 2005; Botes and Cloete, 2010].

Substantial reduction in the quantities of both organic and biological contaminants was achieved using filtration [Savage and Diallo, 2005; Lipp et al., 2009]. Various studies have shown that membranes are effective in producing water with reduced bacterial level but the retentivity depends on the magnitude of the organism challenge levels [Tanny et al., 1979; Madaeni, 1998]. Recovery of viruses (in nano size) using membrane filters have been demonstrated in various studies. They may be captured by sieving mechanism, if the membrane pore size is smaller than the virus particles, or adsorption via electrostatic interactions [Madaeni, 1998]. More recently, filtration using low pressure drop membranes (Microfiltration and Ultrafiltration) with anti-biofouling and anti-viral features are under research in order to overcome the problems of biofouling and virus penetration [Botes and Cloete, 2010]. Other advantages of using membrane for drinking water treatment are its operation easiness and competitive cost [Guo et al., 2010].

On the other hand, it is also important to have particle and chemical-free water for the advance of various industries, for example, semiconductor and pharmaceuticals. The level of purity, which determines the process for contaminant removal, depends on the nature of the contaminants to be removed and the applications [Madaeni, 1998].There is a

need to understand the nanoparticle filtration mechanism by membrane filters fundamentally.

Other than particle removal, filters with different pore sizes are also employed in marine and aquatic research to size-fractionate particle samples for analysis [Laxen and Chandler 1982 and references therein]. Because of the collection mechanisms other than sieving, e.g., diffusion, some particles smaller than the filter pore diameter can be retained. A sharp size cut may not be achieved. Filtration modeling is therefore needed to determine the suitability of particle collection schemes for aquatic particle studies and understand the size distribution of particles retained on the filter [Logan, 1993]. Some studies (e.g. Logan et al., 1993 and literatures cited therein) have applied modified aerosol filtration models in filtration of liquid-borne micron-sized particles. Depending on the types of filters used, the fibrous model and the capillary tube model were applied for prediction. However, the application of aerosol models for liquid-borne particle filtration has not been extended to study nano-sized particles, which are expected to be more influenced by the random diffusion mechanism.

The aims of this work are to 1) obtain the retention efficiencies of nuclepore filters against polystyrene latex (PSL) particles experimentally, and 2) compare the experimental results with our previous study (in Chapter 3) and filtration models modified from those developed for aerosols. To the best knowledge of the authors, this is the first study utilizing the NTA technique in liquid-borne particle filtration application.

4.2 Experiments

Filtration experiments

PSL particles of various sizes (50, 70, 125, 200 and 500 nm) were used as the challenge particles. The desired particle concentration was prepared by diluting the PSL particle suspensions with deionized water, which was assumed to be particle-free. Particle concentration used was about 10^8-10^9 particles/ml, similar to that used in Chapter 3. To

ensure the suspensions were well-dispersed and agglomerate-free, they were sonicated before being used to challenge the filters.

Filtration experiments were performed by using a syringe pump to deliver PSL suspensions to a 47 mm filter holder at a constant rate of 40ml/min. This corresponds to a face velocity (before considering the filter porosity) of $5x10^{-4}$ m/s. The test nuclepore polycarbonate track-etched membrane filter (Whatman) was placed in the filter holder. Filters with rated pore sizes 400, 200, 100 and 50 nm were used. A pressure gauge was used to monitor the pressure build up during the filtration test. The liquid downstream of the filter was collected. All procedures were made in duplicates. The experimental details are similar to those in Chapter 3, except that a syringe pump, instead of peristaltic pump, was used to deliver the suspensions.

NTA measurements

The number concentrations and size distribution of the particles in the suspensions upstream and downstream of the filter were determined by the NTA technique. Filipe et al. [2010] performed a comprehensive evaluation of size distribution measurements by the NTA technique. However, determination of filtration efficiency relies on the accurate measurement of particle concentration in the suspensions. We performed the concentration calibration of NTA by 150 nm PSL particles and found that measurements are reliable within a concentration range of 10^8-10^{10} particles/ml and a correction factor may be needed to determine the actual concentration depending on the camera gain values used during the measurements (Refer to Chapter 2). Five measurements were made for each suspension sample, and the averaged values were used for calculating the filtration efficiency as:

$$\text{Efficiency} = 1 - \frac{\text{Downstream Concentration}}{\text{Upstream Concentration}} \qquad \text{Equation 4-1}$$

4.3 Filtration model description

In air filtration studies, generally, two different models are available to describe the particle collection characteristics of membrane filters: the 1) capillary tube model [Spurny et al., 1969; Rubow and Liu, 1986; Cyrs et al., 2010] and 2) fibrous filter model [Brown, 1993; Wang et al., 2008 a,b; Wang et al., 2011]. Nuclepore filters are thin polycarbonate membranes which have a straight "capillary tube"-like pore structure of uniform diameter (Figure 4-1). Based on the assumptions made in the capillary tube model (discussed in this section), it is suitable for describing the nuclepore filter geometry. The capillary tube model was found to successfully predict aerosol removal by nuclepore filter over a wide aerosol size range [Rubow and Liu, 1986].

a)

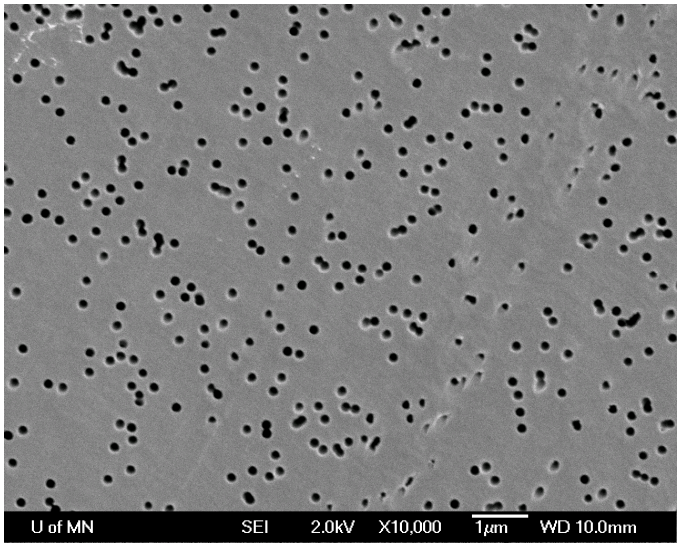

b)

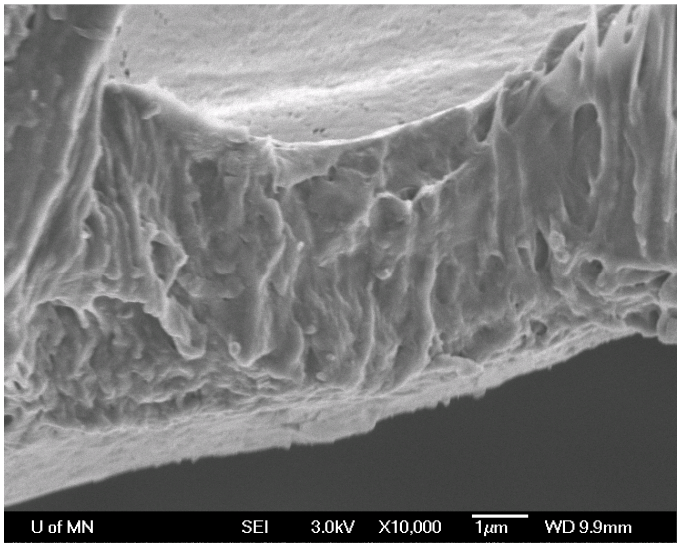

Figure 4-1. SEM images of nuclepore filters: a) Top view showing the cylindrical and uniform pores of the filter (200nm rated), b) Side view showing the filter thickness is approximately 4 μm.

The model works by 1) assuming a simplified filter geometrical description, 2) mathematically describing the fluid flow-field through the filter and 3) determining particle retention based on various collection mechanisms individually. The particle deposition mechanisms include 1) inertial impaction, 2) interception, 3) diffusion and 4)

gravitational settling [Rubow and Liu, 1986]. Gravitational setting is neglected in this work because it is efficient for large particles (micron-sized) only.

Major assumptions made in the capillary tube model include:

1) The filter can be represented by an assembly of uniformly-distributed capillary tubes of circular cross section.
2) The fluid is undergoing incompressible laminar flow.
3) The tubes are perpendicular to the filter surface and parallel to the fluid flow direction.
4) Particles are deposited on a clean filter.
5) Particles are collected once they are carried to the filter medium. Particle-filter interactions are not considered.
6) There is no particle blow-off from the filter surfaces.

The particle collection mechanisms are briefly discussed as follows:

Inertial impaction

Particles are deposited on the filter surface by impaction due to the finite mass and momentum of the particles and the change in direction as the fluid converges into the pore openings [Rubow and Liu, 1986]. The particle collection by inertial impaction is negligible in liquid filtration because of the high viscosity of the fluid. For simplicity, this mechanism is not considered in this study. Further discussion on the validity of neglecting the impaction mechanism is given in the next section.

Interception

Interception occurs when the streamline carrying a particle passes within a distance equal to or less than the particle's radius from the edge of the pore opening [Rubow and Liu, 1986]. There have been several studies on this mechanism (e.g.: Smith and Philips, 1975; Smith et al., 1976; John et al., 1978), and we adopted the one from John et al. 1978, since

it was found to fit the data best. All particles are intercepted when they are larger than the pore openings. The collection efficiency can be expressed as:

$n_R=(2R-R^2)^{3/2}$ for $R<1$

$n_R=1$ for $R>=1$ Equation 4-2

where the interception parameter R is the ratio of the particle to pore diameter, $D_{particle}/D_{pore}$.

Diffusion

Particles smaller than the pore size pass into the pore and diffuse towards the tube wall. Particles in contact with the tube wall are collected. The diffusion theory in Spurny et al. [1969] suggested that the collection efficiency can be expressed as (applicable for $N_D>0.001$):

$$n_D = 1 - \left[0.81904e^{-3.6568N_D} - 0.09752e^{-22.3045N_D} - 0.03248e^{-56.95N_D} - 0.0157e^{-107.6N_D}\right]$$

Equation 4-3

where N_D is the dimensionless parameter defined as $N_D=4LD/D_{particle}^2U$, and

D = Particle diffusion coefficient

L = Filter thickness

U = Fluid velocity

Overall filter efficiency

The overall efficiency is the sum of the removal by individual mechanisms, and is given as [Rubow and Liu, 1986; Logan, 1993; Spurny et al., 1969]:

$E_T=\alpha(n_R+n_D)$ for $R<1$

$E_T=1$ for $R>=1$ Equation 4-4

where α is the sticking coefficient of particles with the filter. The significance of α will be discussed in the next section.

Details of the filtration model can be referred to Rubow and Liu, 1986; Logan, 1993 and Spurny et al., 1969.

4.4 Results and discussions

Nanoparticle tracking vs aerosolization technique

Figures 4-2 to 4-5 show the results from the experiments and modeling for nuclepore filters rated at 400, 200, 100 and 50 nm, respectively. Modeling results using the sticking coefficient of 1.00 and 0.15 are both shown.

In Chapter 3, we proposed an aerosolization method to quantify nanoparticle concentration in suspensions, and applied it to measure the retention efficiency of PSL particles by nuclepore filters rated at 400 and 200nm. It was found that retention can be mainly attributed to the sieving mechanism. The experiments also found non-zero efficiency for particles smaller than the rated pore size, indicating the retention of diffused/intercepted smaller particles by adsorption also played a role. In this study, a new approach -- the NTA technique -- was used for particle concentration measurement. As shown in Figures 4-2 and 4-3, the efficiencies measured by the NTA technique are comparable to the fittings reported in Chapter 3, differing by less than 15%. Therefore, we have the confidence in this new technique for filter evaluation.

Modeling results

As shown in Figures 4-2a to 4-5a, removal of small particles is dominated by diffusion mechanism, which increases its efficiency with decreasing particle size. In the larger

particle regime, particle removal is accomplished by interception, which increases its efficiency with particle size. The modeling results exhibit the typical Most Penetrating Particle Size (MPPS) characteristics [Hinds 1999], if no correction by the sticking coefficient is made, i.e., $\alpha=1$.

a)

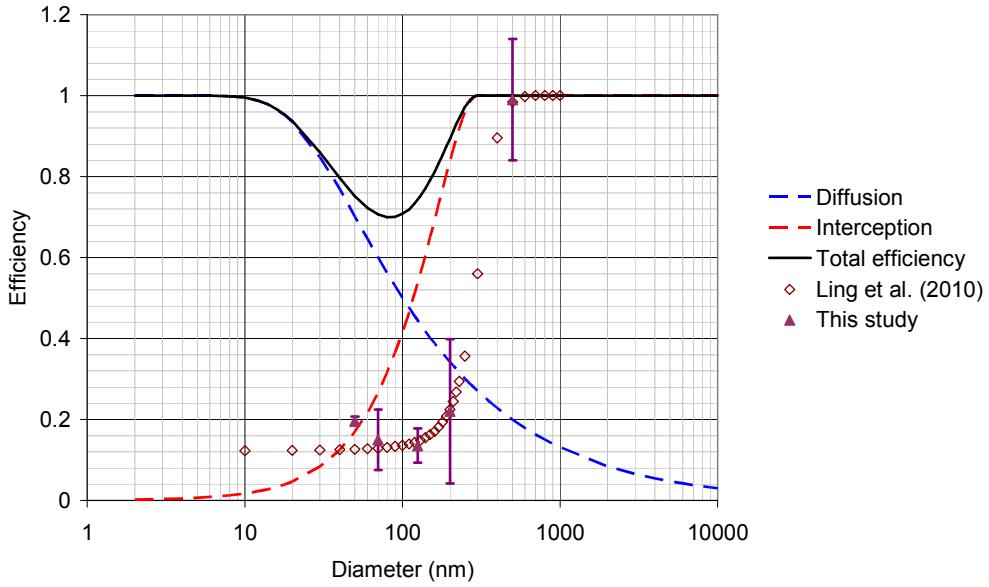

b)

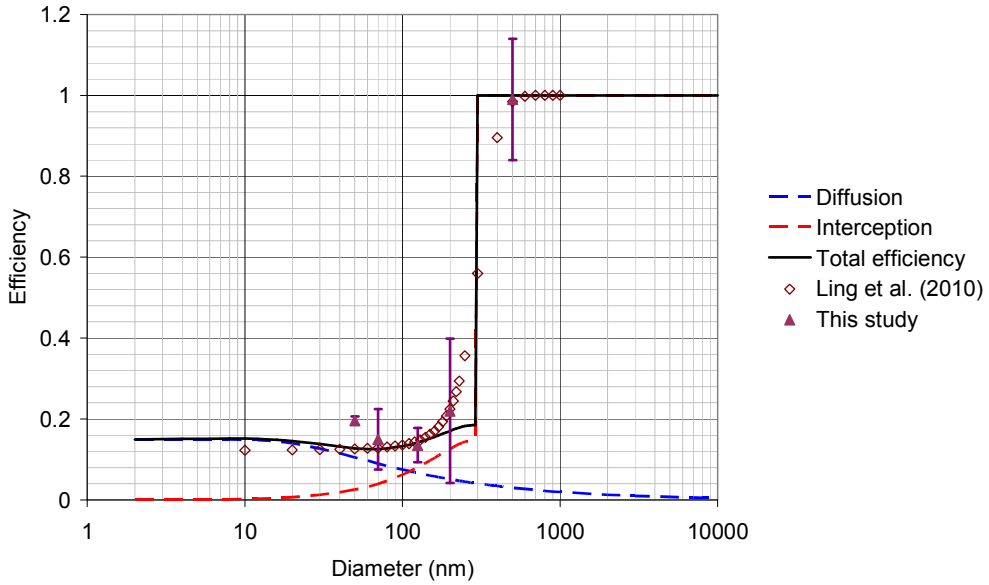

Figure 4-2. Filtration efficiency of a 400 nm rated nuclepore filters from the capillary tube model and experiment: a) Sticking coefficient = 1.00. b) Sticking coefficient = 0.15. Pore diameter of 300 nm was used in the model, as observed from the SEM. Data indicated as Ling et al. (2010) are the same as that reported in Chapter 3.

a)

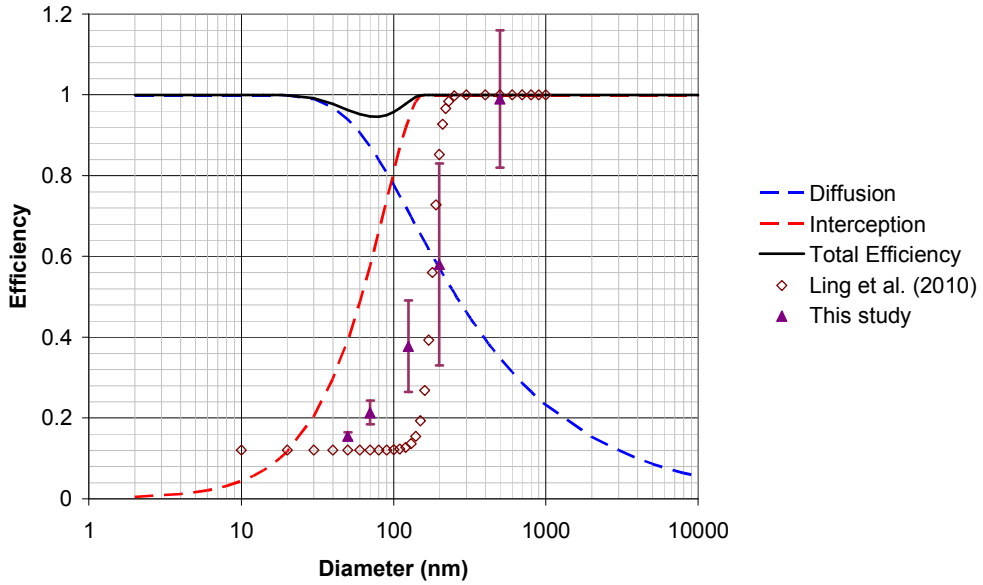

b)

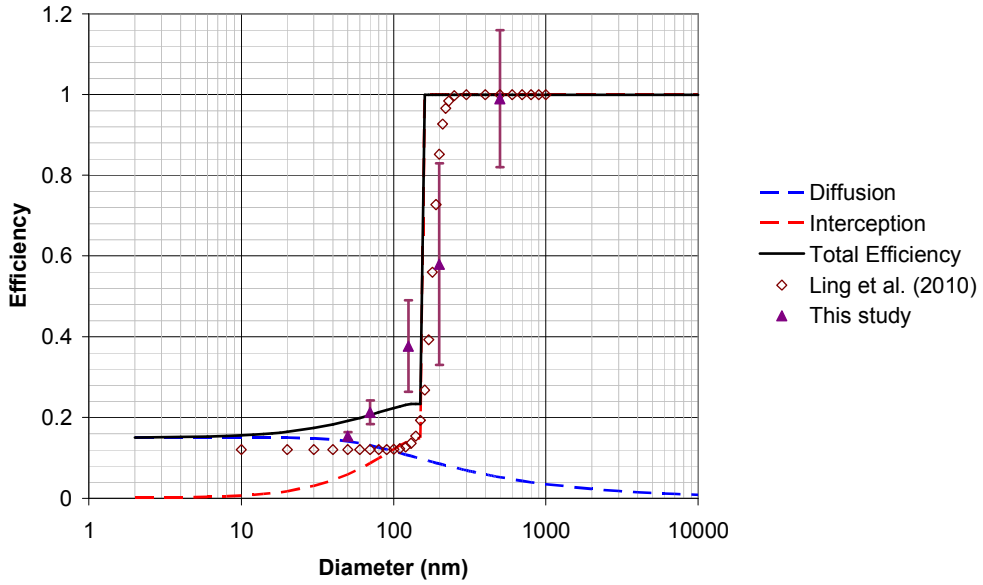

Figure 4-3. Filtration efficiency of a 200 nm rated nuclepore filters from the capillary tube model and experiment: a) Sticking coefficient = 1.00. b) Sticking coefficient = 0.15. Pore diameter of 157 nm was used in the model, as observed from the SEM. Data indicated as Ling et al. (2010) are the same as that reported in Chapter 3.

a)

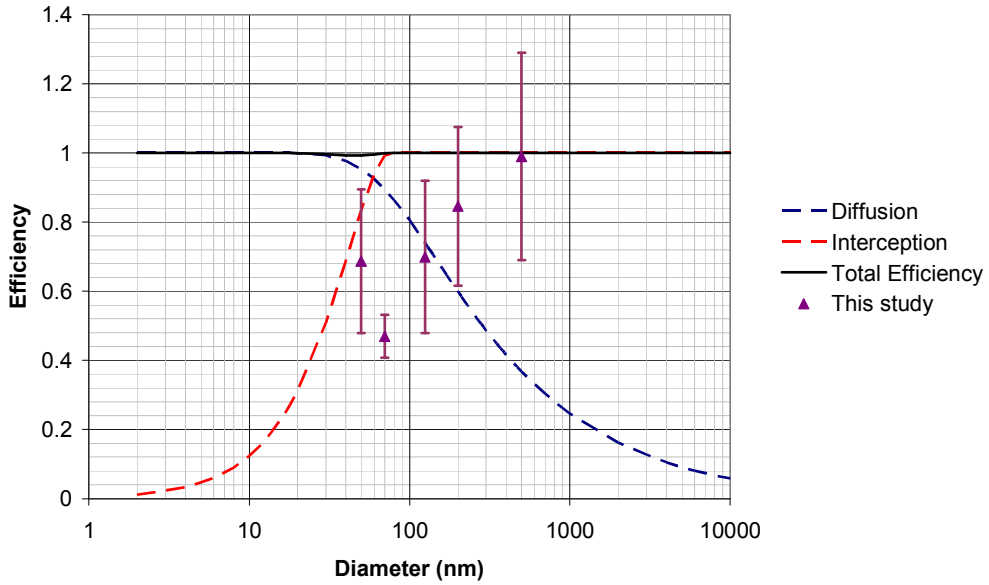

b)

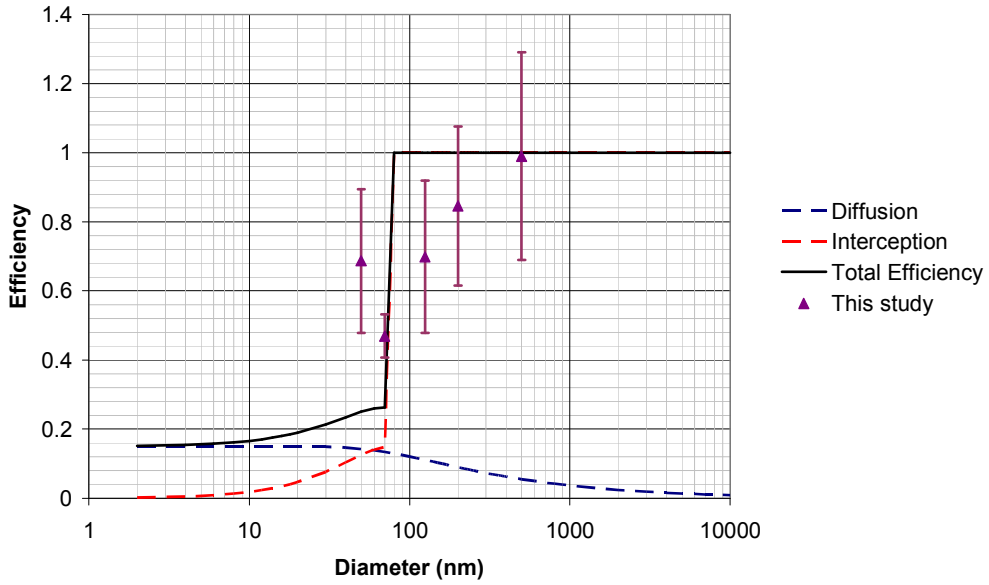

Figure 4-4. Filtration efficiency of a 100 nm rated nuclepore filters from the capillary tube model and experiment: a) Sticking coefficient = 1.00. b) Sticking coefficient = 0.15. Pore diameter of 76 nm was used in the model, as observed from the SEM. Data indicated as Ling et al. (2010) are the same as that reported in Chapter 3.

a)

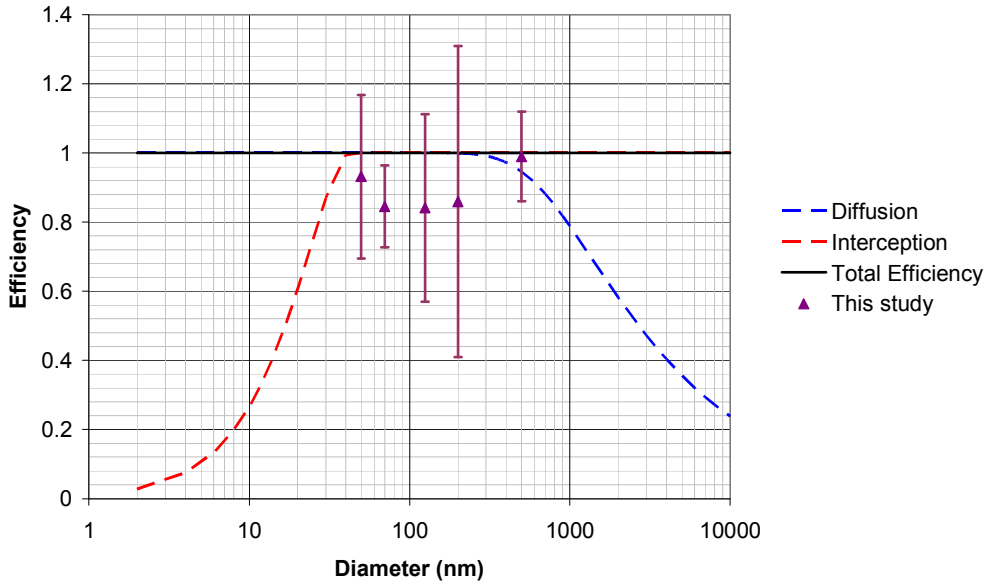

b)

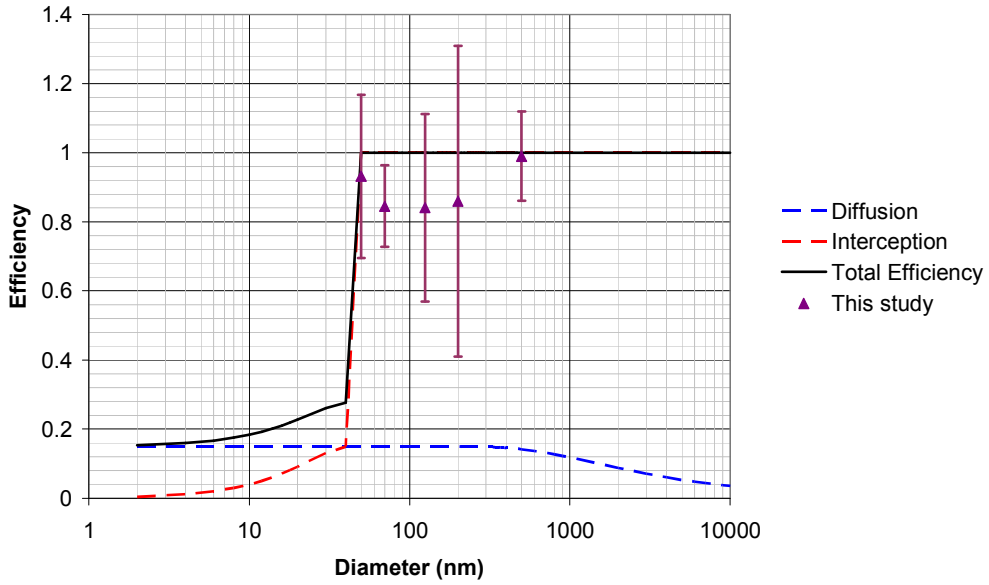

Figure 4-5. Filtration efficiency of a 50 nm rated nuclepore filters from the capillary tube model and experiment: a) Sticking coefficient = 1.00. b) Sticking coefficient = 0.15. Pore diameter of 43 nm was used in the model, as observed from the SEM. Data indicated as Ling et al. (2010) are the same as that reported in Chapter 3.

Modeling vs experimental results

Figures 4-2a to 4-5a show that the model over-estimates the filtration efficiency when compared to the experimental results. To better represent the efficiencies obtained from experiments, the sticking coefficient (α) in Equation 4-4 in the filtration model was adjusted. The optimum value was found to be 0.15 for experiments with all the four nuclepore filter samples (Figures 4-2b to 4-5b).

If a microscopic approach is used to describe the filtration process, it involves two steps: 1) The transport of the particle from the suspension to the vicinity of the surface and 2) the subsequent attachment of particles on the filter surface [Yao et al., 1976]. Particles carried by the liquid will be transported close to the filter surface by impaction, interception and diffusion, as described in the previous section. After being brought close to the medium surface, the surface interactions between the particle and the medium surface will determine whether the particle will get collected or not. Surface interactions mainly involve van der Waals and double layer forces acting at short distance below 5 nm, and the combined effects of the two will determine the attachment efficiency [Lee 1992].

If the condition is favorable, that is the particles and the filter surface are of opposite charge, the combined force is always attractive. The attachment probability is close to one. For example, positively charged membranes are likely to be effective to remove negatively charged viruses from water via depth filtration. Therefore, pressure drop will not be compromised for having small pore sizes to capture nanometer-sized virus particles [Madaeni 1998]. However, if particles and filter are of the same polarity of charge, there exist a repulsive force between each other, and the particle has to have a high enough inertia to overcome the energy barrier to get attached to the filter surface. Overall particle collection efficiency is determined by the 1) rates of particle transport (by interception and diffusion) and 2) attachment efficiency (described by α), which can be represented by Equation 4-4.

Therefore, the sticking coefficient (α) can be understood as the fraction of collisions, occurring between the suspended particles and filter, which results in successful adhesion out of the total number of collisions [Yao et al. 1971; Logan 1993]. Experiments in this work suggest that about 15% of particle collisions with the wall of the filter pores result in successful attachment. The sticking coefficient also corrects 1) the possible overestimation of particle collection by the model and 2) the entrainment of collected particles by the incoming fluid. Because of the relatively small sticking coefficient found for the PSL-water-nuclepore filter system, the particle removal performance of the nuclepore filters can be roughly explained by the sieving mechanism.

The value of the sticking coefficient will vary depending on the chemistry of the system: 1) filter media, 2) particles (surface charge) and 3) fluid (ionic strength, concentration of coagulant etc.). Spurny et al. [1969] reported a sticking coefficient of 0.15 for nuclepore filters for airborne particle filtration. In liquid-borne filtration, studies reported the sticking coefficient ranging from 0.09 to >1.00 for various particles and filter materials in aqueous media [Table 4 in Logan, 1993].

In the cases of the nuclepore fitlers rated at 100 nm and 50 nm (Figure 4-4 and 4-5), collection efficiencies obtained experimentally were not 100% even for particles significantly larger than the pore size. This is likely due to the fact that the PSL particles used for challenging the filters have a certain size distribution. The smaller particles, which belong to the lower end of the distribution, may get though the filter pores, causing efficiency less than 100%.

Several discrepancies between the actual experimental conditions and the capillary tube model assumptions should be considered. Points 1) and 2) cause the model to overestimate the filtration efficiency, whereas point 3) causes underestimation.

1) The model was developed to describe particle deposition on a clean filter. Loading of particles on the filter surface and blocking of the pores by collected particles affect the model accuracy. For example, a) the reduction of pore diameter by the particles

collected on the tube walls causes the fluid velocity to increase; b) deposition of particles at/close to the pore opening prevents further collection of particles within the tube wall. Therefore, the theory should be successful in predicting initial collection efficiencies, before the filter is deposited with too many particles. Figure 4-6 shows the Scanning Electron Microscopy (SEM) images of filters after being challenged with PSL particles. It shows that not all pores were filled up by particles at the end of the experiments, suggesting that the assumption of the model that particles are deposited onto a clean filter is reasonable. Cake filtration regime has not been reached until the end of each challenging.

2) The model only considers the transport of the particles to the vicinity of the filter surface but not the short distant surface interactions between particles and filter. Nuclepore filters and PSL particles are negatively charged in water. This creates conditions that do not favor particle collection.
3) Particle collection by diffusion onto the filter upper surface is not considered by the model.

a)

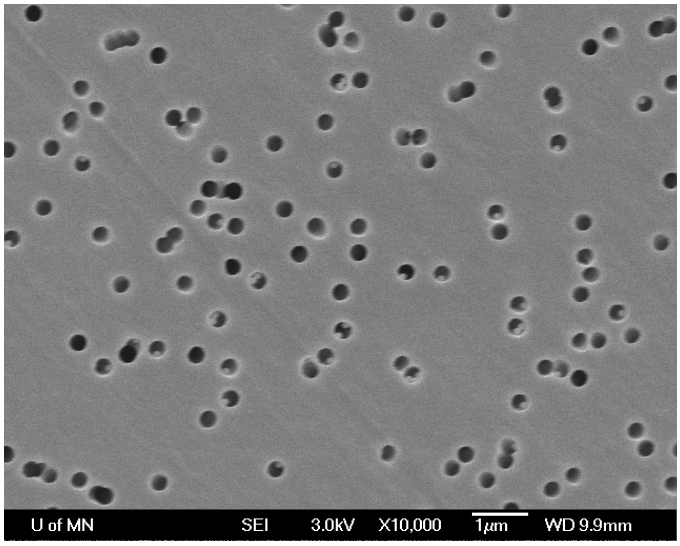

b)

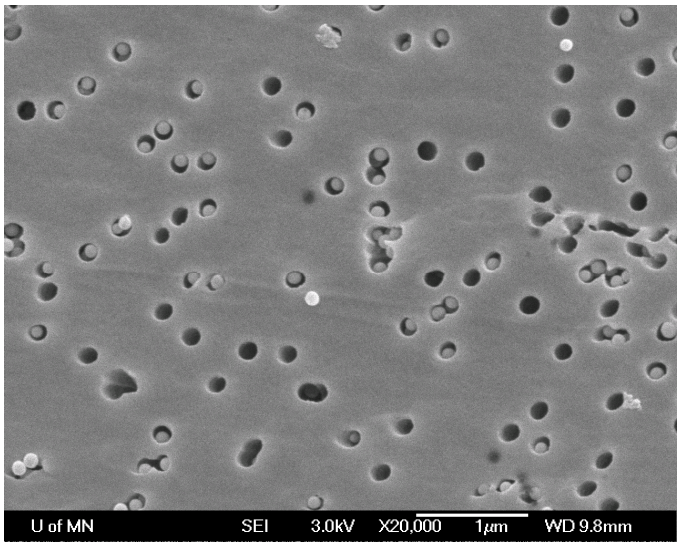

Figure 4-6. SEM images of nuclepore filters after being challenged with 125nm PSL particles: a) 400 nm rated NPF. b) 200 nm rated nuclepore filters.

It should also be noticed that the impaction mechanism was not included in the modeling. Assuming the flow field near the pore entrance can be approximated by converging streamlines described by parabolas, the particle collection efficiency contributed by inertial impaction (n_I) is [Rubow and Liu 1986]:

$$\eta_I = \frac{2E_i}{1+\beta} - \frac{E_i^2}{(1+\beta)^2}$$

where

$$E_i = 2St\sqrt{\beta} + 2St^2\beta\exp\left(-\frac{1}{St\sqrt{\beta}}\right) - 2St^2\rho_P$$

$$\beta = \frac{\sqrt{P}}{1-\sqrt{P}}$$

Equation 4-5

and the Stokes number St is defined as: $St = \frac{CD_{particle}^2\rho_p U_0}{9\mu D_{pore}}$

where

P = porosity of the filter

ρ_p = particle density

μ = fluid viscosity

C = Cunningham slip correction

Modeling with the impaction mechanism considered for 400nm nuclepore filter is shown in Figure 4-7. Because of the high viscosity of the fluid (water in this case) compared to air, the Stokes number is small, leading to the insignificant contribution of impaction to the overall efficiency, compared to air filtration case. Physically, a fluid with high viscosity allows particles to better follow the path of the streamlines, therefore diminishing the chance of particle collection by deviating from the streamlines. As shown in Figure 4-6, most particles are collected within the pores, instead of on the top of the filter surface. This indicates that the assumption of neglecting the impaction collection mechanism is valid.

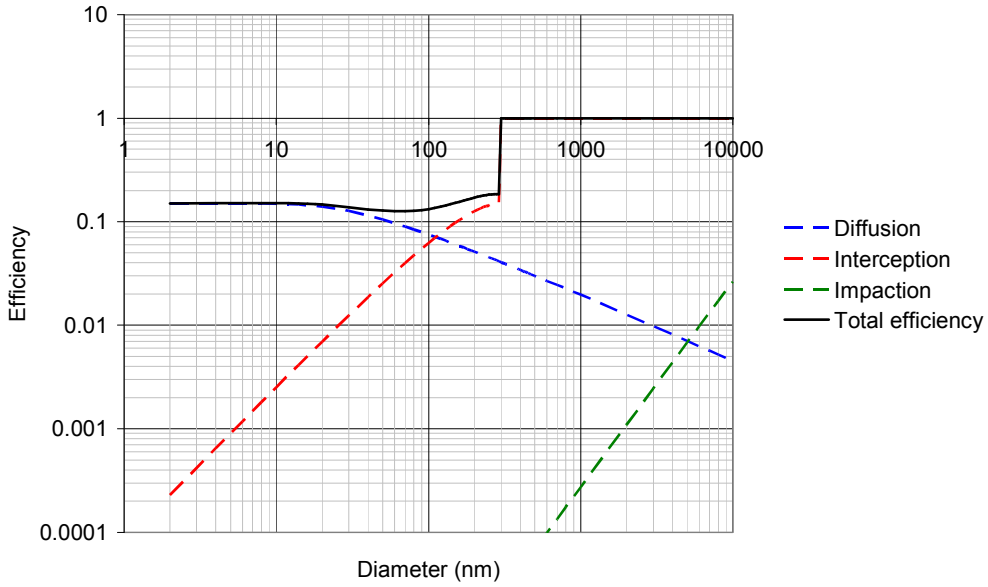

Figure 4-7. Filtration efficiency of a 400 nm rated nuclepore filters predicted from the capillary tube model with initial impaction considered. Log scale was used for the vertical axis.

4.5 Summary

Membrane filtration of liquid-borne nanoparticles has found applications in water purification. This work aims to experimentally obtain retention efficiencies of nuclepore filters against PSL particles and to compare the results with models modified from those developed for aerosol filtration. The NTA technique was used for evaluating filtration efficiency. Efficiencies determined by the NTA technique are comparable with data obtained with the aerosolization method (Chapter 3). Experimental results were compared with the prediction by the capillary tube model, which can describe the particle retention characteristics of the nuclepore filters when the proper sticking coefficient, equals to 0.15, is used. It is understood that the sticking coefficient is dependent on the materials of the fluid, filter medium and particles. Further studies on the relation of the material dependency of the sticking coefficient will be useful for modeling filtration performance.

Chapter 5

Evaluation of nanometer-rated liquid filter by gold, polystyrene latex and silica particles of different concentrations

5.1 Introduction

Liquid filtration has found many applications in environmental health and safety control as well as industrial processes [Jassby et al., 2010; Lecoanet et al., 2004, Seminario et al., 2002]. For industrial process, in biopharmaceutical industry, microfiltration is used for sterile filtration of fermentation media, buffers, product proteins and virus [Loh et al., 2009]. In semiconductor industry, membrane filters are often used to remove small particles from process liquids, e.g.: Ultra Pure Water (UPW) and diluted hydrofluoric acid used in recirculating etch baths [Zahka et al., 1993; Kelly et al., 2000]. Requirements for contamination control in semiconductor industry have become more and more stringent as the feature size of devices shrinks. Nowadays, in order to improve the production yield, filtration is expected to be capable of removing particles of 30 nm from the water and chemicals used in the advanced critical process steps [Nose et al., 2007; Wali et al., 2009].

Bubble point method is commonly used for determining the equivalent membrane cylindrical pore size. Although this does not directly reflect the retention efficiency of the membrane, studies have found good correlation between 1) pore size rated by bubble point method and 2) retention efficiency measured with microorganisms and hard spherical particles. However, the correlation will depend on the types of filters which have different structures, surface characteristics and thickness [Zahka and Grant, 1991]. To directly measure retention efficiency against particles, the common way is to use optical particle counters (OPC), which generally have a lower detection limit of about 50 nm, to measure the particle concentration upstream and downstream of the membrane filter. In order to measure retention efficiency against particles smaller than 50 nm, there

have been studies reporting the use of fluorescent nanoparticles and gold nanoparticles to challenge the filter. Retention efficiency is determined by measuring the fluorescent signals and gold content (with Inductively Coupled Plasma Mass Spectrometry, ICP-MS) as an indication for particle concentration [Takehito et al., 2009]. The major drawback for inferring particle concentration based on the bulk special properties is that there is limited information on particle size.

Therefore, more recent studies have suggested other techniques for counting and sizing nanoparticles which can be applied for evaluating high efficiency nanometer-rated filters. The first technique is the aerosol method, which basically disperses the liquid-borne particles into airborne form to be measured by more sensitive aerosol instruments (Chapter 3). The aerosol method yields very good resolution in particle size measurements. The major drawback is that it requires high particle concentration for the measurements (about > 1E9 particle/ml) , due to the various particle losses during aerosolization process and Differential Mobility Analyzer (DMA) classification. The second technique is the Nanoparticle Tracking Analysis (NTA), which counts the particles by optical method and sizes them based on their Brownian motion. This technique shows some biases when measuring polydisperse particles and has a relatively narrow window of concentration appropriate for measurement (Chapter 3).

Sieving is the generally relied mechanism for the filtration of sub-micron and nano-particles from liquids [Zahka and Grant, 1991; Kelly et al., 2000; Beuscher 2010]. Particles are removed from the liquids and captured when they are too large to pass through the pore openings. It depends on the relative size of the particles to pores only, but not the chemistry of or interactions between the particles, filters and liquids. For particles smaller than the pore size of a filter, particles can be captured by adsorption via diffusion and interception mechanisms, which depends on the particle-filter surface interactions. Attractive interactions enhance the approach and attachment of particles to the filter surface, and repulsive interactions hinder the particles from getting close enough

to the filter surface to be captured. If the repulsive interactions are very large, particle retention is limited to sieving only [Duclos-Orsello et al., 2004].

Particle- filter surface interactions in liquids are governed by the electrostatic and van der Waals interactions. Other highly specific interaction potentials can be assumed negligible. Electrostatic interactions may be attractive or repulsive, depending on the sign of the electrostatic potential of the particles and filter media. The van der Waals interactions are generally attractive forces acting between two materials [Duclos-Orsello et al., 2004]. Recently, filtration by surface-modified membranes has been studied. The surface-modified membrane is almost neutral under most pH conditions and minimizes the electrostatic force (attractive or repulsive) between particles and filter surface, regardless of the signs of their charge. When the attractive van der Waals forces are playing the role primarily, particle retention can be enhanced by interception and diffusion collection mechanisms [Duclos-Orsello et al., 2004; Kelly et al., 2000].

The DLVO theory, which describes the combined effects of van der Waals attractions (W_{vdw}) and electrostatic interactions (W_{edl}) between particle and filter surface immersed in a liquid, can be applied to explain the capture of particles smaller than filter pore size by adsorption [Kelly et al., 2000]. The overall DLVO interactions (W_{DLVO}) can be given as:

$$W_{DLVO}=W_{edl} + W_{vdw} \qquad \text{Equation 5-1}$$

Van der Waals interactions are dependent on the geometry as well as the physical and chemical properties of the interacting bodies. The van der Waals interactions for sphere-surface geometry, which is applicable for representing the case of particle-filter surface interactions, can be expressed as:

$$W_{vdw} = -\frac{A_{123}R}{6D}$$ Equation 5-2

where:

A_{123} = Hamaker constant of the interacting materials (1: particle, 2: fluid medium, 3: membrane)

R = Particle radius

D = Separation distance between sphere and surface

Hamaker constant can be estimated by:

$$A_{132} = \left(\sqrt{A_{11}} - \sqrt{A_{33}}\right) \times \left(\sqrt{A_{22}} - \sqrt{A_{33}}\right)$$ Equation 5-3

where A_{11}, A_{22} and A_{33} are the Hamaker constants of the materials interacting in vacuum [Oliveira, 1997].

When solid bodies are immersed in a liquid medium, they show a generalized tendency to acquire an electrical surface charge. The potential energy arising from the approaching of two charged bodies depends on the geometry of the interacting bodies and electrical behavior during interactions [Oliveira, 1997]. For a particle interacting with a flat surface across a monovalent electrolyte, the electrostatic interaction energy per unit area can be expressed as follows:

$$W_{edl} = RZ\exp(-\kappa D)$$

$$Z = 64\pi\varepsilon\varepsilon_0\left(\frac{kT}{e}\right)^2 \tanh\left(\frac{e\psi_1}{4kT}\right)\tanh\left(\frac{e\psi_2}{4kT}\right)$$ Equation 5-4

$$\kappa = \left(\frac{\rho_\infty e^2}{\varepsilon\varepsilon_0 kT}\right)^{1/2}$$

where:

ε = Dielectric constant of the material

ε_0 = Dielectric permittivity of free vacuum space (8.854×10^{-12} $C^2J^{-1}m^{-1}$)

k = Boltzmann constant

T = Absolute temperature

e = Electronic charge (1.602×10^{-19} C)

ψ_1, ψ_2 = Surface potential of materials (1: particle, 2: membrane surface)

ρ_∞ = Bulk electrolyte concentration

There is a practical difficulty in determining the actual surface potentials. Thus, in practice, they are replaced by zeta potential, which can be obtained by micro-electrophoresis [Oliveira, 1997]. Whether the interactions are attractive or repulsive depends on the charge sign of the two surfaces. The magnitude of the electrostatic interaction will depend on the values of the surface potentials of the particles and filter surface and κ. The quantity $1/\kappa$ is referred to as the Debye length and characterizes the rate of decay of the potential with separation distance. The higher the electrolyte concentration, i.e., ionic strength, the lower the repulsion energy barrier is for two surfaces having the same sign of charge [Oliveira, 1997; Kelly et al., 2000]. When the overall W_{DLVO} interactions are favorable (attractive or slightly repulsive), particles can be more efficiently retained by adsorption via interception and diffusion, in addition to sieving.

In this study, we measured the retention efficiency of a nanometer-rated membrane filter against nanoparticles of different materials, sizes, concentrations and size distributions, as a function of particle loading. The objectives of this work are to 1) compare the retention efficiency of the membrane filter measured under different conditions, 2) explain the results using sieving mechanism and the DLVO theory, and 3) discuss the suitability of using different particle materials for filter testing.

5.2 Experiments

Materials

The membrane filter under test is PTFE-type, which is a common material for liquid chemical filters [Zahka et al., 1993]. It has a pore size rated at 50 nm by the manufacturer using bubble point measurement. Water flows across the filter with a face velocity of 0.07 cm/s at pressure drop of 10 psi. The zeta potential is about -30 mV at pH =7 [Simon et al., 1996; Soster et al., 2005; manufacturer information]. A variety of particle suspensions were used to challenge the filter. This includes monodisperse gold and polystyrene latex particles, with sizes 80, 50 and 30 nm as well as silica particles with sizes of 50 and 30 nm. In addition, a mixture of equal number concentration of gold particles of different sizes (80, 50 and 30 nm) was also prepared as one of the challenge suspensions. The desired particle concentration of each challenge suspension was adjusted by properly diluting bulk suspensions as purchased with deionized water. Table 5-1 lists the information of the particle suspensions used for the filtration experiments.

Table 5-1. Information of the particle suspensions used for filtration experiments

Material	Specified particle size (nm)	Particle concentration (particles/ml)	Zeta potential[1] (mV)	Conductivity μS/cm)
Monodisperse particles				
Gold	80	2E9 1E10	-37 *	NA
	50	2E9 9E9 - 1E10 4E10 -5E10	-37 *	NA
	30	3E9 9E9 4E10	-33 +	39
PSL	80	2E9 1E10 5E10	-50 +	NA
	50	1E10 - 2E10 5E10 3E11	NA	NA
	30	5E10 1E11 3E11 - 4E11	NA	29
Silica	50	3E8	-40 +	NA
	30	1E9 4E9	NA	8
Polydisperse particles				
Gold	80/50/30	3×2E9	NA	NA

Note1:

Zeta potential values reported are at pH =7. It is understood that ions and other dissolved impurities affect the zeta potential. However, the measurements of zeta potential with the corresponding instruments requires a certain particle concentration. The desired concentration for zeta potential measurements was adjusted by deionized water dilution. The pH was not manipulated [Limbach, et al., 2008]. Values marked with "*" are information from particle suppliers or literatures [Itano et al., 1995]. Values marked with "+" are measured with NanoSight NS500.

Filtration experiments

The filtration experiment was performed using a set up of a Millipore vacuum filter holder and flask. A new membrane filter was used in each test. Isopropyl alcohol (IPA) was first applied to activate (wet) the membrane filter. The filter was then flushed with deionized water to remove IPA trapped inside the filter. After that, filter was challenged with different sets of test suspensions. Filtration experiment was conducted under constant trans-membrane pressure at 10 psi, as the driving force for the water flow. Transient retention efficiency is determined by measuring particle concentration upstream and downstream of the filter as a function of time during the filtration process. After that, the filter was flushed with particle-free deionized water again and the concentration of the particles present in the flushed water was measured to determine the amount of particles entrained by the water flow. Particle measurements were performed using the aerosol and Nanoparticle Tracking Analysis (NTA) techniques (discussed in following paragraphs). Retention efficiency is calculated as: $1 - \frac{\text{Downstream Particle Concentration}}{\text{Upstream Particle Concentration}}$.

Aerosolization technique

Our group has applied the aerosol technique for counting and sizing liquid-borne nanoparticles. In brief, a dispersion tool is used to aerosolize a liquid suspension and a Scanning Mobility Particle Sizer (SMPS) is used for measuring the aerosolized particles after solvent evaporation. A proportional correlation between airborne and liquid-borne particle concentration has been demonstrated, provided that proper precautions are taken to 1) separate and distinguish real particles from residue particles and 2) ensure the generation of singlet particles. In this study, the suspension samples taken from the filtration experiment were dispersed by a TSI nanoparticle nebulizer, which is designed to disperse droplets with a nominal size of 300 nm. The small droplet size can ensure singlet particle generation and reduce the size of residue particles which may interfere with the solid particles of interest. A SMPS, consisting of an aerosol classifier (Model

3080, TSI) and a condensation particle counter, was used to measure the airborne particle size distribution. The liquid-borne particle concentration was determined by integrating the particle peak of the measured SMPS size distribution. The true number concentration will require a pre-calibration to the nebulizer-SMSP system.

NTA measurements

The suspension samples taken from the filtration experiment were characterized for their size distribution and concentration by the NTA technique (NanoSight LM10, NanoSight Ltd., United Kingdom). NTA determines particle size distribution based on the diffusive Brownian motion of nanoparticles using video microscopy. The Stoke-Einstein equation provides the relation of particle's size and diffusive root mean square displacement. NTA also determines the particle concentration based on the number of particles visualized in the video microscopy. To ensure consistency and improve the statistical accuracy of the measurements, we performed five repeated 60-minute measurements for each sample, with constant parameter settings. All data were analyzed using the instrument software (NanoSight, version 2.3). It should be noted that NTA measures well for particle concentration between 1E7 to 1E9 particles/ml. Therefore, for certain samples, proper dilution with deionized water were needed.

Polydisperse particle measurements

In Chapter 3, we have compared the size distribution measurement of mixed 80, 50 and 30 nm gold particles by the aerosolization technique and NTA. Results have shown that the aerosolization technique gives more accurate representation for polydisperse distribution, while the NTA shows bias to the larger particles. Therefore, only the aerosolization technique was used to measure particle concentration of samples taken from the filtration experiments using mixed gold particles. The retention efficiency at a certain particle size is determined by taking ratio of the upstream and downstream

particle counts at the corresponding particle size read from the size distributions measured by SMPS.

5.3 Results and discussions

Monodisperse particle test: decreasing trend

The retention efficiency of the membrane filter challenged with monodisperse 50 nm gold particles of different concentrations is shown in Figure 5-1, as a function of filtration progress. For each test with particles of a certain concentration, three downstream samples were taken at different times during the filtration process. Particle measurement was made with the aerosol technique. Within each test, the retention efficiency decreases as the filtration process proceeds. Comparing tests using different concentrations, the retention efficiency decreases with increasing suspension concentration. The observation suggests that retention efficiency decreases with particle loading, due to increase in either time or particle concentration.

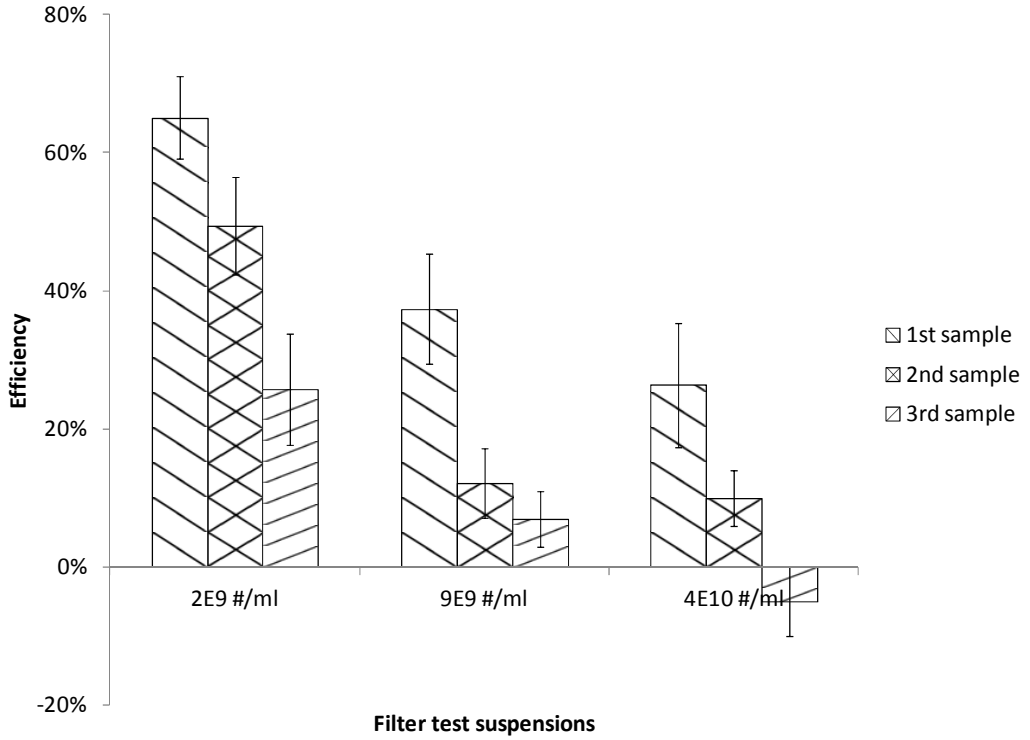

Figure 5-1. Retention efficiency of tested membrane filter at different times, measured using 50 nm gold particles of different concentrations.

To generalize the retention efficiency results obtained with different particle concentrations and at different times, we plotted the results as a function of cumulative volume of test particles, which is defined as the products of 1) volume of a particle, 2) particle number concentration and 3) total volume of suspension that has passed through the filter. Figure 5-2 (a-c) shows the results for 80, 50 and 30 nm particles of different materials (gold, PSL and SiO_2). The upper axis indicates the cumulative particle volume relative to the bulk volume of the membrane filter. Retention efficiency data from different test particle concentrations collapse into the same trend, which decreases rapidly in the beginning and followed by a more gradual decrease. The measurements made by aerosol technique and NTA are generally comparable with each other, suggesting the validity of the two methods. Since retention efficiency is given by the ratio of the measured upstream and downstream particle concentrations, uncertainty in obtaining the actual particle concentration is negligible.

a)

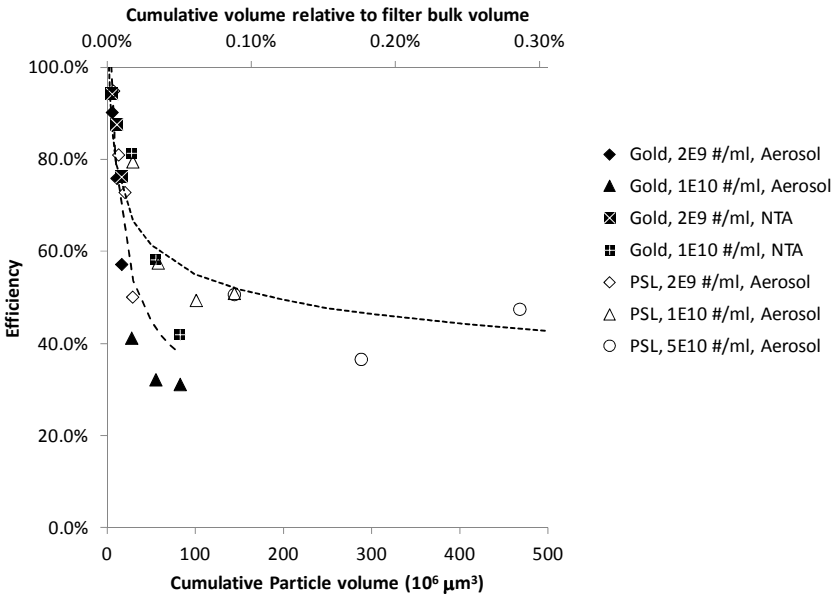
Cumulative volume relative to filter bulk volume
0.00%
0.10%
0.20%
0.30%
100.0%
80.0%
60.0%
40.0%
20.0%
0.0%
Efficiency
0
100
200
300
400
500
Cumulative Particle volume (10⁶ µm³)
Gold, 2E9 #/ml, Aerosol
Gold, 1E10 #/ml, Aerosol
Gold, 2E9 #/ml, NTA
Gold, 1E10 #/ml, NTA
PSL, 2E9 #/ml, Aerosol
PSL, 1E10 #/ml, Aerosol
PSL, 5E10 #/ml, Aerosol

b)

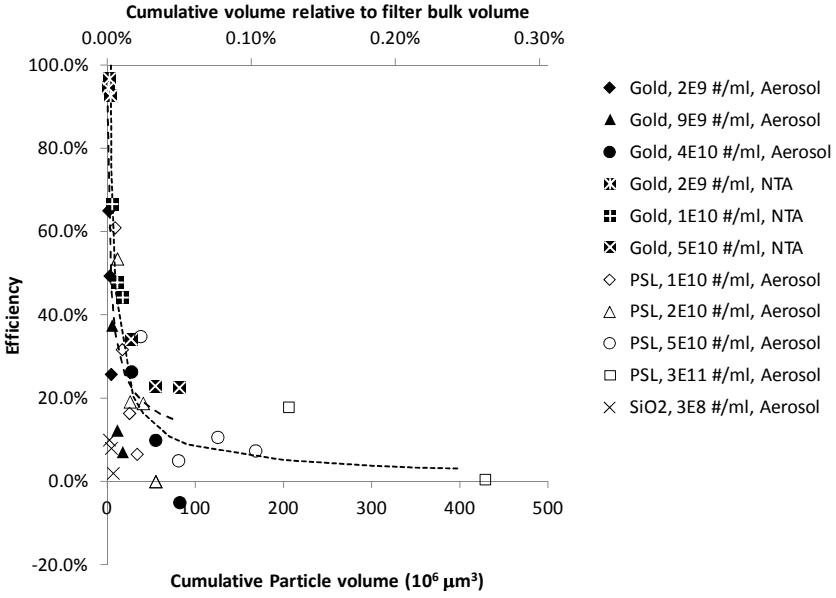
Cumulative volume relative to filter bulk volume
0.00%
0.10%
0.20%
0.30%
100.0%
80.0%
60.0%
40.0%
20.0%
0.0%
-20.0%
Efficiency
0
100
200
300
400
500
Cumulative Particle volume (10⁶ µm³)
Gold, 2E9 #/ml, Aerosol
Gold, 9E9 #/ml, Aerosol
Gold, 4E10 #/ml, Aerosol
Gold, 2E9 #/ml, NTA
Gold, 1E10 #/ml, NTA
Gold, 5E10 #/ml, NTA
PSL, 1E10 #/ml, Aerosol
PSL, 2E10 #/ml, Aerosol
PSL, 5E10 #/ml, Aerosol
PSL, 3E11 #/ml, Aerosol
SiO2, 3E8 #/ml, Aerosol

c)

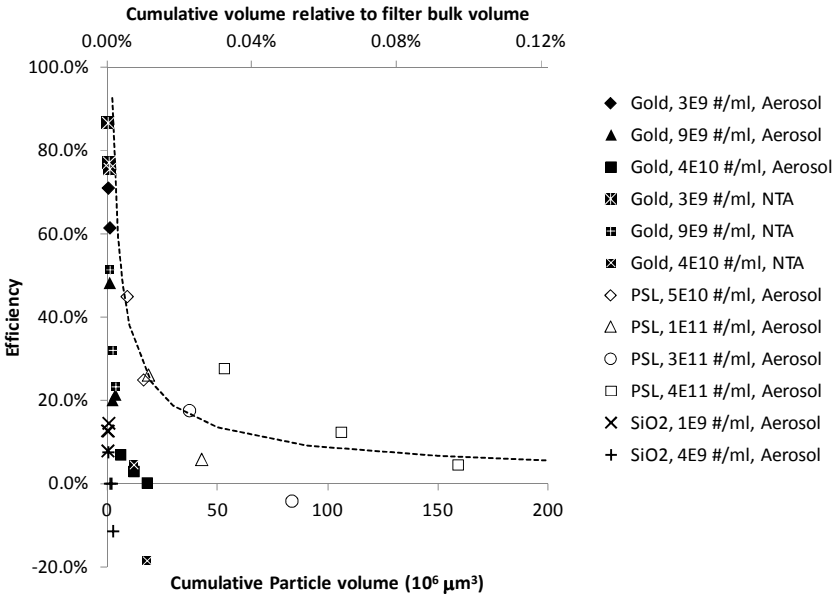

Figure 5-2. Retention efficiency results as a function of cumulative particle volume for a) 80, b) 50 and c) 30 nm particles of different materials: gold, PSL and silica. The legend indicates the material, number concentration and method of concentration determination.

The decreasing trend of retention efficiency of membrane filters as a function of particle loading has been reported by previous studies [Zahka and Grant, 1991, Lee and Liu, 1994; Beuscher 2010]. These studies challenged the filter with particles which are larger than or equal to the rated pore size. Therefore, the observation can be readily explained by pore blockage due to sieving. Membrane filters can be regarded as having pores of a certain size distribution. The decrease in retention efficiency with particle loading is caused by some of the smaller pores in the membrane filter becoming plugged by the particles when captured. When an appreciable amount of particles have plugged those smaller pores, the mean pore size of the filter increases, and this forces more fluid to flow through the larger pores.

In this study, we also challenged the membrane filter with particles size (30 nm) that is smaller than its rated pore size (50 nm). In this case, the probability for particle capture by sieving is low. However, under favorable conditions, i.e., attractive or slightly repulsive interactions between particles and membrane surface, particles can also be captured by adsorption via interception and diffusion onto the pores that are bigger than the particle size. According to the capillary tube model [Rubow and Liu, 1986], the efficiency of particle capture by interception increases with increasing value of the ratio of particle diameter to pore diameter, i.e., $D_{particle}/D_{pore}$ (for $D_{particle}/D_{pore}$ <1). Therefore, the chance for particle capture by interception decreases as more particles are intercepted onto the walls of the pores of relatively smaller diameter. In addition, particles captured by adsorption may be entrained off by the fluid passing through the pores. Collectively, 1) increase in filter mean pore size due to pore plugging, 2) decrease in favorable sites for particle intercepting onto walls of the pores and 3) entrainment of adsorbed particles lead to the decrease of the retention efficiency as particle loading increases. Although not shown in Figure 5-2, retention efficiency will stop decreasing and rise when further loadings occur as a particle cake has built up on the filter surface [Lee and Liu, 1994]. More discussions on particle adsorption and entrainment will be given in the following sections.

Retention efficiency is dependent on particle size. The larger the particles, the higher the efficiency for the same particle cumulative volume, as shown in Figure 5-3. This observation can be easily explained with the sieving concept discussed in the previous sections. Previous studies have also reported similar trends for PVDF and PTFE membrane filters [Zahka and Grant, 1991]. In addition, the filter has similar retention efficiency for 80 nm gold and PSL particles at different cumulative particle volumes, because they are primarily captured by sieving mechanism, which is independent of particle material/chemistry. There are larger differences between gold and PSL for smaller particles, i.e., 50 and 30 nm, because these particles are captured mainly by adsorption, which is dependent on particle chemistry. It should be noted that retention efficiency data for silica particles, which are much lower than those for PSL and gold

particles, are not included in Figure 5-3. The significant difference will be discussed in the following sections. As the retention efficiency is decreasing with particle loading, the filter's initial retention efficiency can be obtained by extrapolating plots in Figure 5-2 to zero loading. The initial retention efficiency, considered to be the retention efficiency at cumulative particle volume of 5 μm^3, is also plotted in Figure 5-3. The initial retention efficiency increases with increasing test particle sizes.

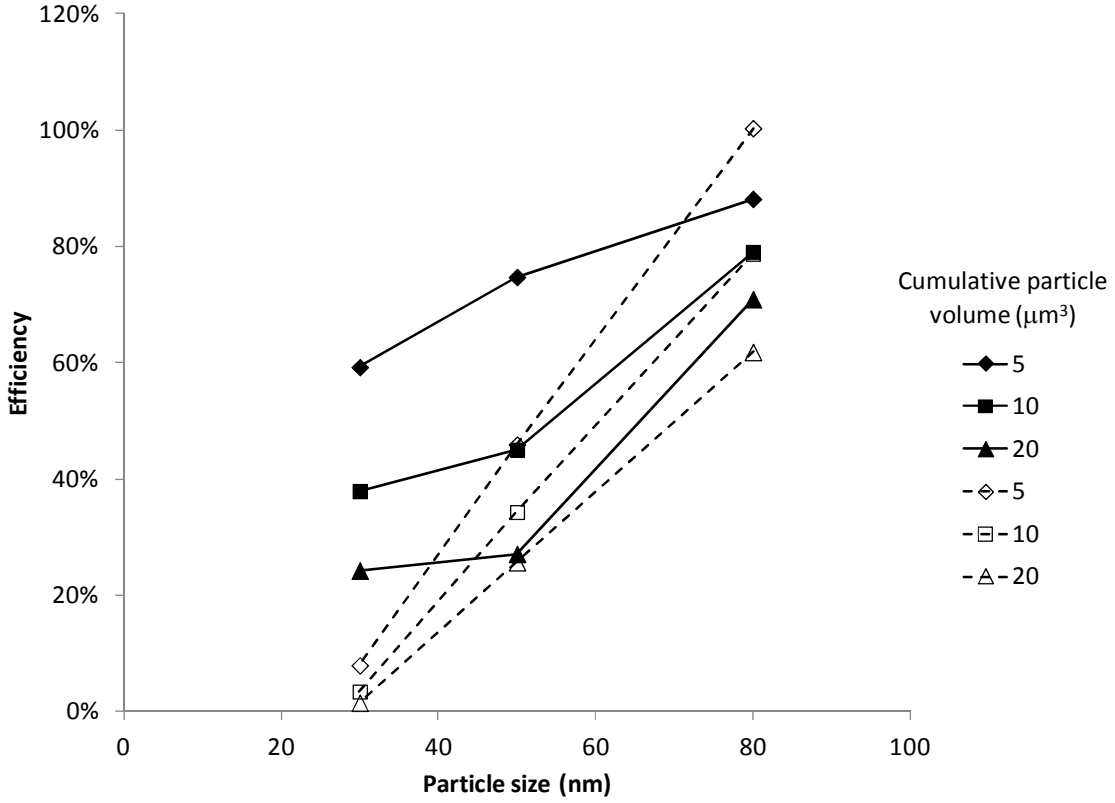

Figure 5-3. Retention efficiency as a function of particle size at different cumulative volume. Solid and open symbols represent results from PSL and gold particles, respectively.

Monodisperse particle test: particle material dependence

According to Figure 5-2, it can be seen that, at the same cumulative particle volume, silica particles show much lower retention efficiency than that for gold and PSL particles. To explain the observation, we notice that Equations 5-1 to 5-4 describing the DLVO theory indicate that the interactions between particles and filter surfaces are dependent on the material properties of the particles, membrane filters and liquid medium. The zeta potential of PTFE membrane in water (at roughly pH =7) is about -30 mV. The zeta potentials of the gold, PSL and silica particles show similar values at pH=7, as indicated in Table 5-1. However, as shown in Equation 5-4, the rate of decay the electrostatic interaction energy with separation distance is characterized by the quantity $1/\kappa$. κ is proportional to the electrolyte concentration, which is related to the amount of dissolved substances present in the particle suspensions. The conductivity of the solution is a good indicator for the electrolyte concentration, i.e., ionic strength [Limbach et al., 2008]. As also shown in Table 5-1, the conductivity of silica colloid is much lower than those for gold and PSL particles, which have similar values.

Based on the conductivity measurements, we estimated the electrolyte concentration for the test particle suspensions and plotted the interaction energies between the membrane filter and particles of different materials (Figure 5-4). The plots in Figure 5-4 suggest that silica particles experience higher repulsion interactions over a longer distance than PSL and gold particles. In other words, the higher ionic strength (or ion concentrations) of PSL and gold suspensions causes a decrease in the magnitude of energy barrier and favors adhesion of particles to the filter surface [Oliveira, 1997; Limbach et al., 2008]. In a filtration test using Si_3N_4 particles and hydrofluoric acid solution with different concentration, i.e., different pH values, it has been reported that retention efficiency for Si_3N_4 particles increases when the solution has high hydrofluoric acid concentration and low pH. The authors explained the results with the fact that high ionic strength of the solution partially masked the electrostatic repulsion between particles and the filter and therefore allowed an increase in particle retention efficiency. [Kelly et al., 2000]. Therefore, the conditions for particle capture by adsorption via interception and diffusion

are less favorable for silica suspension, which has a lower ionic strength. Filtration of silica particles can be described as: 1) more electrostatically hindered for interception and diffusion and 2) more sieving-dominant, compared to that for PSL and gold particles [Kelly et al., 2000]. The difference in retention efficiency between silica and gold particles can be considered to be due to particle adsorption via interception and diffusion. It should be noted that we did not intentionally adjust the electrolyte concentration. We prepared the test colloids with different particle concentration by diluting the original colloids (as purchased from the supplier) with deionized water. Therefore, the amount of dissolved substances present in each test particle suspension is due to the original colloids. Considering the choice of particle suspensions for filter retention efficiency determination, in addition to particle size, shape, size distribution, it is also important to concern about the ionic strength of the electrolyte solution, which will affect the adsorption efficiency of particles to the filter surface. In general, the lower the ionic strength, the higher the energy barrier for particle adsorption (for particles and filter surface having the same charge sign), i.e., lower retention efficiency.

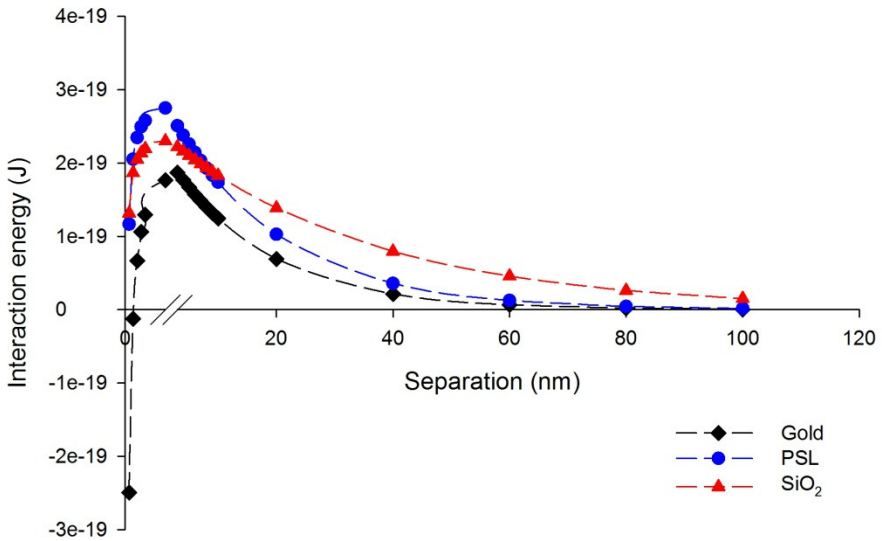

Figure 5-4. Computed DLVO energy profiles between filter surface and 50 nm particles of different materials.

Polydisperse vs monodisperse particle tests

For practical consideration, real life particles that membrane filters are expected to handle are polydisperse, instead of monodisperse. Figure 5-5 shows the retention efficiency measured using mixed 80, 50 and 30 nm gold particles of equal number concentration. The results are compared to that measured with monodisperse gold particles. From Figure 5-5a, the retention efficiencies of 80 and 50 nm gold particles measured with monodisperse and polydisperse particles are comparable to each other. This indicates that the presence of smaller particles has little effects on the retention efficiency of bigger particles. However, for the smaller particles (30 nm), the presence of the bigger particles increases their retention efficiency compared to that obtained with monodisperse particles. This observation can be explained by similar sieving arguments. Since 30 nm particles are less efficiently captured, they do not significantly plug the pores and affect the retention efficiency of 80 and 50 nm particles. On the other hand, the 80 nm particles captured, either by sieving or interception/diffusion, block portion of the smaller pores of the membrane filter and build up extra platform (inner cake within the filter thickness) for collecting the smaller particles. Studies have also reported higher retention efficiency and slower breakthrough for filtration of polydisperse particles than monodisperse particles. However, it should be noted that the retention efficiency for polydisperse particles is dependent on the size distribution of the particles tested and whether there present particles big enough for blocking the pores [Lee and Liu, 1994; Zahka and Grant, 1991].

a)

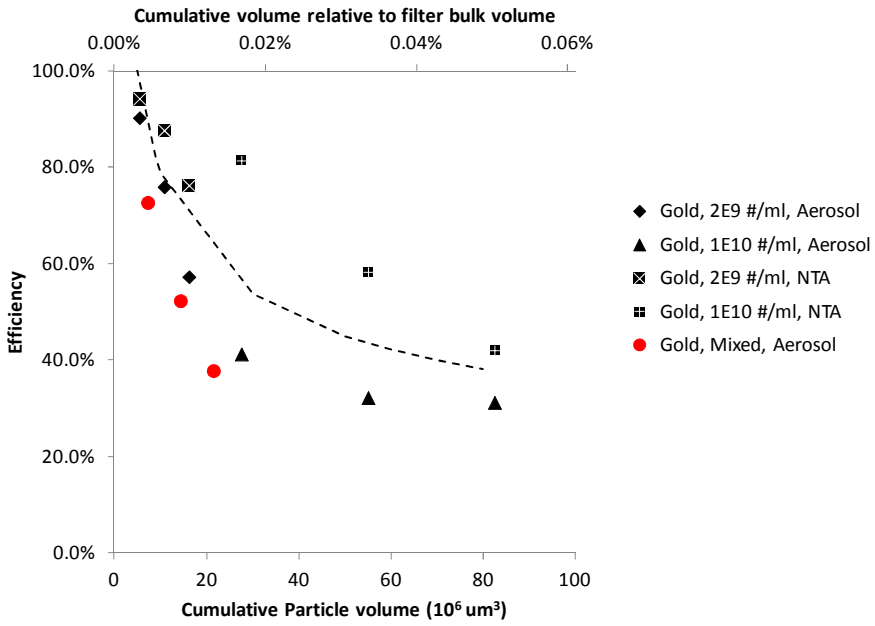
Cumulative volume relative to filter bulk volume
0.00%
0.02%
0.04%
0.06%
100.0%
80.0%
60.0%
40.0%
20.0%
0.0%
Efficiency
0
20
40
60
80
100
Cumulative Particle volume (10⁶ um³)
Gold, 2E9 #/ml, Aerosol
Gold, 1E10 #/ml, Aerosol
Gold, 2E9 #/ml, NTA
Gold, 1E10 #/ml, NTA
Gold, Mixed, Aerosol

b)

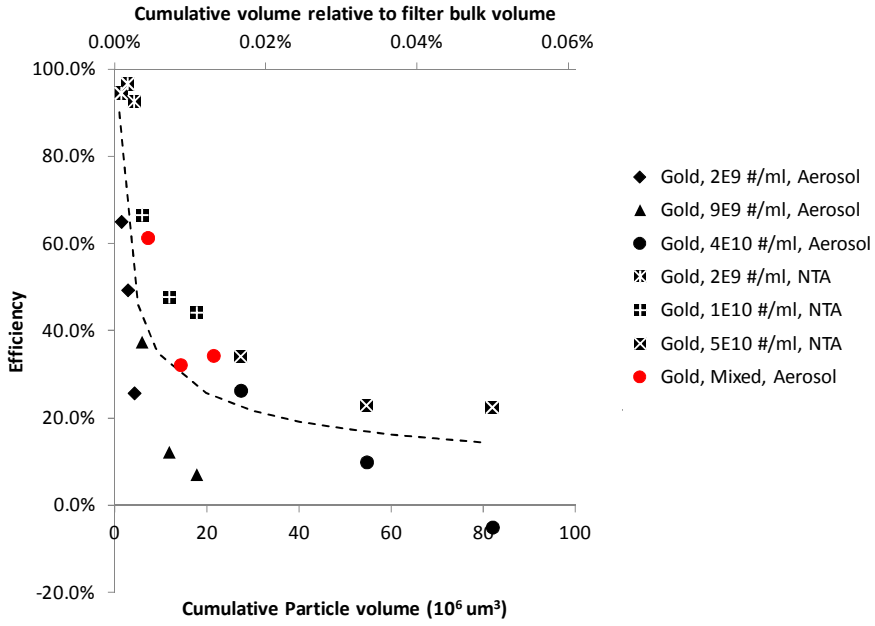
Cumulative volume relative to filter bulk volume
0.00%
0.02%
0.04%
0.06%
100.0%
80.0%
60.0%
40.0%
20.0%
0.0%
-20.0%
Efficiency
0
20
40
60
80
100
Cumulative Particle volume (10⁶ um³)
Gold, 2E9 #/ml, Aerosol
Gold, 9E9 #/ml, Aerosol
Gold, 4E10 #/ml, Aerosol
Gold, 2E9 #/ml, NTA
Gold, 1E10 #/ml, NTA
Gold, 5E10 #/ml, NTA
Gold, Mixed, Aerosol

c)

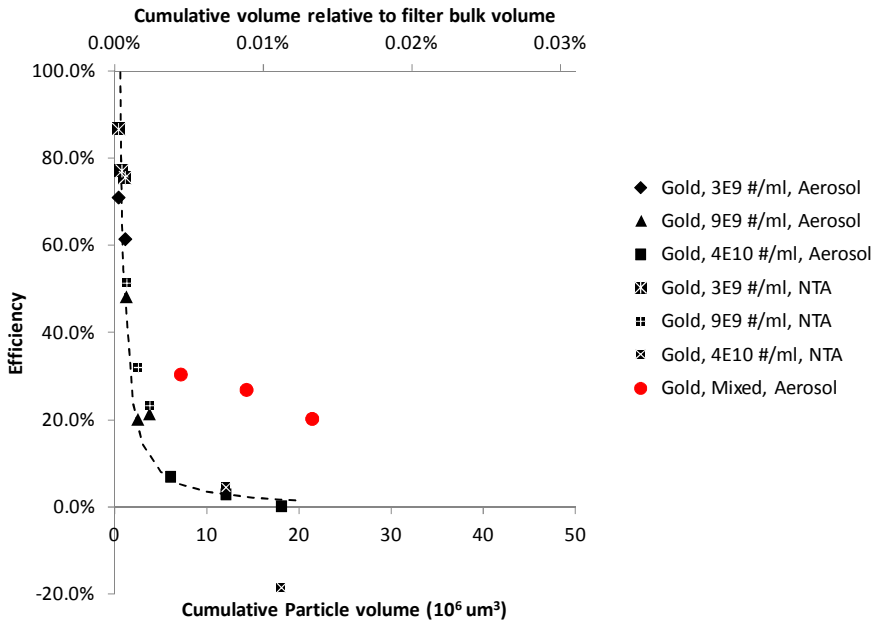

Figure 5-5. Comparison of the retention efficiency of a) 80, b) 50 and c) 30 nm gold particles between that measured with monodisperse and mixed (poludisperse) particles.

Particle entrainment

Figure 5-6 describes entrainment of gold particle by the fluid at the end of the filtration test. The percentage of particles entrained is calculated as follows:

$$Entrainment\ \% = \frac{number\ of\ particles\ entrained\ by\ 20\ ml\ water}{number\ of\ particles\ captured\ by\ the\ filter} \qquad \text{Equation 5-5}$$

Results indicate that particle entrainment can contribute up to 11% of extra particle penetration. This is considered to be relatively insignificant to the measured retention efficiency. However, to be more exact, the actual retention efficiency of the membrane filter excluding the effects of entrainment can be corrected as: $(1 - Eff_{Observed}) = (1 - Eff_{Filter}) \times (1 - Eff_{Entrainment})$. It should be noted that results reported in Figures 5-1, 5- 2 and 5-5 are not corrected by this expression.

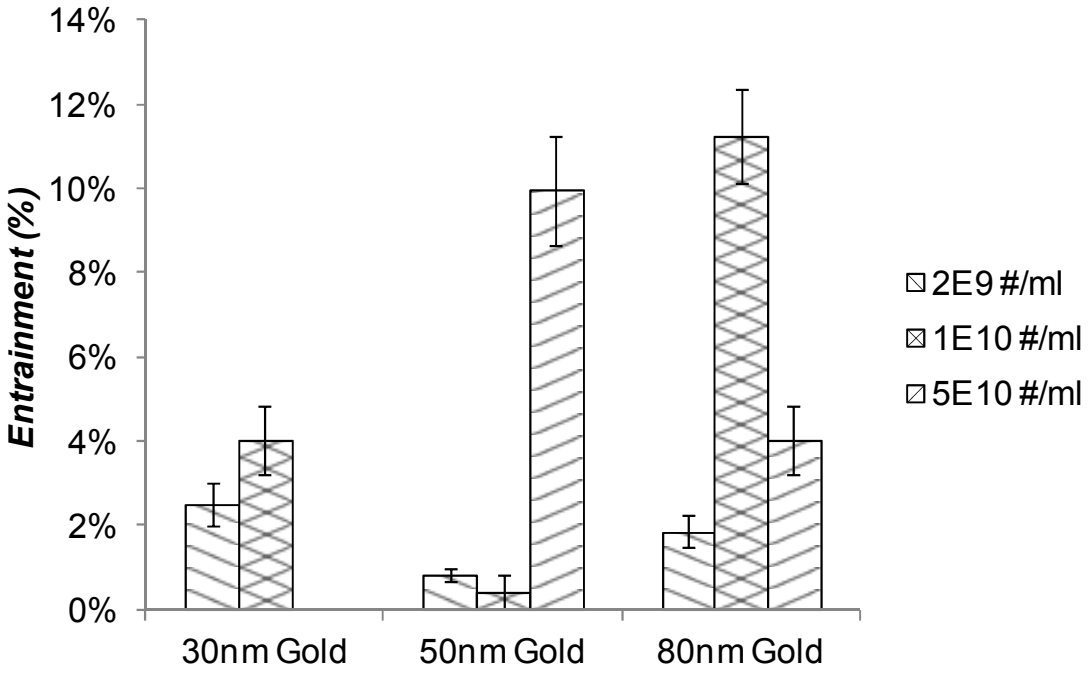

Figure 5-6. Percentage of particle entrainment measured with gold particles of different sizes.

Application to cleanroom filtration

As shown in Figure 5-2, the top horizontal axes indicate the volume of particles relative to the bulk filter volume. These plots can provide estimation for how long these filters can maintain the performance before breakthrough. In this study, filtration experiments were performed using suspensions with concentration of E9-E11 particles/ml, which is much higher than that found in typical semiconductor process fluids. Literatures have reported that most semiconductor process fluids contain between 1-200 particles/ml (> 500nm) [Zahka and Grant, 1991]. Nanoparticles may present with higher concentration, but should still be several orders of magnitude lower than the concentration being used in this study. The high concentrations of test particles were used due to the limitation of the measurement techniques.

Considering filter testing for Ultra Pure Water (UPW) used in semiconductor manufacturing, silica particles are preferred over PSL and gold particles. Firstly, silica

particles are naturally present in UPW, while PSL and gold particles are rarely found in UPW. Therefore, silica will provide a more realistic challenge to the filters. In addition, from the discussion on particle material dependence in the previous section, it was seen that silica particles showed the lowest retention efficiency. This will represent the worst case scenario at the challenge test, i.e. sieving dominant with minimum favorable surface interactions. It has been suggested that surface modification can adjust the surface charge of gold particles, making them more representative to filtration conditions in UPW. However, this will lead to extra cost for filter evaluation [SEMI, 2012]. Table 5-2 summaries the properties of different particles tested in this work.

Table 5-2. Summary of properties of different particle materials tested in this work.

	Gold	**PSL**	**Silica**
Monodispersity	Good for all sizes	Good for particles > 50 nm	Dependent on manufacturers and batches
Detection	ICP-MS	NA	ICP-MS
Observed retention performance	Better	Better	Worst
Representative to actual contaminant in UPW	No	No	Yes

Note: The Detection section lists alternative method for particle detection other than optical particle counters. ICP-MS is the short form of Inductively coupled plasma mass spectrometry [SEMI, 2012].

The materials presented in this chapter are preliminary results on effects of different parameters on the retention efficiency measurements during filter evaluation. More systematic study on the factors affecting filtration performance will be desirable: 1) electrolyte concentration/ ionic strength of solutions, 2) pH value of solution, 3) surface properties of membranes and particles. In addition, for nanoparticle filtration, an appreciable fraction of the particles are captured by interception or diffusion, which can potentially be entrained by incoming fluids. Therefore, it will be worthwhile to

investigate the effects of the listed parameters on the entrainment of captured particles. Table 5-3 lists the properties of different particle and filter materials for considerations.

Table 5-3. Properties of different particle and filter materials

Particle materials	**Isoelectric point**	**Membrane materials**	**Isoelectric point**
Silica	~2	Polysulfone	~3
Silicon nitride (Si_3N_4)	~6	Polyvinylidene fluoride (GVHP)	~5
Alumina (Al_2O_3)	~7	Anodized aluminum oxide (Anopore)	~7

Note: Isoelectric point indicates the pH value at which the material carries no net surface charge [Kim et al., 1996; Yu and Somasundaran, 1996; Knutsen and Davis, 2006].

5.4 Summary

Liquid filtration has found many applications in environmental health and safety control as well as industrial processes. Sieving mechanism, which depends only on the relative size of the particles to pores, is primarily used to describe the filtration of liquid-bone sub-micron and nano-particles. Particles smaller than the pore size of a filter can still be captured by diffusion and interception mechanisms (adsorption), when the particle-filter surface interactions are favorable as described by the electrostatic and van der Waals interactions (DLVO theory). In this study, we measured retention efficiency of a 50 nm-rated PTFE type filter against nanoparticles of different materials (gold, PSL and silica), sizes (80, 50 and 30 nm) concentrations (2E9 -4E11 particles/ml) and size distributions (monodisperse and polydisperse). For monodisperse particle test, a decreasing trend as a function of cumulative particle volume has been observed. This can be explained by the sieving mechanism. Comparing the decreasing trend among different particle materials, we observed that silica particles have much lower retention efficiency compared to PSL and gold particles of the same size. The observation can be explained in part, by the interplay among membrane, particle and liquid media properties. Silica, gold and PSL particles have different concentration of dissolved substances, as indicated by the

electrolyte conductivity. The DLVO theory indicates that the lower ionic strength of silica particles experience higher repulsion interactions over a longer distance than PSL and gold particles. Finally, it is observed that retention efficiency is higher for test run with polydisperse particles than that with monodisperse particles.

Chapter 6

Numerical modeling of nanoparticle filtration: effects of loaded particles on the retention efficiency

6.1 Introduction

Filtration of liquid-borne particles by membrane filters usually gives a decreasing trend of retention efficiency as a function of particle loading [Beuscher 2010, Zahka and Grant, 1991]. The rate of retention efficiency decrease will depends on the particle properties, pore size distribution and other filtration parameters. The observation is usually described by the pore blockage model [Lee and Liu, 1994]. The model assumes membrane filter captures particles as a sieve and completely retains all particles larger than its rated pore size. Membrane filters are usually tested with monodisperse particles for determining their filtration efficiency. However, real-world particles are likely to be polydisperse [Lee at al., 1994]. It has been observed that the retention efficiency is always lower when membrane filters are challenged with monodisperse particles than the case when they are challenged with polydisperse particles or a mixture of particles with some larger sizes. It is believed that the larger particles captured by the filter enhance the collection efficiency of the smaller particles by providing extra platform or inner cake as a collection site. However, this only provides a qualitatively explanation to the observation.

One of the challenge of modeling a membrane filtration is to accurately represent the membrane structure. There are many different types of membrane filters. They can be made of different materials, e.g.: cellulose esters, polyvinyl chloride, nylon, polyproplene, polyvinyldene fluoride (PVDF), polytetrafluoroethylene, polycarbonate, sintered metal and others. The manufacturing process can be casting, stretching, additive leach, sintering, track-etching, etc [Rubow and Liu, 1986]. Scanning electron microscopy (SEM) images of different types of conventional membrane filters are shown in Figure 6-1. These figures show 1) the inter-connected void space of the membrane and 2) the fiber-like nature of the connecting links in the filter structure. An exception is the

nuclepore filter, which has a straight capillary tube like pore structure. Ideally, the model should be based on the exact geometric representation. However, due to complex and random nature of the void spaces within the membrane, numerical modeling of particle penetration through membrane filters haven been approached by comparing the fluid flow field to a simplified structure [Rubow and Liu, 1986]. Researchers have used two different models to describe the particle collection characteristics: 1) the capillary tube model [Menton, 1978; Menton 1979; Heidam 1981; Smutek and Pich, 1974; Parker and Buzzard, 1978; Kanaoka et al., 1978; Spurny et al., 1969; Smith and Phillips 1975] and 2) the fibrous filter model [Logan 1993; Friedlander 1958; Pich, 1966]. The choice of an appropriate model is not straightforward. The capillary tube model is commonly used for describing the transient filtration process with particle loading, while the fibrous model has been used for predicting aerosol particle deposition in clean membranes. The basics of the two models are described in the following paragraphs.

a) b)

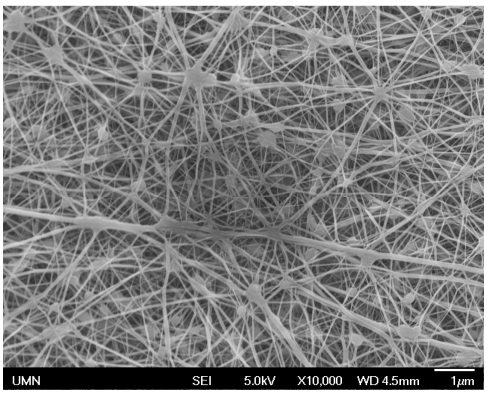

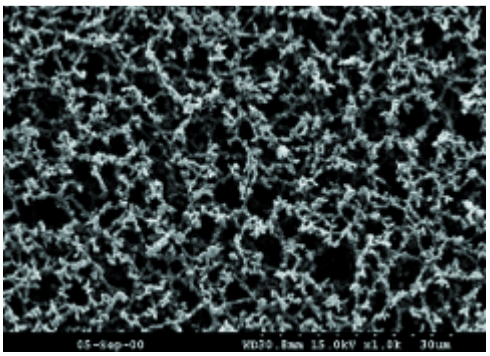

c)

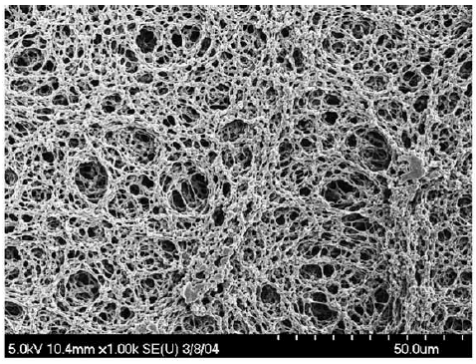

Figure 6-1. SEM images of different membrane filters: a) PTFE, b) cellulose acetate and c) PVDF [Whatman, Singh et al., 2005]

In capillary tube model, the filter is represented by an assembly of straight capillary tubes of circular cross section. The tubes are parallel to each other and perpendicular to the filter surface. The diameter of the tubes is assumed to be equal to the diameter of the pores in the real filter [Rubow and Liu, 1986; Heidam 1981]. The fluid flow field through the pore is relatively straight-forward to represent. Researchers have obtained numerical and analytical solutions for uniform and parabolic velocity profiles at the pore entrance [Spurny et al., 1969, Smith et al., 1976]. The model also assumes that there is no flow interaction between neighboring pores. The retention efficiency of a pore will be same as that of a clean filter. There has been little study on the change in retention efficiency in a partially blocked pore.

For fibrous filters, common theoretical model is to study particle collection onto 1) a straight cylindrical element, as a representation of a single fiber, or 2) a structured array

of it, lying parallel to each other and perpendicular to the direction of the fluid flow [Friedlander 1958; Hinds 1998]. Kuwabara has derived fluid flow field for a system of cylindrical elements, known as the cell model. It accounts for the interference caused by adjacent cylindrical elements [Kuwabara 1959]. This simplification has limited accounting for the random nature of the membrane filter. The fibrous model determines the particle collection efficiency of a single fiber, η. The collection efficiency of an overall filter can be determined by material balance around a single fiber, according to the following derivations [Friedlander 1958; Hinds 1999]:

The removal efficiency of a single fiber is defined as:

$$\eta = \frac{b}{d_f} \qquad \text{Equation 6-1}$$

The number of fibers per unit filter area can be given as:

$$\alpha = \frac{\frac{1}{4}\pi {d_f}^2 n}{1}$$
$$n = \frac{4\alpha}{\pi {d_f}^2} \qquad \text{Equation 6-2}$$

In a differential filter thickness *dh*, in the flow direction, the fractional particle removal (per unit cross-sectional area) is given as:

$$\gamma = b \times n \times dh = \eta d_f \frac{4\alpha}{\pi {d_f}^2} dh = \eta \frac{4\alpha}{\pi d_f} dh \qquad \text{Equation 6-3}$$

The overall particle removal can be determined as:

$$-\frac{dN}{N} = \gamma dh$$

$$\int_{Nin}^{Nout} \frac{dN}{N} = \int_{0}^{H} -\gamma \, dh$$

$$ln\frac{N_{out}}{N_{in}} = -\gamma H \qquad \text{Equation 6-4}$$

$$P = \frac{N_{out}}{N_{in}} = e^{-\gamma H} = exp\left[\frac{-4\alpha\eta H}{\pi d_f}\right]$$

where:

d_f = Fiber diameter

α = Solid fraction

N = Concentration of particles passing through

η = Single fiber removal efficiency

b = Width which corresponds to the region of flow completely cleared of all particles by the cylinder

dh = Differential thickness of filter

n = Number of fibers in a unit area

γ = Fractional particle removal (per unit cross-sectional area)

In general, the value of η represents the initial efficiency of clean, un-loaded filters. As particles load onto the fiber, the value of η will change.

To describe the fluid flow field and particle capture efficiency through a pore or across a single fiber, both analytical and numerical solutions have been reported, with various assumptions and simplifications. With the advance in computational fluid dynamics (CFD) techniques, studying filtration problems with more realistic, less-simplified, 3-dimensional filter model structures is possible. For example, the Fluent and CFX CFD codes have been applied to model the non-woven filtration process in random 3-D

geometries [Wang et al. 2006; Hosseini and Tafreshi 2010; Ling et al., 2012]. The aim of this work is to study the effects of the presence of larger particles on membrane filter's retention efficiency of smaller particles, using ANSYS CFX.

6.2 Modeling approach

Numerical modeling was performed to study the filtration efficiency of 30 nm particles for the following cases:

1) Capillary tube model
    a) a clean cylindrical tube
    b) a cylindrical tube partially blocked by a larger particle
2) Single fiber model
    a) a clean straight cylindrical element, as a representation of a single fiber
    b) a cylindrical element with a larger particle attached onto it

The modeling conditions were applied to match with those used in the experiments described in the previous chapter. The simulation domain was constructed using ANSYS Design Module. Pore size distribution of membrane filters is usually described using the Gamma distribution [Beuscher 2010; Johnston 1998]:

$$f(x) = \frac{\beta^a}{\Gamma(a)} x^{a-1} e^{-\beta x} \qquad \text{Equation 6-5}$$

where:

a = Distribution shape factor, indicator of the broadness of the distribution

β = Scale factor

$\Gamma(a)$ = (a-1)!

Beuscher reported that the pore size distribution of a 30 nm rated PTFE filter can be represented by gamma distribution with a=2 and β=0.015 [Beuscher 2010]. The

distribution is shown in Figure 6-2. It can be seen that only 18% of the pore is smaller than 50 nm. Therefore, we estimated that there are higher fraction of pores larger than its rated pore size for the PTFE membrane used in our experiments, which is rated at 50 nm. The simulation domain for case 1 is a cylindrical volume with a wider inlet opening. The length of the cylindrical pore are estimated based on the membrane thickness. We simulated the cases in which the pores have a diameter of 100 and 200 nm. Pores larger than 100 nm are expected to be present in a high fraction and large enough to capture particles by interception instead of sieving. The inlet opening dimensions are adjusted based on the porosity of the membrane filter. Porosity is the fraction of void volume in the filter and is assumed to be 0.1. An example of the simulation domain for case 1b), i.e., a cylindrical tube partially blocked by a particle, is shown in Figure 6-3. Since particle capture by interception is likely to take place near the pore opening, the particle is located immediately below the pore opening. Because of symmetry, only half of the cylindrical pore is simulated.

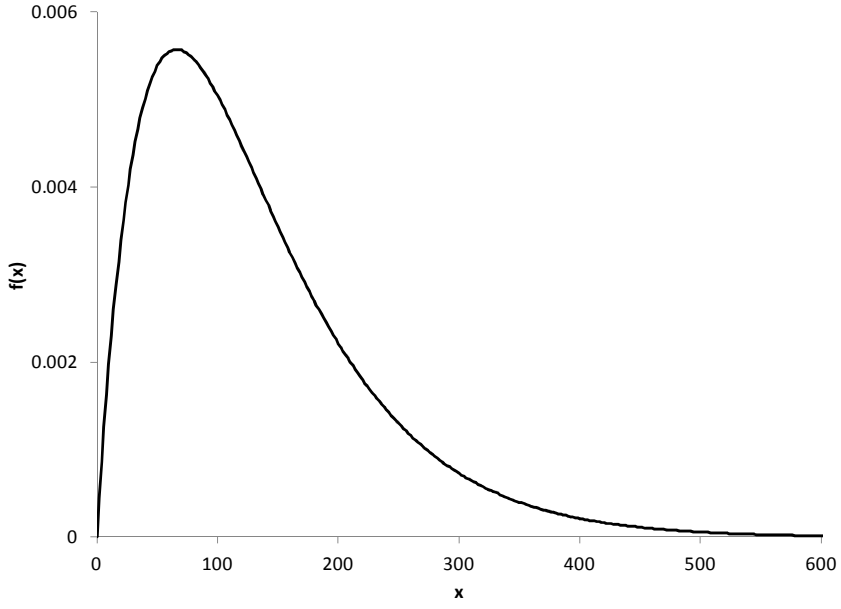

Figure 6-2. Gamma distribution with a=2 and β=0.015, representing the pore size distribution of a 30 nm rated PTFE membrane.

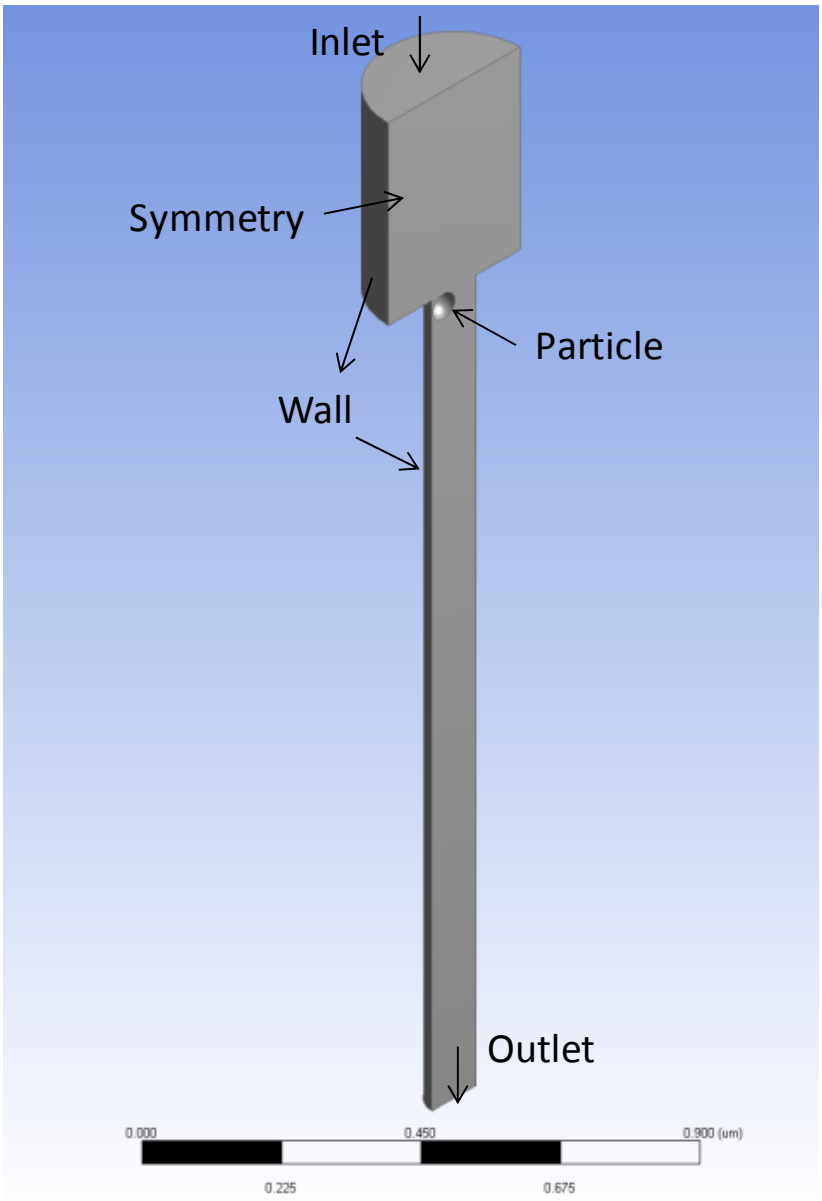

Figure 6-3. Simulation domain for the case of a cylindrical tube (diameter = 100 nm) partially blocked by a 50 nm particle.

The simulation domain for the case 2a, i.e., a clean straight cylindrical element, is a rectangular box of fluid with dimensions 0.5 µm by 1 µm by 3 µm (Figure 6-4a). The diameter of the cylinder is 50 nm, average fiber diameter based on the observation from SEM images of the FTPE membrane (Figure 6-1a). The fiber is located 1µm from the

inlet and 2µm from the outlet. The distance is longer than the suggested value such that the simulation results will be independent of where the inlet and outlet boundary conditions are prescribed [Wang et al., 2011]. For case 2b, we study the cases when a particle is captured at 0 degree and 45 degree measured from the direction of inlet fluid flow (Figure 6-4b, 6-4c). Symmetry conditions are set for the four remaining sides of the simulation domain.

a)

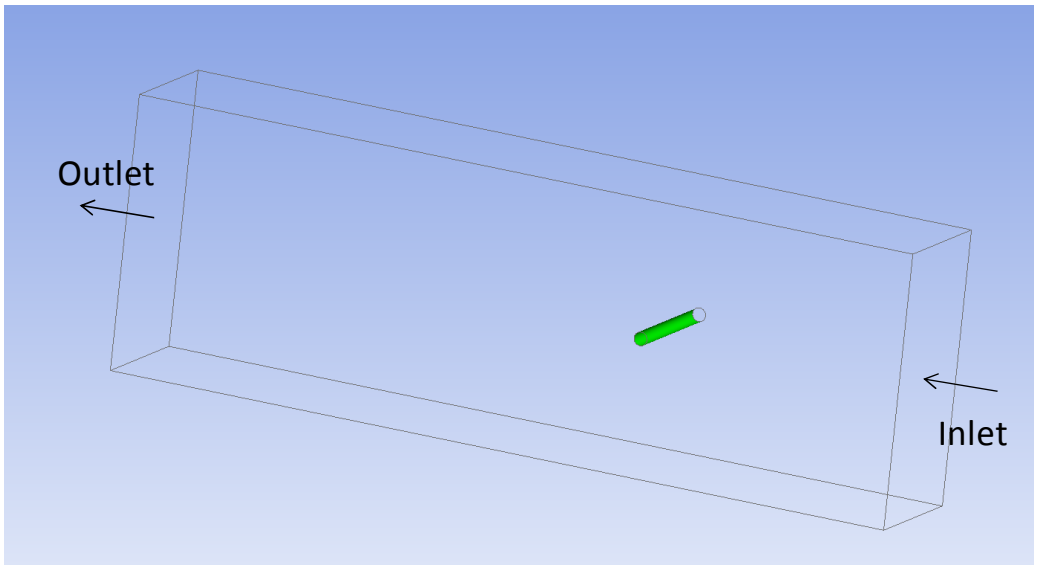

b)

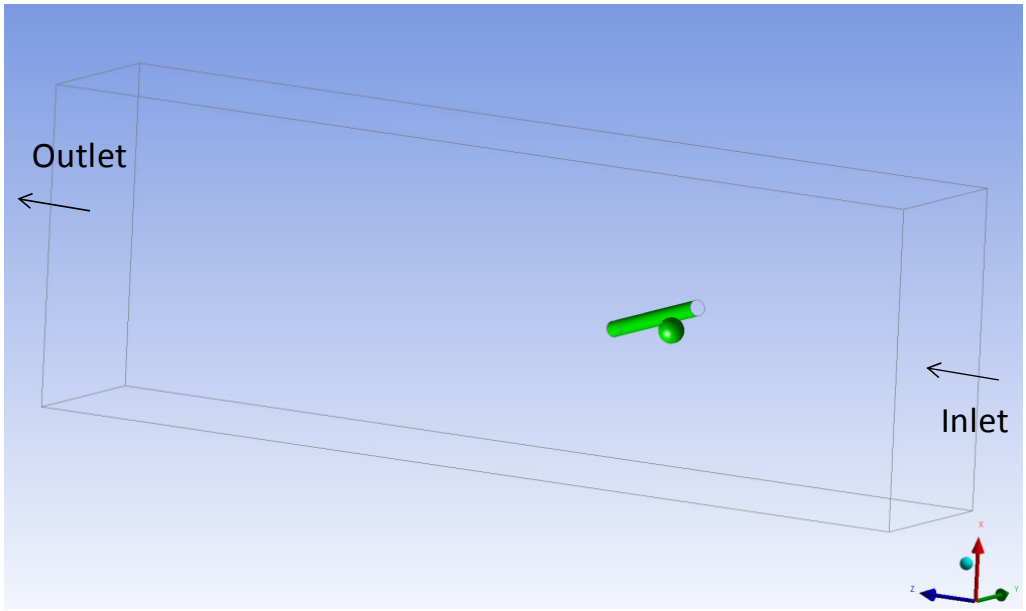

c)

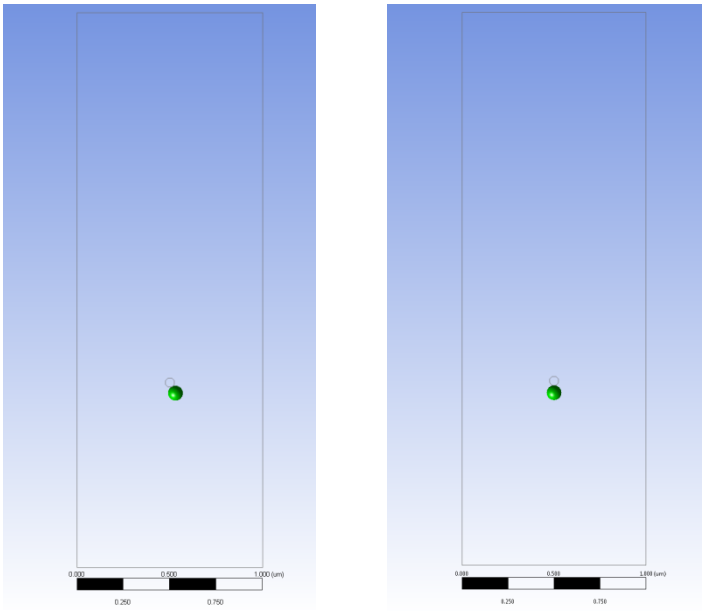

Figure 6-4. Simulation domain for single fiber model: a) clean straight cylindrical element representing a bare fiber (50 nm in diameter), b) a cylindrical element with a particle (80 nm) attached onto it, c) Top view of the simulation domain to indicate the location of particle on the cylindrical element.

We performed the numerical simulation using the computational fluid dynamic code CFX, ANSYS. The simulation can be considered to have two parts: 1) fluid flow and 2) particle tracking. The fluid flow through the domain is simulated by solving the steady state incompressible Navier-Stokes equation and the continuity equation.

Navier-Stokes

$$\rho\left(u\frac{\partial u}{\partial x}+v\frac{\partial u}{\partial y}+w\frac{\partial u}{\partial z}\right)=-\frac{\partial P}{\partial x}+\mu\left(\frac{\partial^2 u}{\partial x^2}+\frac{\partial^2 u}{\partial y^2}+\frac{\partial^2 u}{\partial z^2}\right) \quad \text{x-direction}$$

$$\rho\left(u\frac{\partial v}{\partial x}+v\frac{\partial v}{\partial y}+w\frac{\partial v}{\partial z}\right)=-\frac{\partial P}{\partial y}+\mu\left(\frac{\partial^2 v}{\partial x^2}+\frac{\partial^2 v}{\partial y^2}+\frac{\partial^2 v}{\partial z^2}\right) \quad \text{y-direction} \qquad \text{Equation 6-6}$$

$$\rho\left(u\frac{\partial w}{\partial x}+v\frac{\partial w}{\partial y}+w\frac{\partial w}{\partial z}\right)=-\frac{\partial P}{\partial z}+\mu\left(\frac{\partial^2 w}{\partial x^2}+\frac{\partial^2 w}{\partial y^2}+\frac{\partial^2 w}{\partial z^2}\right) \quad \text{z-direction}$$

Continuity

$$\frac{\partial u}{\partial x}+\frac{\partial v}{\partial y}+\frac{\partial w}{\partial z}=0 \qquad \text{Equation 6-7}$$

As for the boundary conditions, uniform velocity profile, which is perpendicular to the inlet surface, is prescribed at the inlet of the simulation domain. The inlet velocity corresponds to the conditions used in our experiments, i.e. face velocity = 0.07 cm/s. On the surfaces of the pore wall, attached particle and fiber, no slip condition is applied, i.e. all components of velocity equal to zero.

To simulate particle capture, particles are added to the simulation domain using the Particle Transport Model of CFX. It uses the Lagrangian approach to describe motion of a particle across the simulation domain using the force balance equation [ANSYS CFX manual]:

$$m\frac{du_{particle}}{dt}=f\left(u_{fluid}-u_{particle}\right)=F_{drag} \qquad \text{Equation 6-8}$$

CFX gives the trajectories of the particle centers. The particle capture mechanisms considered include impaction and interception. Particles, possessing finite mass and momentum, are captured by impaction onto a surface when they deviate from the fluid streamline as the fluid changes direction due to the presence of obstacles. Particles are captured by interception when they follow the fluid streamlines but travel within a

distance equal to or less than the particle's radius from the surface. In our simulations, the consideration of particle size for interception capture is taken into account by comparing the distance of the particle center to the surface of the pore/fiber/captured particle. We released 2500 particles distributed evenly on the inlet surface of the simulation domain and followed their trajectories. The penetration can be determined by comparing number of particles going into and out of the simulation domain. Particle diffusion takes place along the whole length of the cylindrical pore and all surface of the fibers. Therefore, we expect that the effects of the presence on a larger particle near the pore opening or on the fiber surface on diffusion particle capture is less significant compared to impaction and interception. Therefore, particle capture due to diffusion is not considered in this study. Additionally, the electrostatic forces and other surface interaction forces on particles are assumed to be negligible.

Mesh with tetrahedral cells is used to discreticize the simulation domain. The mesh is very fine near the surfaces of the pore, cylindrical element or attached particle, where large fluid velocity gradient is expected. The size of cells gradually increase as the distance from the surfaces becomes larger. We have ensured the simulation results are grid-independent and the numerical uncertainty in the solution presented is <10%, calculated using the method suggested by Celik et al. [Celik et al., 2008].

6.3 Results and discussions

Capillary tube model

Figure 6-5 shows the vector plot of water flow through the capillary pore, with a particle attached near the pore opening. The pore opening and particle diameters are 100 nm and 50 nm, respectively. The vectors are colored by velocity magnitude. The water entering the domain at face velocity = 0.07 cm/s, same as the experimental condition. Entering the pore, the velocity is highest when the fluid bends abruptly due to the presence of captured particle. After passing the particle, it resumes the typical parabolic velocity profile quickly. Representative tracks of 30 nm particles are shown in Figure 6-6. The tracks

show the trajectories of the particle centers. Most particles successfully penetrate the capillary pore. Particle A impacts onto the 50 nm particle previously captured. Particle B impacts onto the pore opening. Particles C, D, E represent those that are too close to the surface of the particle or pore, and collected by interception.

a)

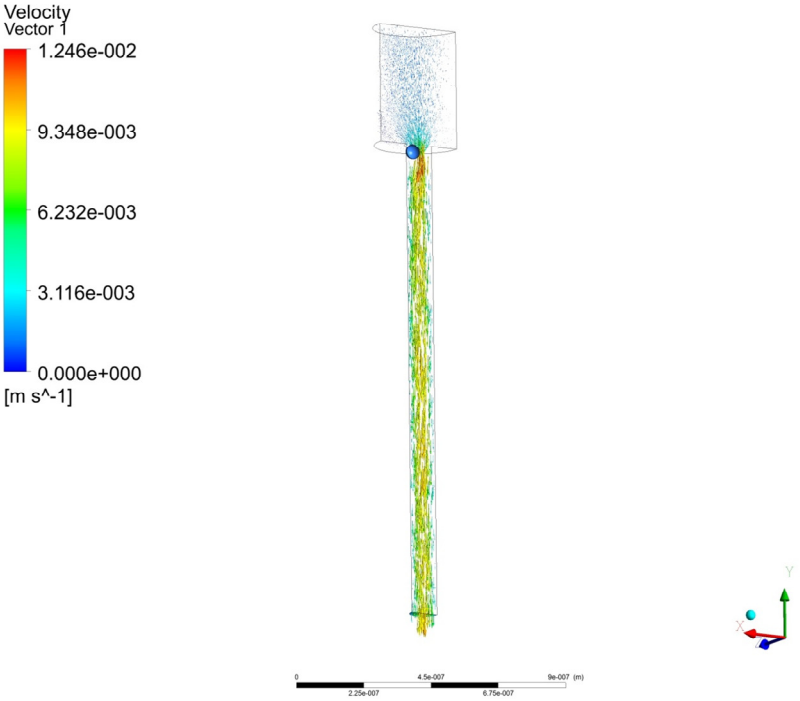

b)

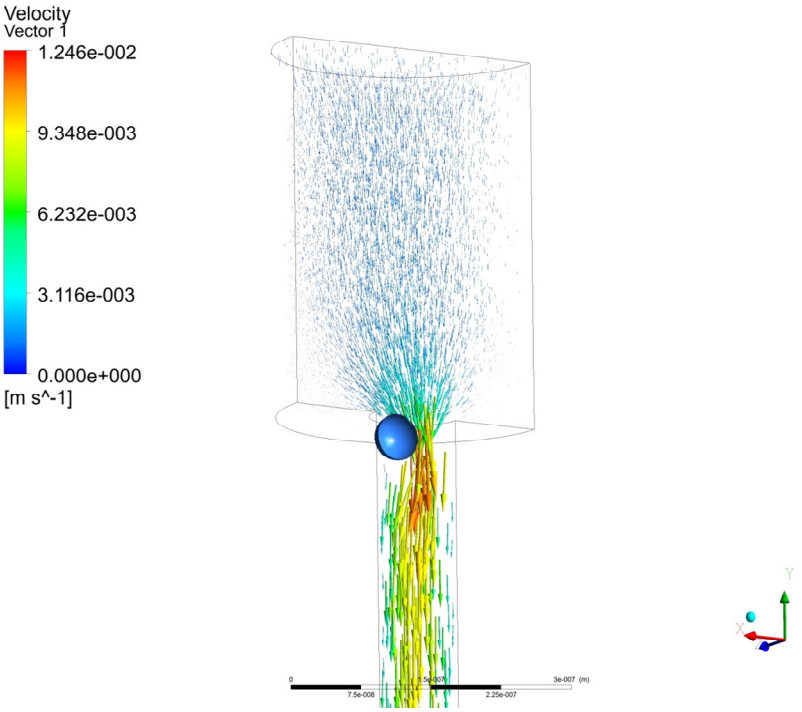

Figure 6-5. Vector plot of water flowing through the capillary pore blocked by a particle near the inlet: a) Full view, b) Zoomed-in view at the inlet portion.

a)

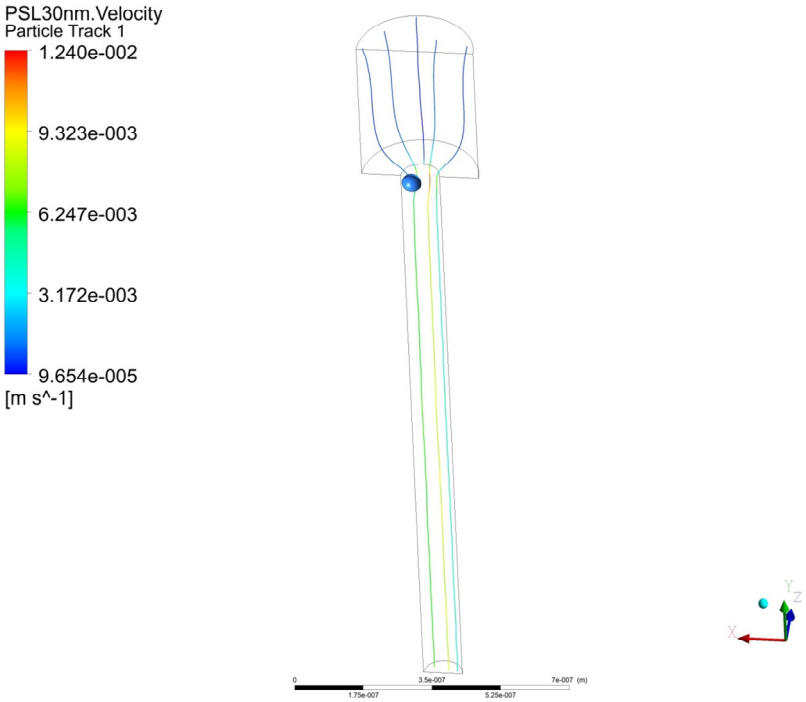

b)

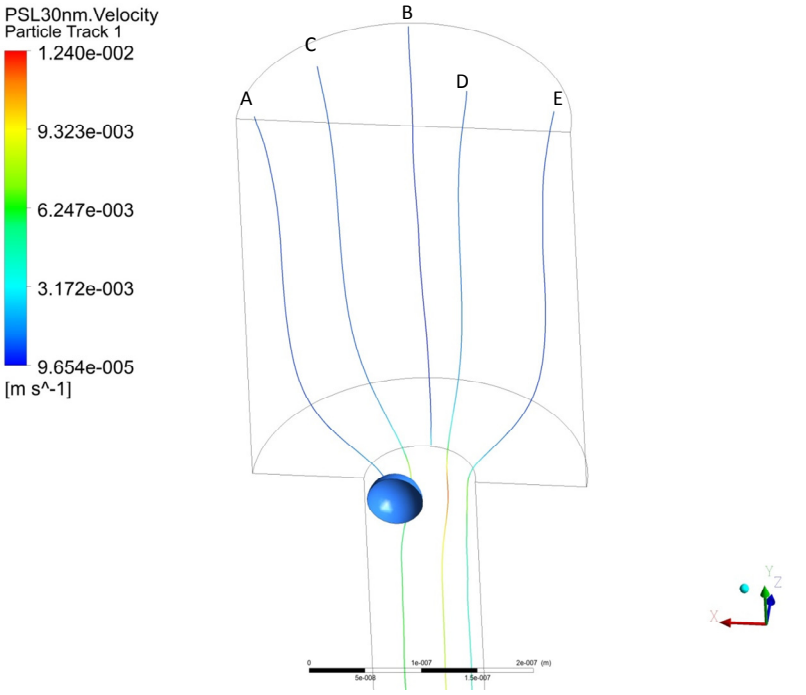

Figure 6-6. Representative tracks of 30 nm particles flowing through the capillary pore blocked by a particle near the inlet: a) Full view, b) Zoomed-in view at the inlet portion.

Figure 6-7 summarizes the results of the numerical simulation for different cases. It plots the retention efficiency of 30 nm particles by a cylindrical pore as a function of the size of the particle previously captured at the pore opening. A clear un-blocked pore is represented at zero particle size on the horizontal axis. Cases include cylindrical pore diameter of 100 and 200 nm. We did not perform the simulations for smaller cylindrical pores because particles are very likely to be captured by direct size exclusion (i.e., sieving) if there is a particle previously captured at the pore opening. For example, an 80 nm pore with a 50 nm particle captured at the pore opening will directly capture a 30 nm particle. The particle retention efficiency of a clear un-blocked pore as predicted by different capillary tube models is also shown [John et al., 1979; Rubow and Liu, 1986]. There is considerable difference between different capillary tube model expressions. The disagreement is probably caused by the approximations used to solve for the flow-field at the pore inlet. For example, John et al. [1976] assumed a fully developed parabolic velocity profile at the pore entrance. It is expected that would cause considerable disagreements as particle interception mainly take place at the pore inlet. In fact, disagreements have been noted and compared among other similar capillary tube models reported in the literatures [Heidam 1981]. In general, our results are comparable to the widely used capillary tube model expressions, suggesting the validity of the simulation results.

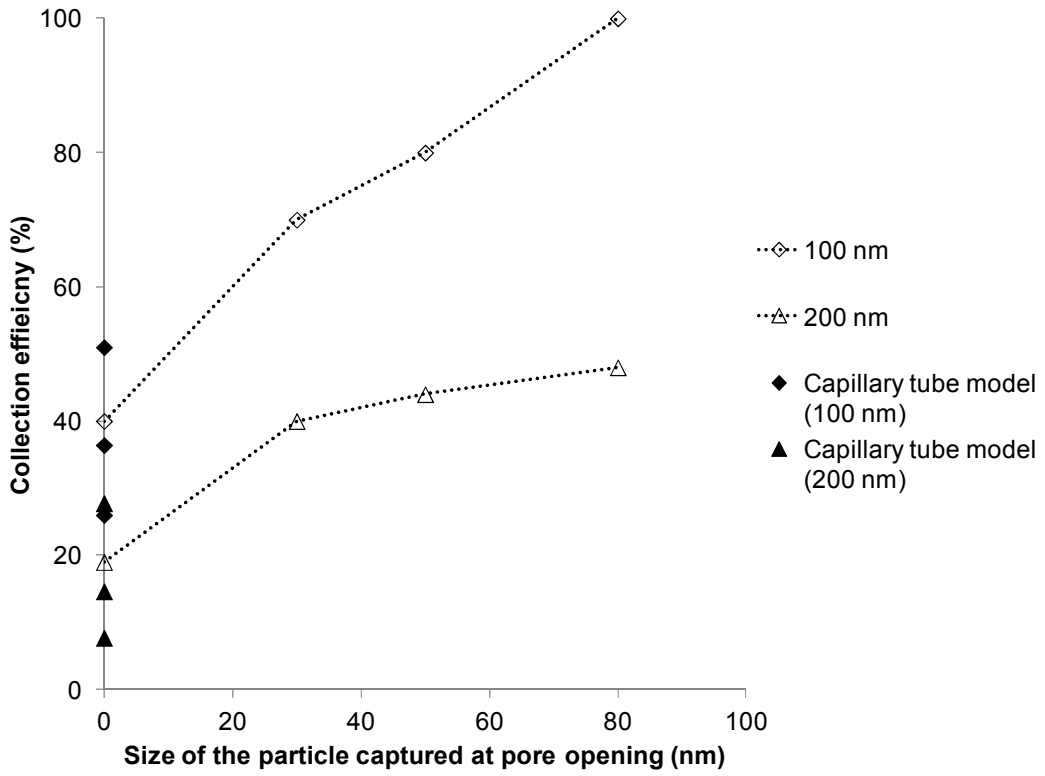

Figure 6-7. Summary of the numerical simulation results for capillary tube model of different cases: Collection efficiency of 30 nm particles by impaction and interception at different pore sizes (100 and 200 nm) and with/without a particle previously captured at the pore opening.

The simple way of modeling membrane filtration is to 1) represent a filter by layers of parallel pores with a certain pore size distribution and 2) determine if particles can pass through different layers and get out of the filter based on size exclusion (sieving) mechanism . Particles larger than the pore size are considered to be captured. The corresponding pores are completely plugged and not available for further particle passage. It has been reported that such model can represent the retention behavior of common membranes [Lee and Liu, 1992; Beuscher, 2010]. However, these models ignore the probability for a pore to capture a particle smaller than the pore size by adsorption, and the effects of partially blocked pores. The simulation results reported can

be incorporated into such models to better represent the fate of particles smaller than the pore size when they transverse across the membrane filter.

Single fiber model

Simulations on a bare cylindrical element were first performed to determine the probable locations that a particle will be captured at. Figure 6-8 shows the vector plot of water flow across the bare cylindrical element. Fluid enters the simulation domain with uniform profile. It can be seen that the velocities are close to zero near the cylinder surfaces and the velocity magnitude is largest at the symmetric planes. Figure 6-9 shows the representative tracks of 80 nm particles flowing across the cylindrical element. Since the tracks only represent the trajectories of the particle centers, a grey surface covering locations corresponding to a distance of the particle radius from the cylindrical element was included in Figure 6-9 to indicate where particle interceptions take place. In other words, particle centers hitting the grey cylinder will be captured by interception, and tracks after that are not valid. It can be seen that particles can be impacted onto the cylindrical element at close to 0 degree, measured from the direction of the inlet fluid flow. On the other hand, particles can also be captured by intercepting onto the cylindrical element at higher degree. Therefore, in the subsequent study, two cases will be considered: a particle is captured at 1) 0 degree and 2) 45 degree measured from the direction of fluid flow.

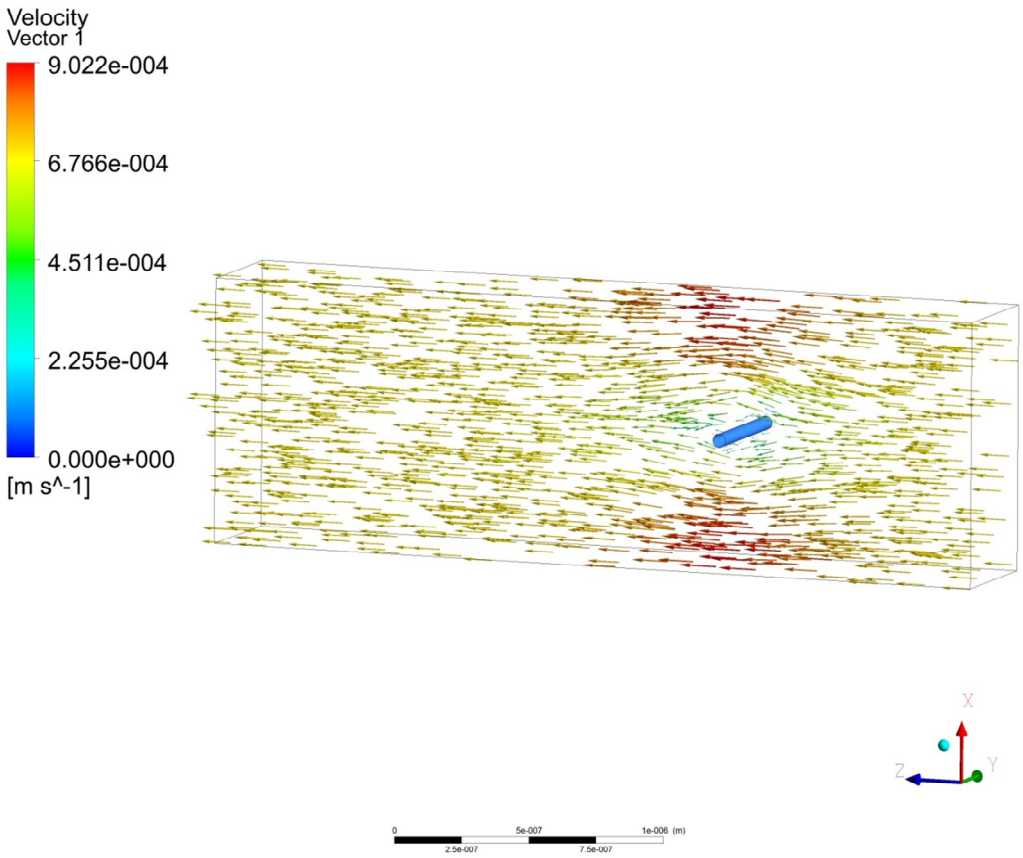

Figure 6-8. Vector plot of water flowing across a clean straight cylindrical element.

a)

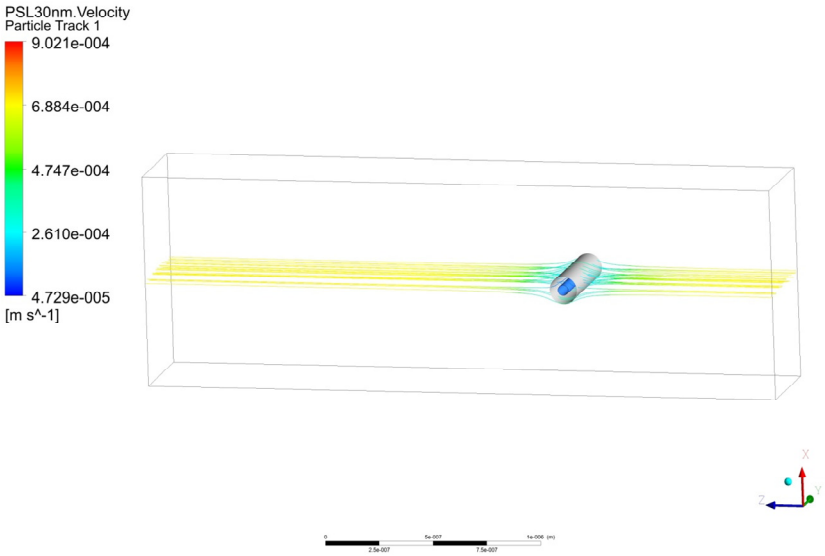

b)

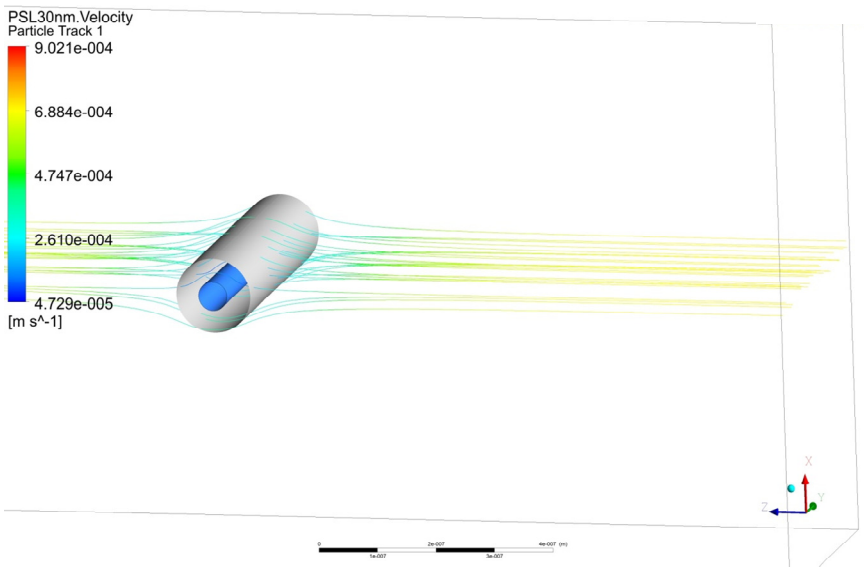

Figure 6-9. Representative tracks of 80 nm particles flowing across a cylindrical element (represented in blue, 50 nm in diameter): a) Full view, b) Zoomed-in view near the element. The tracks show the trajectories of the particle centers. The grey surface shown in the figure represents a distance of the particle radius from the cylindrical element. Therefore, tracks of particle centers hitting the grey cylinder will be captured by interception.

Representative tracks of 30 nm particles flowing across the cylindrical element with an 80 nm particle previously captured are shown in Figure 6-10 and Figure 6-11. It can be seen that the presence of the 80 nm particle can cause additional particle capture onto it. Figure 6-12 shows the computed single fiber efficiency due to impaction and interception for different simulation conditions. The classical single fiber efficiency [Hinds, 1998] due to interception on a clean fiber is also included in Figure 6-12 for comparison. The difference between the classical single fiber efficiency and the simulation result in this study can be explained by the assumed flow field. In determining the classical single fiber efficiency, the Kuwabara's flow field was applied [Kuwabara, 1979]. The Kuwabara flow was developed analytically with conditions which are different from our study: 1) Fluid medium is air; 2) Inertia effect is assumed to be negligible, because the Renoylds number for the flow is much smaller than unity, i.e. Stokes' flow; and 3) Flow field of an array of fibers, instead of an isolated fiber, are considered. Therefore, the effects of neighboring fibers are taken into account. In our study, the Reynolds number is higher because of the higher density of water than air.

a)

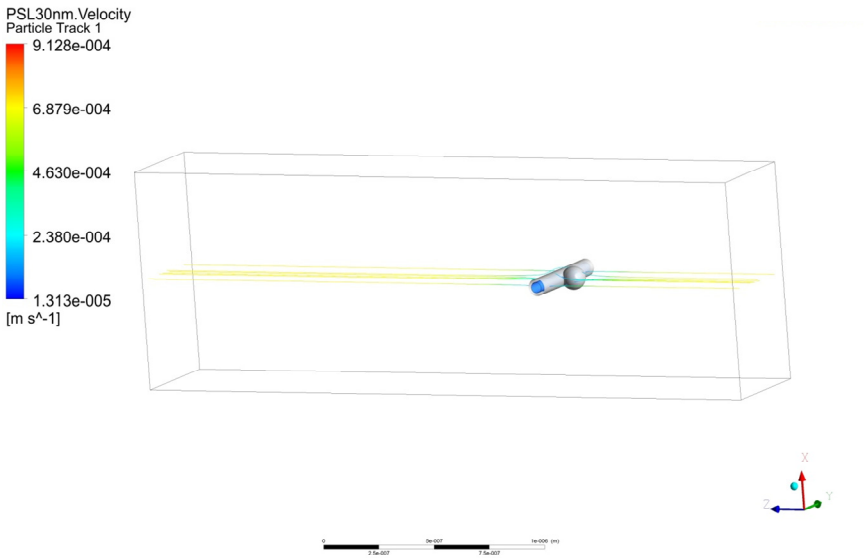

b)

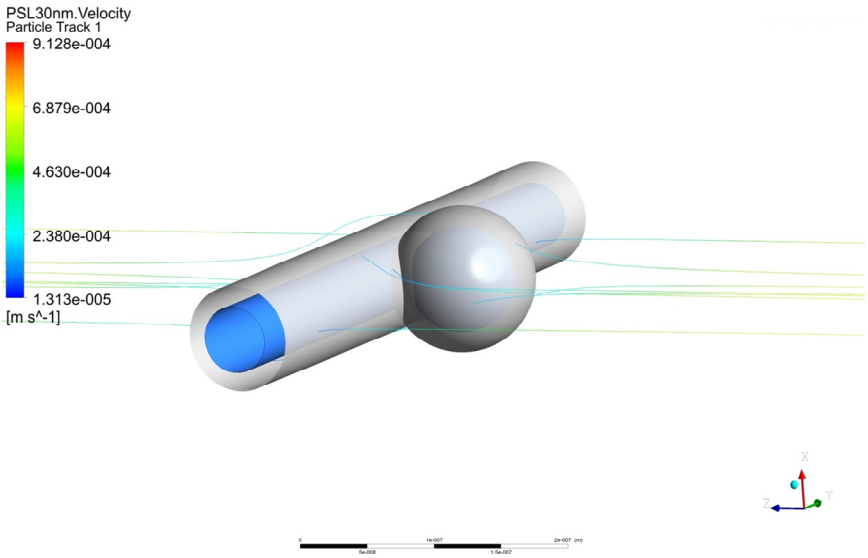

Figure 6-10. Representative tracks of 30 nm particles flowing across a cylindrical element with a particle deposited it at zero degree measured from the fluid flow direction: a) Full view and b) Zoomed-in view near the cylindrical element. The tracks show the trajectories of the particle centers. The grey surface shown in the figure represents a distance of the particle radius from the cylindrical element. Therefore, tracks of particle centers hitting the grey cylinder will be captured by interception.

a)

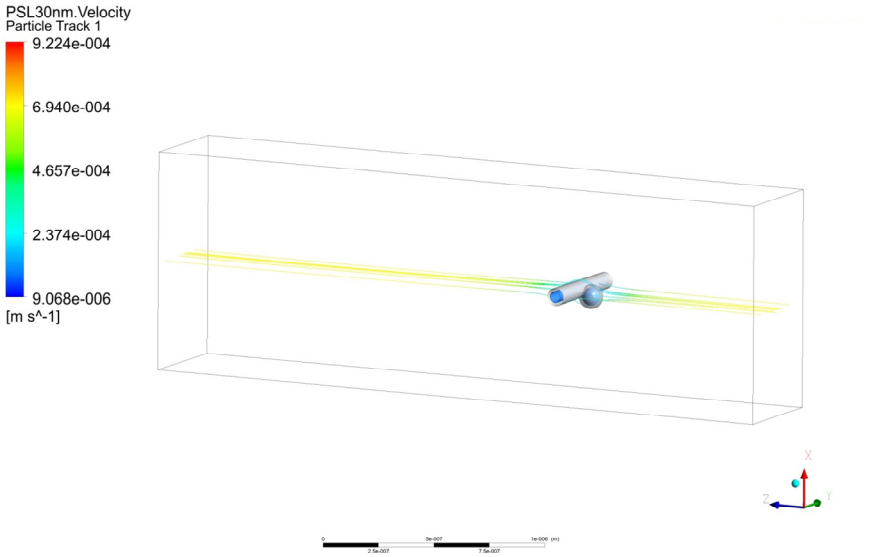

b)

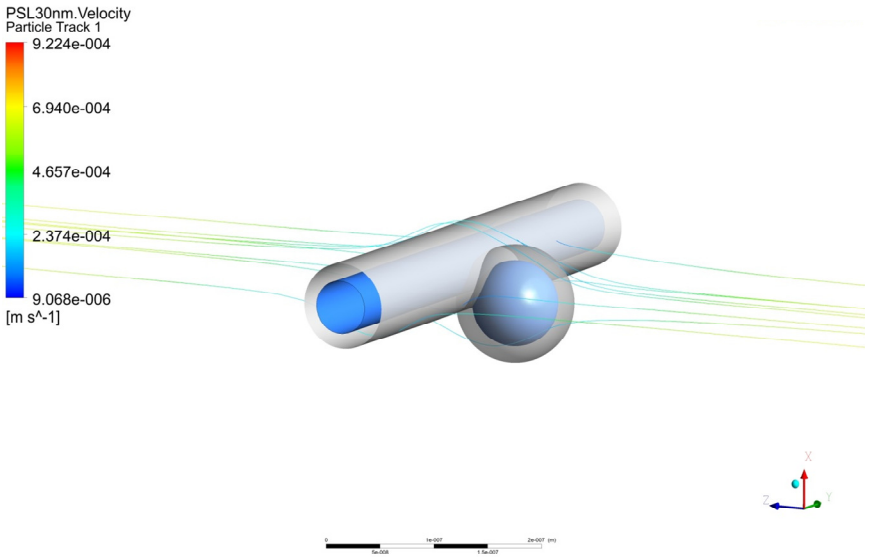

Figure 6-11. Representative tracks of 30 nm particles flowing across a cylindrical element with a particle deposited it at 45 degree measured from the fluid flow direction: a) Full view and b) Zoomed-in view near the cylindrical element. The tracks show the trajectories of the particle centers. The grey surface shown in the figure represents a distance of the particle radius from the cylindrical element. Therefore, tracks of particle centers hitting the grey cylinder will be captured by interception.

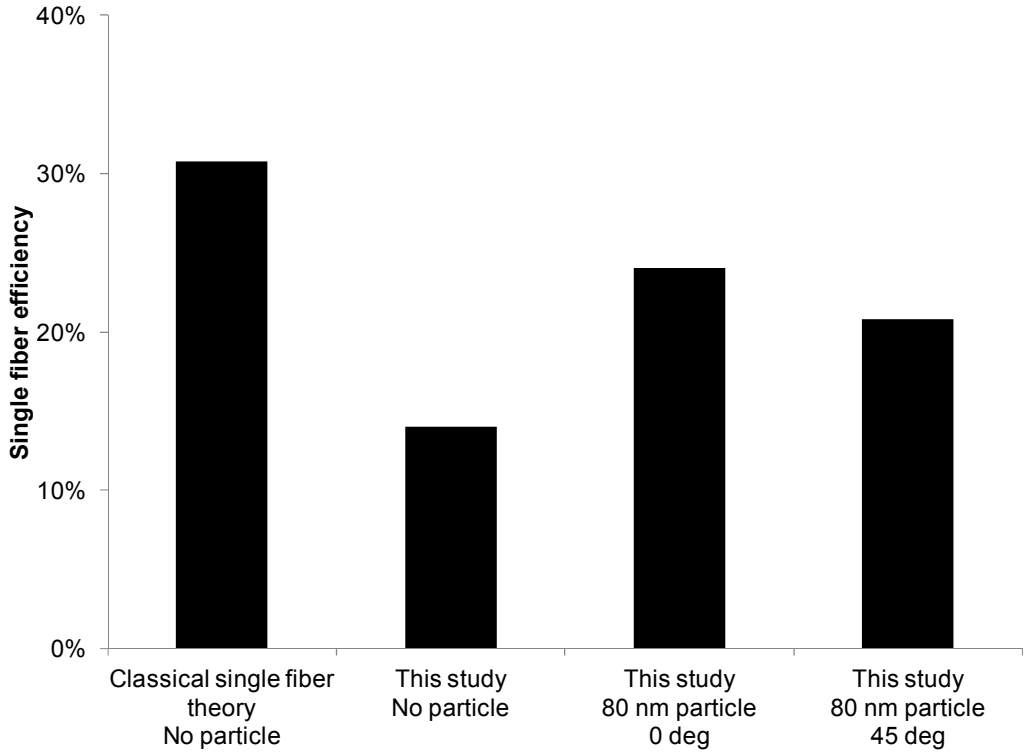

Figure 6-12. Collection efficiency at different simulation conditions based on simulations

On the other hand, the presence of a 80 nm particle on the cylindrical element can enhance the capture of 30 nm particles. It should be noted that the results represented in Figure 12 are obtained for a cylindrical element with length 0.5 μm having a 80 nm particle attached at the middle. The single fiber efficiency, as defined in Equation 6-1, in cases which a particle is attached should be 226% and 189% for the particle attached at 0 and 45 degree from the inlet flow, respectively. The effects for particle located at 0 degree relative to the inlet flow is slight higher. With the information of the filter physical characteristics, the single fiber efficiency results can be incorporated into Equation 6-4 to determine the overall filtration efficiency. The simulation results can explain the higher collection efficiency due to a previously captured particle. However, the single fiber theory alone cannot account for the observed decreasing trend with particle loading of membrane filters. Therefore, a combined multi-layer pore blockage model and single

fiber theory can potentially be explored to describe the transient filtration performance of membrane filters.

6.4 Summary

We have presented results of numerical simulation by ANSYS CFX for change in membrane filter's collection efficiency due to the presence of a particle previously captured within the filter. Because of the complex porous structure of the membrane, we simplified our study into two cases: 1) capillary tube model and 2) single fiber model. From the capillary tube model, it was found that the presence of a particle captured near the pore opening can increase the collection efficiency of 30 nm particles by about two times, depending on the relative size of the particles to the pore. The information can be incorporated into pore blockage model which considers filters as multiple layers of parallel pores. From the single fiber model, a particle attached on the fiber can increase the single fiber efficiency by 10 times, depending on the location of the particle attached. The simulation results can explain the higher collection efficiency due to a previously captured particle. However, the single fiber theory alone cannot account for the observed decreasing trend with particle loading.

Chapter 7

Accomplishments and recommendations

7.1 Summary of accomplishments

The objectives of this thesis are to 1) explore methods for characterizing liquid-borne nanoparticles and 2) apply these methods to study nanoparticle filtration problems. The characterization techniques and filtration technologies of liquid-borne nanoparticles were studied. For particle characterization, the aerosolization technique was developed and the Nanoparticle Tracking Analysis (NTA) technique was evaluated. The applicability of these techniques for liquid filtration was demonstrated. For nanoparticle filtration, laboratory procedures to evaluate nanometer-rated liquid filters were developed. Initial and transient filtration performance of filters against nanoparticles of different materials were studied. Numerical modeling is attempted to understand the experimental observations. The studies accomplished within this dissertation are summarized as follows.

Chapter 2 discusses the use of the Nanoparticle Tracking Analysis (NTA) technique for liquid-borne nanoparticle characterization. NTA was first calibrated and it was shown that, with proper software settings, NTA concentration measurements agree well with the number concentration estimated by suspension mass concentration. Since the dynamic concentration range is limited, it is important to ensure the measurements are made within the acceptable concentration range. A single sample should be diluted and the NTA concentration measurements for the original and diluted samples should agree. The application of NTA is also demonstrated by a study on the nanoparticles produced during abrasive waterjet cutting and electrical discharge machining processes. Nanoparticles, with peak size between 100 and 200 nm, are present in water samples collected from these processes. SEM analysis suggested that these nanoparticles are mostly non-spherical and agglomerated. The safety procedures for handling and disposal of used filters should be considered.

Chapter 3 demonstrates the use of aerosol instruments for characterzing liquid-borne nanoparticles. Conventional atomizer, electrospray generator and nanoparticle nebulizer (TSI) were used for dispersing suspensions into airborne form. After solvent evaporation, SMPS is used for counting and sizing the insoluble nanoparticles. This method can quantify liquid-borne particles as small as 30 nm, which cannot be analyzed by state-of-the-art liquid particle counters. The sizing resolution is shown to be better than the NTA technique, by measuring a suspension containing mixed 30, 50 and 80 nm gold particles. The applicability of this technique for filtration study is also discussed.

In Chapter 4, the aerosol and NTA techniques discussed in the previous chapters were applied to study initial filtration efficiency of standard nuclepore filters. The retention efficiencies of nuclepore filters against PSL nanoparticles were experimentally determined. Results were compared with the predictions by capillary tube model, which was originally developed for aerosol filtration. Particles smaller than the pore size have a low, but non-zero retention efficiency. By applying a proper sticking coefficient, equal to 0.15, the model can describe the particle retention characteristics of the nuclepore filters.

Chapter 5 reports the experimental studies on the filtration performance of a 50 nm- rated Polytetrafluoroethylene (PTFE) membrane filter. The effects of loading, size distribution and materials of test particles were examined. For monodisperse particle test, a decreasing trend as a function of cumulative particle volume has been observed. This can be readily explained by the sieving mechanism. Comparing the decreasing trend among different particle materials, we observed that silica particles have much lower retention efficiency compared to PSL and gold particles of the same size. The observation can be explained in part, by the interplay among membrane, particle and liquid media properties. Silica, gold and PSL particles have different amount of dissolved substance concentration, as indicated by the electrolyte conductivity. The DLVO theory indicates that the lower ionic strength of silica particles experience higher repulsion interactions over a longer distance than PSL and gold particles.

In Chapter 6, CFD simulations were performed to understand the observations from the liquid filtration experiments. We attempted to understand the change in membrane filter's collection efficiency due to the presence of a particle previously captured within the filter. Because of the complex porous structure of the membrane, simplified cases were used: 1) capillary tube model and 2) single fiber model. According to the capillary tube simulations, a particle captured near the pore opening can increase the collection efficiency of 30 nm particles by about two times, depending on the relative size of the particles to the pore. The information will be useful for making the multi-layer pore blockage model more realistic. From the single fiber model, a particle attached on the fiber can increase the single fiber efficiency by about 10 times. While the single fiber theory alone cannot account for the general decreasing efficiency with particle loading, the simulation results can explain the higher collection efficiency due to a previously captured particle. Therefore, a combined multi-layer pore blockage model and single fiber theory can possibly describe the transient filtration performance.

7.2 Recommendations

Liquid-borne nanoparticle filtration is still a relatively new field of studies. More work is needed to understand the behaviors and mechanisms, in order to improve the designs of nanometer-rated liquid filters for different applications. The following recommendations, inspired by this thesis study, are for future research related to liquid-borne nanoparticle characterization and filtration:

1. For understanding the environmental, health and safety effects of nanoparticles, the sources of unintentionally generated nanoparticles will need to be identified. The information of the physical and chemical properties as well as the quantity of the nanoparticles will be useful for nanoparticle exposure modeling study.

2. In this study, time-averaged filtration efficiency of nuclepore filters was reported. However, as indicated in the results of Chapter 5, nuclepore filters may also exhibit

varied filtration performance during particle loading. A more detailed study on the filtration performance of nuclepore filters will provide data for comparison with modeling.

3. As indicated in Chapter 5, several parameters affect the nanoparticle filtration performance: the size, shape, degree of agglomeration and size distribution of particles, surface charges of particles and filters as well as pH values and ionic strength of the solution. All these parameters should be systematically studied to gain better understanding on the filtration problems (Refer to Table. 5-3).

4. With the use of silica and PSL as challenge particles, the smallest particle size achievable is about 20 nm. Gold nanoparticle suspensions are available down to about 5 nm. Another option for test particles is quantum dots, which has size of 1-7 nm. The surface charge of quantum dots can be tailor-made possess different charge polarity. Surface charge modification to nanoparticles can facilitate the study of the effects of a single parameter on filtration performance.

5. In this thesis study, the decreasing trend of filtration efficiency, due to blockage of small pores of the filters, has been observed. However, the cake filtration regime has not been systemically studied. The cake structure and porosity are expected to differ due to particle size, shape and loading rate. This will deserve further investigation.

6. Finally, for filtration modeling, more systematic numerical study on the fibrous model and capillary tube model will be needed to generalize the effects of pre-captured particles on subsequent filtration efficiency. The results can then be applied to pore blockage model which describes membrane filter as a multiple layers of straight pores.

Bibliography

American Society for Testing and Materials, *Standard terminology relating to nanotechnology*. **2006**.

Benn, T.M. and Westerhoff, P. Nanoparticle silver released into water from commercially available sock fabrics. *Environ. Sci. Technol.* **2008,** *42,* 4133-4139.

Beuscher, U. Modeling Sieving Filtration using Multiple Layers of Parallel Pores. *Chem. Eng. Technol.* **2010,** *33,* 1377-1381.

Biswas, P. and Wu, C. Nanoparticles and the environment. *J. Air Waste Manage. Assoc.* **2005,** *55,* 708-746.

Bondoc Jr, L. and Fitzpatrick, S. Size distribution analysis of recombinant adenovirus using disc centrifugation. *Journal of Industrial Microbiology and Biotechnology* **1998,** *20,* 317-322.

Botes, M. and Eugene Cloete, T. The potential of nanofibers and nanobiocides in water purification. *Crit. Rev. Microbiol.* **2010,** *36,* 68-81.

Bowen, W.R. and Jenner, F. Theoretical descriptions of membrane filtration of colloids and fine particles: an assessment and review. *Adv. Colloid Interface Sci.* **1995,** *56,* 141-200.

Boxall, A.B.; Tiede, K.; Chaudhry, Q. Engineered nanomaterials in soils and water: how do they behave and could they pose a risk to human health? *Nanomedicine* **2007,** *2,* 919-927.

Brown, R.C. *Air filtration: an integrated approach to the theory and applications of fibrous filters*. Pergamon press New York, **1993**.

Cabanillas, E.; Granovsky, M.; Ratner, M. TEM AND SEM Studies of Micro and Nanoparticles Obtained by Electroerosion Discharge Machining Process in Liquid N2. *Acta Microscopica* **2010,** *19,* 190-195.

Cabanillas, E. Micro and nano particles produced by waterjet abrasion. *Acta Microscopica* **2010,** *19,* 105-108.

Celik, I.B.; Ghia, U.; Roache, P.J. Procedure for estimation and reporting of uncertainty due to discretization in CFD applications. *Journal of fluids Engineering-Transactions of the ASME* **2008,** *130(7).*

Chang, I.; Le Clech, P.; Jefferson, B.; Judd, S. Membrane fouling in membrane bioreactors for wastewater treatment. *J. Environ. Eng.* **2002,** *128,* 1018-1029.

Chen, Z.; Meng, H.; Xing, G.; Chen, C.; Zhao, Y.; Jia, G.; Wang, T.; Yuan, H.; Ye, C.; Zhao, F. Acute toxicological effects of copper nanoparticles in vivo. *Toxicol. Lett.* **2006,** *163,* 109-120.

Cyrs, W.; Boysen, D.; Casuccio, G.; Lersch, T.; Peters, T. Nanoparticle collection efficiency of capillary pore membrane filters. *J. Aerosol Sci.* **2010,** *41,* 655-664.

Derjaguin, B. A theory of the heterocoagulation, interaction and adhesion of dissimilar particles in solutions of electrolytes. *Discuss. Faraday Soc.* **1954,** *18,* 85-98.

Domingos, R.F.; Baalousha, M.A.; Ju-Nam, Y.; Reid, M.M.; Tufenkji, N.; Lead, J.R.; Leppard, G.G.; Wilkinson, K.J. Characterizing manufactured nanoparticles in the

environment: multimethod determination of particle sizes. *Environ. Sci. Technol.* **2009,** *43,* 7277-7284.

Duclos-Orsello, C.; Kelly, W.P.; Grant, D.C.; Zahka, J.; Thom, V. Neutral adsorptive capture of particles by membranes: network modeling near the membrane isoelectric point. *J. Membr. Sci.* **2004,** *237,* 167-180.

Duke, S.D. Particle retention testing of 0.05 to 0.5 micrometer membrane filters. *Fluid/Particle Separation Journal* **1988,** *1,* 75-78.

Elsaied, H.E.; Sato, M.; Naganuma, T. Viable Cytophaga-like Bacterium in the 0.2 μm-Filtrate Seawater. *Syst. Appl. Microbiol.* **2001,** *24,* 618-622.

Farré, M.; Gajda-Schrantz, K.; Kantiani, L.; Barceló, D. Ecotoxicity and analysis of nanomaterials in the aquatic environment. *Analytical and Bioanalytical Chemistry* **2009,** *393,* 81-95.

Filipe, V.; Hawe, A.; Jiskoot, W. Critical evaluation of Nanoparticle Tracking Analysis (NTA) by NanoSight for the measurement of nanoparticles and protein aggregates. *Pharm. Res.* **2010,** *27,* 796-810.

Friedlander, S. Theory of aerosol filtration. *Industrial & Engineering Chemistry* **1958,** *50,* 1161-1164.

Gallego-Urrea, J.A.; Tuoriniemi, J.; Hassellöv, M. Applications of particle-tracking analysis to the determination of size distributions and concentrations of nanoparticles in environmental, biological and food samples. *TrAC Trends in Analytical Chemistry* **2011,** *30,* 473-483.

Geise, G.M.; Lee, H.; Miller, D.J.; Freeman, B.D.; McGrath, J.E.; Paul, D.R. Water purification by membranes: the role of polymer science. *Journal of Polymer Science Part B: Polymer Physics* **2010,** *48,* 1685-1718.

Grant, D.C. and Liu, B.Y. Sieving capture of liquidborne particles by microporous membrane filtration media. *Particle & Particle Systems Characterization* **1991,** *8,* 142-150.

Grant, D.C.; Liu, B.Y.; Fisher, W.G.; Bowling, R.A. Particle capture mechanisms in gases and liquids: an analysis of operative mechanisms in membrane/fibrous filters. *The Journal of Environmental Sciences* **1989,** *32,* 43-51.

Greenwald, R.; Bergin, M.H.; Carrico, C.M.; Grant, D. New real-time technique to measure the size distribution of water-insoluble aerosols. *Environ. Sci. Technol.* **2005,** *39,* 4967-4973.

Gregory, J. *Particles in water: properties and processes.* CRC Press, **2005**.

Gudimetla, P.; Wang, J.; Wong, W. Kerf formation analysis in the abrasive waterjet cutting of industrial ceramics. *J. Mater. Process. Technol.* **2002,** *128,* 123-129.

Guo, H.; Wyart, Y.; Perot, J.; Nauleau, F.; Moulin, P. Low-pressure membrane integrity tests for drinking water treatment: A review. *Water Res.* **2010,** *44,* 41-57.

Han, J.; Fu, J.; Schoch, R.B. Molecular sieving using nanofilters: past, present and future. *Lab on a Chip* **2008,** *8,* 23-33.

Handy, R.D.; von der Kammer, F.; Lead, J.R.; Hassellöv, M.; Owen, R.; Crane, M. The ecotoxicology and chemistry of manufactured nanoparticles. *Ecotoxicology* **2008,** *17,* 287-314.

Hassellöv, M.; Readman, J.W.; Ranville, J.F.; Tiede, K. Nanoparticle analysis and characterization methodologies in environmental risk assessment of engineered nanoparticles. *Ecotoxicology* **2008,** *17,* 344-361.

Heidam, N.Z. Review: Aerosol fractionation by sequential filtration with Nuclepore filters. *Atmospheric Environment (1967)* **1981,** *15,* 891-904.

Henriquez, R.R.; Ito, T.; Sun, L.; Crooks, R.M. The resurgence of Coulter counting for analyzing nanoscale objects. *Analyst* **2004,** *129,* 478-482.

Hinds, W.C. *Aerosol technology: properties, behavior, and measurement of airborne particles*. John Wiley & Sons, 2nd edition, **1999**.

Ho, K. and Newman, S. State of the art electrical discharge machining (EDM). *Int. J. Mach. Tools Manuf.* **2003,** *43,* 1287-1300.

Hogan, C.J.; Kettleson, E.M.; Ramaswami, B.; Chen, D.; Biswas, P. Charge reduced electrospray size spectrometry of mega-and gigadalton complexes: whole viruses and virus fragments. *Anal. Chem.* **2006,** *78,* 844-852.

Hosseini, S. and Tafreshi, H.V. 3-D simulation of particle filtration in electrospun nanofibrous filters. *Powder Technol* **2010,** *201,* 153-160.

International Organization for Standardization. *Hydraulic fluid power: Verification of fabrication integrity and determination of the first bubble point*. Geneva. **1985.**

International Organization for Standardization. *Nanotechnologies– Terminology and Definitions for Nano-objects–Nanoparticle, nanofibre, and nanoplate.* Norme, TS 27687. **2008**.

Israelachvili, J.N. *Intermolecular and surface forces: revised third edition.* Academic press, 2011.

Itano, M.; Kezuka, T.; Ishii, M.; Unemoto, T.; Kubo, M.; Ohmi, T. Minimization of particle contamination during wet processing of Si wafers. *J. Electrochem. Soc.* **1995,** *142,* 971-978.

Ito, T.; Sun, L.; Henriquez, R.R.; Crooks, R.M. A carbon nanotube-based Coulter nanoparticle counter. *Acc. Chem. Res.* **2004,** *37,* 937-945.

Jahanmir, S.; Ramulu, M.; Koshy, P. *Machining of ceramics and composites.* CRC Press, **1999**.

Jassby, D.; Chae, S.; Hendren, Z.; Wiesner, M. Membrane filtration of fullerene nanoparticle suspensions: Effects of derivatization, pressure, electrolyte species and concentration. *J. Colloid Interface Sci.* **2010,** *346,* 296-302.

John, W.; Reischl, G.; Goren, S.; Plotkin, D. Anomalous filtration of solid particles by Nuclepore filters. *Atmospheric Environment (1967)* **1978,** *12,* 1555-1557.

Johnston, P.R. Revisiting the most probable pore-size distribution in filter media: the gamma distribution. *Filtration Sep.* **1998,** *35,* 287-292.

Kaegi, R.; Wagner, T.; Hetzer, B.; Sinnet, B.; Tzvetkov, G.; Boller, M. Size, number and chemical composition of nanosized particles in drinking water determined by analytical microscopy and LIBD. *Water Res.* **2008,** *42,* 2778-2786.

Kanaoka, C.; Emi, H.; Aikura, T. Collection efficiency of aerosols by micro-perforated plates. *J. Aerosol Sci.* **1979,** *10,* 29-41.

Kelly, W.P.; Grant, D.C.; Zahka, J. Optimization of filter properties for recirculating etch baths. *J. IEST* **2000,** *43,* 30-40.

Kim, K.; Fane, A.; Nystrom, M.; Pihlajamaki, A.; Bowen, W.; Mukhtar, H. Evaluation of electroosmosis and streaming potential for measurement of electric charges of polymeric membranes. *J. Membr. Sci.* **1996,** *116,* 149-159.

Knotter, D.M.; Wolters, S.A.; Kasanrokijat, M.A. Particle Concentration Measurements in Process Liquids Using Light-Scattering Techniques. *Particul. Sci. Technol.* **2007,** *25,* 435-447.

Knutsen, J.S. and Davis, R.H. Deposition of foulant particles during tangential flow filtration. *J. Membr. Sci.* **2006,** *271,* 101-113.

Kuwabara, S. The forces experienced by randomly distributed parallel circular cylinders or spheres in a viscous flow at small Reynolds numbers. *Journal of the Physical Society of Japan* **1959,** *14,* 527.

Ladner, D.; Steele, M.; Weir, A.; Hristovski, K.; Westerhoff, P. Functionalized nanoparticle interactions with polymeric membranes. *J. Hazard. Mater.* **2012,** *211,* 288-295.

Laxen, D.P. and Chandler, I.M. Comparison of filtration techniques for size distribution in freshwaters. *Anal. Chem.* **1982,** *54,* 1350-1355.

Lecoanet, H.F.; Bottero, J.; Wiesner, M.R. Laboratory assessment of the mobility of nanomaterials in porous media. *Environ. Sci. Technol.* **2004,** *38,* 5164-5169.

Lee, H.S.; Chae, S.K.; Liu, B.Y. Size Characterization of Liquid - Borne Particles by light scattering counters. *Particle & Particle Systems Characterization* **1989,** *6,* 93-99.

Lee, J.; Liu, B.Y.; Rubow, K.L. Latex sphere retention by microporous membranes in liquid filtration. *J. IES* **1993,** *36,* 26-36.

Lee, J. and Liu, B.Y. An experimental study of particulate retention by microporous membranes in liquid filtration. *KSME Journal* **1994,** *8,* 69-77.

Lee, J. and Liu, B.Y. A filtration model of microporous membrane filters in liquids. *KSME Journal* **1994,** *8,* 78-87.

Lee, J.; Liu, B.; Rubow, L.; Yoo, S. Filtration of Real-World Particles in Liquids by Microporous Membranes. *J. IES* **1994,** *38,* 19-25.

Lee, J.K. Particulate retention by microporous membrane filters in liquid filtration. *PhD Thesis, University of Minnesota*, **1992.**

Lenggoro, I.W.; Widiyandari, H.; Hogan Jr, C.J.; Biswas, P.; Okuyama, K. Colloidal nanoparticle analysis by nanoelectrospray size spectrometry with a heated flow. *Anal. Chim. Acta* **2007,** *585,* 193-201.

Lenggoro, I.W.; Xia, B.; Okuyama, K.; de la Mora, Juan Fernandez Sizing of colloidal nanoparticles by electrospray and differential mobility analyzer methods. *Langmuir* **2002,** *18,* 4584-4591.

Limbach, L.K.; Bereiter, R.; Müller, E.; Krebs, R.; Gälli, R.; Stark, W.J. Removal of oxide nanoparticles in a model wastewater treatment plant: influence of agglomeration and surfactants on clearing efficiency. *Environ. Sci. Technol.* **2008,** *42,* 5828-5833.

Lin, M. Synthesis of nanophase tungsten carbide by electrical discharge machining. *Ceram. Int.* **2005,** *31,* 1109-1115.

Ling, T.Y.; Wang, J.; Pui, D.Y. Measurement of retention efficiency of filters against nanoparticles in liquids using an aerosolization technique. *Environ. Sci. Technol.* **2009,** *44,* 774-779.

Ling, T.Y.; Wang, J.; Pui, D.Y. Measurement of filtration efficiency of Nuclepore filters challenged with polystyrene latex nanoparticles: experiments and modeling. *Journal of Nanoparticle Research* **2011,** *13,* 5415-5424.

Ling, T.Y.; Wang, J.; Pui, D.Y. Numerical modeling of nanoparticle penetration through personal protective garments. *Separation and Purification Technology* **2012,** *98, 230-239*.

Ling, T.Y.; Zuo, Z.; Pui, D.Y. Detection and Identification: Instrumentation and Calibration for Air/Liquid/Surface-borne Nanoscale Particles. *Journal of Physics: Conference Series* **2013,** *429,* 012006.

Lipp, P.; Müller, U.; Hetzer, B.; Wagner, T. Characterization of nanoparticulate fouling and breakthrough during low-pressure membrane filtration. *Desalination and Water Treatment* **2009,** *9,* 234-240.

Logan, B.E. Theoretical analysis of size distributions determined with screens and filters. *Limnol. Oceanogr.* **1993,** *38,* 372-372.

Logan, B.E.; Hilbert, T.A.; Arnold, R.G. Removal of bacteria in laboratory filters: models and experiments. *Water Res.* **1993,** *27,* 955-962.

Loh, S.; Beuscher, U.; Poddar, T.K.; Porter, A.G.; Wingard, J.M.; Husson, S.M.; Wickramasinghe, S.R. Interplay among membrane properties, protein properties and operating conditions on protein fouling during normal-flow microfiltration. *J. Membr. Sci.* **2009,** *332,* 93-103.

Lundahl, P.; Stokes, R.; Smith, E.; Martin, R.; Graham, D. Synthesis and characterisation of monodispersed silver nanoparticles with controlled size ranges. *Micro & Nano Letters, IET* **2008,** *3,* 62-65.

Lynch, I.; Dawson, K.A.; Linse, S. Detecting cryptic epitopes created by nanoparticles. *Science Signaling* **2006,** pe14.

Madaeni, S. The application of membrane technology for water disinfection. *Water Res.* **1999,** *33,* 301-308.

Madaeni, S. and Fane, A. Microfiltration of very dilute colloidal mixtures. *J. Membr. Sci.* **1996,** *113,* 301-312.

Manton, M. Brownian diffusion of aerosols to the face of a nuclepore filter. *Atmospheric Environment (1967)* **1979,** *13,* 525-531.

Manton, M. The impaction of aerosols on a nuclepore filter. *Atmospheric Environment (1967)* **1978,** *12,* 1669-1675.

Mavrocordatos, D.; Perret, D.; Leppard, G.G. Strategies and advances in the characterisation of environmental colloids by electron microscopy, *IUPAC Series on Analytical and Physical Chemistry of Environmental Systems,* **2007***, 10,* 345.

McFadyen, P. and Fairhurst, D. High-resolution particle size analysis from nanometres to microns. *Clay Miner.* **1993,** *28,* 531-537.

Menard, A.; Drobne, D.; Jemec, A. Ecotoxicity of nanosized TiO2. Review of in vivo data. *Environmental Pollution* **2011,** *159,* 677-684.

Mizuno, T.; Namiki, A.; Tsuzuki, S. A Novel Filter Rating Method Using Less Than 30-nm Gold Nanoparticle and Protective Ligand. *Semiconductor Manufacturing, IEEE Transactions on* **2009,** *22,* 452-461.

Mohd Abbas, N.; Solomon, D.G.; Fuad Bahari, M. A review on current research trends in electrical discharge machining (EDM). *Int. J. Mach. Tools Manuf.* **2007,** *47,* 1214-1228.

Momber, A.W.; Kovacevic, R.; Momber, A.W.; Kovacevic, R. *Principles of abrasive water jet machining.* Springer London, **1998**.

Mueller, N.C. and Nowack, B. Exposure modeling of engineered nanoparticles in the environment. *Environ. Sci. Technol.* **2008,** *42,* 4447-4453.

Nakao, S. Determination of pore size and pore size distribution: 3. Filtration membranes. *J. Membr. Sci.* **1994,** *96,* 131-165.

Nassar, T.; Rom, A.; Nyska, A.; Benita, S. Novel double coated nanocapsules for intestinal delivery and enhanced oral bioavailability of tacrolimus, a P-gp substrate drug. *J. Controlled Release* **2009,** *133,* 77-84.

Nel, A.; Xia, T.; Mädler, L.; Li, N. Toxic potential of materials at the nanolevel. *Science* **2006,** *311,* 622-627.

Nose, M.; Tsuzuki, S.; Mizuno, T.; Numaguchi, T. Particle removal performance of 20nm rated filters for advanced wet chemical cleaning. *International Symposium on Semiconductor Manufacturing 2007, IEEE,* **2007,** 1-3.

Nowack, B. and Bucheli, T.D. Occurrence, behavior and effects of nanoparticles in the environment. *Environmental Pollution* **2007,** *150,* 5-22.

Oganesyan, V.; Orelovich, O.; Yanina, I.; Apel, P.Y. Study of retention ability of nucleopore membranes. *Colloid Journal* **2001,** *63,* 755-761.

Oliveira, R. Understanding adhesion: a means for preventing fouling. *Exp. Therm. Fluid Sci.* **1997,** *14,* 316-322.

Pandey, A. and Singh, S. Current research trends in variants of Electrical Discharge Machining: A review. *International Journal of Engineering Science and Technology* **2010,** *2,* 2172-2191.

Park, J.Y.; Lim, S.; Han, S.; Park, K. Quantification of a mixture of insoluble submicrometer particles and dissolved solids in water using membrane filtration and aerosolization method. *Aerosol Science and Technology* **2011,** *45,* 1010-1018.

Park, J.Y.; McMurry, P.H.; Park, K. Production of Residue-Free Nanoparticles by Atomization of Aqueous Solutions. *Aerosol Science and Technology* **2012,** *46,* 354-360.

Parker, R. and Buzzard, G. A filtration model for large pore nuclepore filters. *J. Aerosol Sci.* **1978,** *9,* 7-16.

Peralta-Videa, J.R.; Zhao, L.; Lopez-Moreno, M.L.; de la Rosa, G.; Hong, J.; Gardea-Torresdey, J.L. Nanomaterials and the environment: a review for the biennium 2008–2010. *J. Hazard. Mater.* **2011,** *186,* 1-15.

Pich, J. Theory of aerosol filtration by fibrous and membrane filters. *Aerosol Science (Davies, CN, ed.), Academic Press, New York* **1966,** 223-285.

Raabe, O.G. The dilution of monodisperse suspensions for aerosolization. *Am. Ind. Hyg. Assoc. J.* **1968,** *29,* 439-443.

Rezić, I. Determination of engineered nanoparticles on textiles and in textile wastewaters. *TrAC Trends in Analytical Chemistry* **2011,** *30,* 1159-1167.

Rothen-Rutishauser, B.M.; Schürch, S.; Haenni, B.; Kapp, N.; Gehr, P. Interaction of fine particles and nanoparticles with red blood cells visualized with advanced microscopic techniques. *Environ. Sci. Technol.* **2006,** *40,* 4353-4359.

Roco, M.C. Nanotechnology's future. *Sci. Am.* **2006,** *295,* 39-39.

Rosenberger, S.; Laabs, C.; Lesjean, B.; Gnirss, R.; Amy, G.; Jekel, M.; Schrotter, J. Impact of colloidal and soluble organic material on membrane performance in membrane bioreactors for municipal wastewater treatment. *Water Res.* **2006,** *40,* 710-720.

Rubow, K.L. and Liu, B.Y. Characteristics of membrane filters for particle collection. *Fluid filtration: gas* **1986,** *1,* 74-94.

Sadr Ghayeni, S.; Beatson, P.; Fane, A.; Schneider, R. Bacterial passage through microfiltration membranes in wastewater applications. *J. Membr. Sci.* **1999,** *153,* 71-82.

Savage, N. and Diallo, M.S. Nanomaterials and water purification: opportunities and challenges. *Journal of Nanoparticle Research* **2005,** *7,* 331-342.

Schrand, A.M.; Rahman, M.F.; Hussain, S.M.; Schlager, J.J.; Smith, D.A.; Syed, A.F. Metal - based nanoparticles and their toxicity assessment. *Wiley Interdisciplinary Reviews: Nanomedicine and Nanobiotechnology* **2010,** *2,* 544-568.

Semiconductor Equipment and Materials International. *New standard: Guide to evaluate the performance of sub-15 nm filters used in Ultrapure water (UPW)*, Document Number: 5188, **2012**.

Seminario, L.; Rozas, R.; Bórquez, R.; Toledo, P.G. Pore blocking and permeability reduction in cross-flow microfiltration. *J. Membr. Sci.* **2002,** *209,* 121-142.

Sharma, H.S. and Sharma, A. Nanoparticles aggravate heat stress induced cognitive deficits, blood–brain barrier disruption, edema formation and brain pathology. *Prog. Brain Res.* **2007,** *162,* 245-273.

Simon, F.; Hermel, G.; Lunkwitz, D.; Werner, C.; Eichhorn, K.; Jacobasch, H. Surface modification of expanded poly (tetrafluoroethylene) by means of microwave plasma treatment for improvement of adhesion and growth of human endothelial cells. **1996,** *103,* 243-257.

Singh, N.; Husson, S.M.; Zdyrko, B.; Luzinov, I. Surface modification of microporous PVDF membranes by ATRP. *J. Membr. Sci.* **2005,** *262,* 81-90.

Singh, S.; Khulbe, K.; Matsuura, T.; Ramamurthy, P. Membrane characterization by solute transport and atomic force microscopy. *J. Membr. Sci.* **1998,** *142,* 111-127.

Smith, T.N. and Phillips, C.R. Inertial collection of aerosol particles at circular aperture. *Environ. Sci. Technol.* **1975,** *9,* 564-568.

Smith, T.N.; Phillips, C.R.; Melo, O.T. Diffusive collection of aerosol particles on Nuclepore membrane filter. *Environ. Sci. Technol.* **1976,** *10,* 274-277.

Spurny, K.; Lodge, J.P.; Frank, E.R.; Sheesley, D.C. Aerosol filtration by means of Nuclepore filters: Structural and filtration properties. *Environ. Sci. Technol.* **1969,** *3,* 453-464.

Stana-Kleinschek, K.; Ribitsch, V.; Šoster, R.; Brumen, M. Measurements of zeta potential of poly (tetrafluoroethylene) foils. **2005,** *480,* 89-94.

Stern, Otto. The theory of the electrolytic double-layer. *Zeit. Elektrochem.* **1924**, 30, 508-516.

Tanny, G.B.; Strong, D.K.; Presswood, W.G.; Meltzer, T.H. Adsorptive retention of Pseudomonas diminuta by membrane filters. *J. Parenter. Drug Assoc.* **1979,** *33,* 40-91.

Tien, C. and Ramarao, B.V. *Granular filtration of aerosols and hydrosols. Butterworth, Stoneham,MA.* Elsevier, **2007**.

Trushkevych, O.; Collings, N.; Hasan, T.; Scardaci, V.; Ferrari, A.; Wilkinson, T.; Crossland, W.; Milne, W.; Geng, J.; Johnson, B. Characterization of carbon nanotube–thermotropic nematic liquid crystal composites. *J. Phys. D* **2008,** *41,* 125106.

Verwey, EJW; Overbeek, JTG; Nes, KV. *Theory of the stability of lyophobic colloids: the interaction of sol particles having an electric double layer*. New York: Elsevier, **1948**.

Wali, F.; Knotter, D.M.; Mud, A.; Kuper, F.G. Impact of particles in ultra pure water on random yield loss in IC production. *Microelectronic Engineering* **2009,** *86,* 140-144.

Wang, J. Abrasive waterjet machining of polymer matrix composites–cutting performance, erosive process and predictive models. *The International Journal of Advanced Manufacturing Technology* **1999,** *15,* 757-768.

Wang, J.; Kim, S.C.; Pui, D.Y. Carbon nanotube penetration through a screen filter: numerical modeling and comparison with experiments. *Aerosol Science and Technology* **2011,** *45,* 443-452.

Wang, J.; Kim, S.C.; Pui, D.Y. Figure of merit of composite filters with micrometer and nanometer fibers. *Aerosol Science and Technology* **2008,** *42,* 722-728.

Wang, J.; Kim, S.C.; Pui, D.Y. Investigation of the figure of merit for filters with a single nanofiber layer on a substrate. *J. Aerosol Sci.* **2008,** *39,* 323-334.

Wang, J.; Kim, S.C.; Pui, D.Y. Measurement of multi-wall carbon nanotube penetration through a screen filter and single-fiber analysis. *Journal of Nanoparticle Research* **2011,** *13,* 4565-4573.

Wang, J.; Kuriyagawa, T.; Huang, C. An experimental study to enhance the cutting performance in abrasive waterjet machining. *Mach. Sci. Technol.* **2003,** *7,* 191-207.

Wang, Y.; Hammes, F.; Boon, N.; Egli, T. Quantification of the filterability of freshwater bacteria through 0.45, 0.22, and 0.1 μm pore size filters and shape-dependent enrichment of filterable bacterial communities. *Environ. Sci. Technol.* **2007,** *41,* 7080-7086.

Wang, Y.; Hammes, F.; Düggelin, M.; Egli, T. Influence of size, shape, and flexibility on bacterial passage through micropore membrane filters. *Environ. Sci. Technol.* **2008,** *42,* 6749-6754.

Warheit, D.B.; Webb, T.R.; Colvin, V.L.; Reed, K.L.; Sayes, C.M. Pulmonary bioassay studies with nanoscale and fine-quartz particles in rats: toxicity is not dependent upon particle size but on surface characteristics. *Toxicological Sciences* **2007,** *95,* 270-280.

Waterhouse, S. and Hall, G. The validation of sterilising grade microfiltration membranes with Pseudomonas diminuta a review. *J. Membr. Sci.* **1995,** *104,* 1-9.

Weersing, J.R. Light scatter measurements for counting and sizing particles. *Ann. N. Y. Acad. Sci.* **1969,** *158,* 722-730.

Weinberg, H.; Galyean, A.; Leopold, M. Evaluating engineered nanoparticles in natural waters. *TrAC Trends in Analytical Chemistry* **2011,** *30,* 72-83.

Wiesner, M.R.; Lowry, G.V.; Alvarez, P.; Dionysiou, D.; Biswas, P. Assessing the risks of manufactured nanomaterials. *Environ. Sci. Technol.* **2006,** *40,* 4336-4345.

Wu, N.; Wyart, Y.; Liu, Y.; Rose, J.; Moulin, P. An overview of solid/liquid separation methods and size fractionation techniques for engineered nanomaterials in aquatic environment. *Environ. Technol.* **2013,** 1-16.

Yang, L. and Watts, D.J. Particle surface characteristics may play an important role in phytotoxicity of alumina nanoparticles. *Toxicol. Lett.* **2005,** *158,* 122-132.

Yao, K.; Habibian, M.T.; O'Melia, C.R. Water and waste water filtration. Concepts and applications. *Environ. Sci. Technol.* **1971,** *5,* 1105-1112.

Yu, X. and Somasundaran, P. Role of polymer conformation in interparticle-bridging dominated flocculation. *J. Colloid Interface Sci.* **1996,** *177,* 283-287.

Zahka, J.; Anantharaman, V.; Carroll, M.; Vakhshoori, K. Characterization of filters used in recirculated buffered oxide etch baths. *Solid State Technol.* **1993,** *36,* 63-71.

Zahka, J. and Grant, D. Predicting the performance efficiency of membrane filters in process liquids based on their pore-size ratings. *Microcontamination* **1991,** *9,* 23-29.

Zänker, H. and Schierz, A. Engineered Nanoparticles and Their Identification Among Natural Nanoparticles. *Annual Review of Analytical Chemistry* **2012,** *5,* 107-132.

Zhao, C.; Zhou, X.; Yue, Y. Determination of pore size and pore size distribution on the surface of hollow-fiber filtration membranes: a review of methods. *Desalination* **2000,** *129,* 107-123.

Appendix

This appendix contains copies of the copyright permissions granted by the owners of the journals where this work is published or figures were taken from.

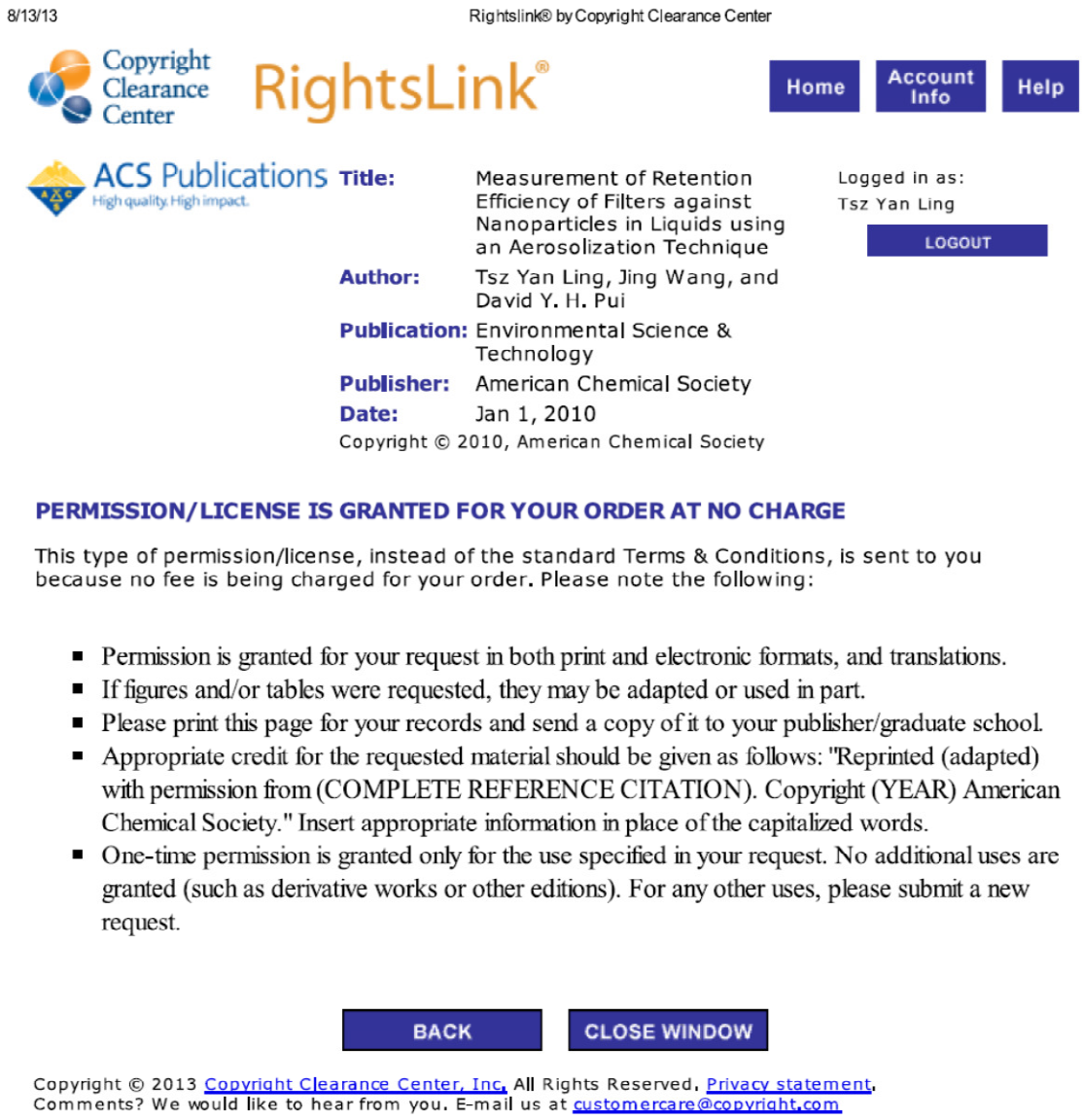

8/13/13 Rightslink® by Copyright Clearance Center

Copyright Clearance Center RightsLink®

Home | Account Info | Help

ACS Publications High quality. High impact.

Title: Measurement of Retention Efficiency of Filters against Nanoparticles in Liquids using an Aerosolization Technique

Author: Tsz Yan Ling, Jing Wang, and David Y. H. Pui

Publication: Environmental Science & Technology

Publisher: American Chemical Society

Date: Jan 1, 2010

Copyright © 2010, American Chemical Society

Logged in as: Tsz Yan Ling

LOGOUT

PERMISSION/LICENSE IS GRANTED FOR YOUR ORDER AT NO CHARGE

This type of permission/license, instead of the standard Terms & Conditions, is sent to you because no fee is being charged for your order. Please note the following:

- Permission is granted for your request in both print and electronic formats, and translations.
- If figures and/or tables were requested, they may be adapted or used in part.
- Please print this page for your records and send a copy of it to your publisher/graduate school.
- Appropriate credit for the requested material should be given as follows: "Reprinted (adapted) with permission from (COMPLETE REFERENCE CITATION). Copyright (YEAR) American Chemical Society." Insert appropriate information in place of the capitalized words.
- One-time permission is granted only for the use specified in your request. No additional uses are granted (such as derivative works or other editions). For any other uses, please submit a new request.

BACK | CLOSE WINDOW

Copyright © 2013 Copyright Clearance Center, Inc. All Rights Reserved. Privacy statement.
Comments? We would like to hear from you. E-mail us at customercare@copyright.com

SPRINGER LICENSE
TERMS AND CONDITIONS

Aug 13, 2013

This is a License Agreement between Tsz Yan Ling ("You") and Springer ("Springer") provided by Copyright Clearance Center ("CCC"). The license consists of your order details, the terms and conditions provided by Springer, and the payment terms and conditions.

All payments must be made in full to CCC. For payment instructions, please see information listed at the bottom of this form.

License Number	3207260694830
License date	Aug 13, 2013
Licensed content publisher	Springer
Licensed content publication	Journal of Nanoparticle Research
Licensed content title	Measurement of filtration efficiency of Nuclepore filters challenged with polystyrene latex nanoparticles: experiments and modeling
Licensed content author	Tsz Yan Ling
Licensed content date	Jan 1, 2011
Volume number	13
Issue number	10
Type of Use	Thesis/Dissertation
Portion	Full text
Number of copies	1
Author of this Springer article	Yes and you are the sole author of the new work
Order reference number	
Title of your thesis / dissertation	Liquid-borne Nanoparticle Characterization and its Application to Nanometer-rated Liquid Filter Evaluation
Expected completion date	Aug 2013
Estimated size(pages)	160
Customer Tax ID	8029894
Total	0.00 USD
Terms and Conditions	

Title: Understanding adhesion: A means for preventing fouling
Author: R. Oliveira
Publication: Experimental Thermal and Fluid Science
Publisher: Elsevier
Date: May 1997

Order Completed

Thank you very much for your order.

This is a License Agreement between Tsz Yan Ling ("You") and Elsevier ("Elsevier"). The license consists of your order details, the terms and conditions provided by Elsevier, and the payment terms and conditions.

Get the printable license.

License Number	3213150232674
License date	Aug 20, 2013
Licensed content publisher	Elsevier
Licensed content publication	Experimental Thermal and Fluid Science
Licensed content title	Understanding adhesion: A means for preventing fouling
Licensed content author	R. Oliveira
Licensed content date	May 1997
Licensed content volume number	14
Licensed content issue number	4
Number of pages	7
Type of Use	reuse in a thesis/dissertation
Portion	figures/tables/illustrations
Number of figures/tables/illustrations	1
Format	both print and electronic
Are you the author of this Elsevier article?	No
Will you be translating?	No
Order reference number	
Title of your thesis/dissertation	Liquid-borne Nanoparticle Characterization and its Application to Nanometer-rated Liquid Filter Evaluation
Expected completion date	Aug 2013
Estimated size (number of pages)	160
Elsevier VAT number	GB 494 6272 12
Customer Tax ID	8029894
Permissions price	0,00 USD
VAT/Local Sales Tax	0,00 USD / 0,00 GBP
Total	0.00 USD